Draft version October 13, 2025
Typeset using LaTeX **twocolumn** style in AASTeX631

The optical photometric variability of Herbig Ae/Be stars from *TESS*

Ann Marie Cody,[1] Lynne A. Hillenbrand,[2] Shreya Chandragiri,[3] and Marvin Morgan[4]

[1] *SETI Institute, 339 Bernardo Ave., Suite 200, Mountain View, CA 94043, USA*
[2] *Department of Astronomy, California Institute of Technology, Pasadena, CA 91125, USA*
[3] *Santa Clara University, Santa Clara, CA 95053, USA*
[4] *Department of Physics, University of California, Santa Barbara, Santa Barbara, CA 93106, USA*

ABSTRACT

We have carried out a photometric time domain study of 188 intermediate-mass young stars observed in Full Frame Image mode with the *TESS* satellite over the first 3.3 years of its mission. The majority of these targets are classified as Herbig Ae/Be stars (HAeBes). All were monitored at optical wavelengths for at least one 27-day *TESS* sector, with many having multiple sectors of data. From a custom aperture photometry pipeline, we produced light curves and analyzed the variability therein, as a function of stellar and circumstellar properties. Based on visual and statistical analysis, we find that ~95% of HAeBes are variable on timescales of 10 minutes to 1 month, with the most common light curve morphology being stochastic. Approximately 15% of the set display quasi-periodic variability. In comparison to sets of low-mass T Tauri stars monitored with optical space telescopes, the Herbig Ae/Be stars display a much lower incidence of "dipper" behaviors (quasi-periodic or aperiodic fading events), as well as periodic modulations. As posited by previous work, we conclude that magnetic starspots are rare on HAeBes, and that the inner circumstellar dust rims of these objects lie at substantially larger radii than for low-mass young stars. Beyond these differences, the accretion dynamics of young stars less than $\sim 7 M_\odot$ appear to be largely consistent based on their time domain properties from data streams of up to three months' duration. We do, however, find tentative evidence for a change in variability amplitude above this mass boundary, particularly for quasi-periodic behavior.

Keywords: Herbig Ae/Be stars (723), Young stellar objects (1834), Pre-main sequence stars (1290), Light curve classification (1954), Time series analysis (1916), Stellar accretion (1578), Circumstellar disks (235)

1. INTRODUCTION

The pre-main sequence (PMS) stage of stellar evolution occupies a key point at the end of star formation, during which stars contract toward eventual main sequence equilibrium. T Tauri stars (masses $\lesssim 2\ M_\odot$) are the most common constituent of the young population, with the classical subtype (CTTS) hosting dusty circumstellar accretion disks. At the high-mass end ($M > 10 M_\odot$), stars do not become optically visible until reaching the main sequence. The intermediate-mass regime is occupied by Herbig Ae/Be stars (HAeBes), with masses of approximately 2 to 10 $M_\odot$ (Herbig 1960; Strom et al. 1972; Waters & Waelkens 1998; Brittain et al. 2023). Like their lower mass counterparts, HAeBes are characterized by spectroscopic signatures of accretion (e.g., hydrogen emission lines) as well as circumstellar dust emission, as signified by (near-)infrared excesses (Hillenbrand et al. 1992; Meeus et al. 2001). They are often found in association with nebulosity, as originally defined by Herbig (1960). That work considered HAeBes to comprise A and B spectral types, but the class is now often extended to include F spectral types as well (van den Ancker et al. 1998).

Of particular interest is how the structure and dynamics of young star-disk systems change as a function of mass. The transition from convective interiors (CTTSs) to radiative interiors (HAeBes) may correlate with other physical differences within and around these stars. For

Corresponding author: Ann Marie Cody
acody@seti.org

example, the magnetospheric accretion paradigm used to explain gas inflow for CTTSs (Calvet & Hartmann 1992; Hartmann et al. 1994, 2016) may break down for the HAeBes. Indeed, spectroscopic observations indicate a change in accretion rate trends between the Herbig Ae and Be regimes (Donehew & Brittain 2011; Mendigutía et al. 2011; Fairlamb et al. 2015). Boundary layer accretion and potentially different inner disk structure has thus been proposed for stars more massive than about 4 $M_\odot$ (Cauley & Johns-Krull 2015; Arun et al. 2019; Wichittanakom et al. 2020). In general, inner disk edges lie at larger distances from higher mass stars, due to their higher luminosities and hence larger sublimation radii (Monnier & Millan-Gabet 2002; Monnier et al. 2005). Other differences, e.g., in dust processing, rim height, outer disk radii, and total dust mass, may exist between CTTSs and HAeBes (Suh 2016; GRAVITY Collaboration et al. 2019, 2021).

One way to probe putative mass dependences in young accreting stars is via comparative investigations of young populations, through the lens of photometric variability. Thousands of CTTSs have been tallied (e.g., Luhman 2022, 2023, and references therein) and monitored from both the ground and space (e.g., Bouvier et al. 1993; Herbst et al. 1994; Cody & Hillenbrand 2018; Venuti et al. 2021; Cody et al. 2022). Based on high-cadence, long-duration (sub-hour continuous cadence over months) space-based monitoring, distinct optical variability patterns have been identified on timescales from minutes to months and amplitudes from 1% to over 100% (Cody et al. 2014). The patterns have been associated with different physical phenomena, including unsteady accretion, occultation by circumstellar dust, and cool or hotspots on the stellar surface.

Likewise, time variations of HAeBes have been the subject of investigation for decades, albeit with smaller numbers of targets and typically less-intensive ground-based monitoring campaigns (e.g., Herbst & Shevchenko 1999; Eiroa et al. 2002; Barsunova et al. 2013; Efimova et al. 2022). Early photometric monitoring revealed variability at many different timescales, and lower amplitude among the Herbig Be stars, compared with the Ae subclass (Finkenzeller & Mundt 1984; Bibo & The 1991; van den Ancker et al. 1998). Additionally, some objects exhibit a tendency toward pronounced fading (up to several magnitudes) on timescales of days to months (The 1994; Dullemond et al. 2003; Uemura et al. 2004). These have been dubbed "UXors" after prototype UX Ori. In an optical photometric monitoring study of 230 HAeBes, Herbst & Shevchenko (1999) observed irregular variations on day to year timescales, which they also categorized as part of the UXor class. Notably, they did not detect periodic variations consistent with hot or cool spots on the stellar surface. Since then, periodic variations *have* been noted, although primarily associated with pulsational instabilities (Marconi & Palla 1998). The question of whether the radiative HAeBes can support large-scale magnetic fields and associated stellar surface spots remains largely unanswered, though progress has been made in making and explaining magnetic field detections in a handful of objects (Järvinen et al. 2019; Hubrig & Schöller 2021). The physical origin of irregular variability also remains the subject of speculation, whether tied to circumstellar occultation (Vioque et al. 2018) or changes in accretion luminosity (Herbst & Shevchenko 1999).

A path forward in understanding the drivers of Herbig Ae/Be star variability and its connections to (circum)stellar physics is through high-cadence space-based photometric monitoring. With the advent of NASA Transiting Exoplanet Survey Satellite (*TESS*) mission (Ricker et al. 2015; Ricker 2019), nearly all-sky optical photometric coverage is now available on timescales from minutes to months and, in many cases, years. In parallel, data from Gaia (Gaia Collaboration et al. 2016) and other missions have made it possible to identify hundreds of new HAeBe candidates based on their photometric properties alone (Vioque et al. 2020).

Using observations from *TESS*, we have embarked on a photometric monitoring study of 188 HAeBes on timescales of minutes to years. In this paper, we define a sample with uniformly derived stellar properties (§2) and create custom light curves for the included stars from Full Frame Images of available *TESS* sectors (§3). Based on those light curves, we then assess HAeBe variability properties via various statistical metrics (§4). Finally, we attempt to correlate these variability properties with circumstellar parameters (§5). We present our key findings in the context of previous works in §6; concluding remarks are provided in §7.

2. STELLAR SAMPLE

In recent decades, imaging and spectroscopic studies have been undertaken to catalog HAeBes across the sky (Hillenbrand et al. 1992; Torres et al. 1995). The canonical list of Thé et al. (1994) serves as a starting point for building a photometric sample, with the caveat that it contains some post-main-sequence star contaminants. These classical Be stars can be difficult to distinguish from HAeBes, as they also display infrared excesses and line emission due to expelled circumstellar material (Rivinius et al. 2013). High-resolution spectroscopic confirmation (e.g., Vieira et al. 2003; Hernández et al. 2004; Carmona et al. 2010) has played a crucial role in disentangling Herbig Be stars from these more evolved systems.

Within the past few years, a flurry of studies have been undertaken to mine WISE, 2MASS, and now the Gaia dataset for the analysis of Herbig Ae/Be star properties and identification of additional candidates. Zhang et al. (2006) assembled a set of 206 HAeBes, later adding in additional stars in the F spectral type regime (Zhang et al. 2022). Vioque et al. (2018, 2020) developed a larger catalog based on machine learning to identify over 1300 potential new Herbig Ae/Be stars. While the contamination fraction of classical Be stars here is likely low, spectroscopic confirmation for the majority of new candidates has not yet been reported in the literature.

In terms of probing HAeBe variability properties, it is advantageous to select as large as possible a sample that is both clean and homogeneous. For our photometric monitoring study, we therefore adopted the catalog presented by Guzmán-Díaz et al. (2021), dubbed the "HArchiBe." The HArchiBe draws confirmed young stars from the above-cited compilations and also includes uniformly derived sets of stellar and disk parameters. From its spectral type list, we discarded stars listed as being K or M. A few G stars are present in the HArchiBe, and we do retain those for the purpose of continuity with previous low-mass samples. The spectral type distribution of our adopted set, after removal of stars with missing or compromised *TESS* photometric data (as described in §3), is shown in Figure 1.

We provide these spectral types, along with crossed-matched stellar identifiers and *TESS* magnitudes for our photometric sample, in Table 1. With the 21″ size of *TESS* pixels, blending is an issue of consideration. The multiplicity of HAeBes was investigated recently by Thomas et al. (2023), and the fraction of stars with companions was reported to be over 50%. In Table 1, we note which stars are either known multiples or photometric blends in *TESS* imaging, as indicated by the TESS Input Catalog (TIC; Paegert et al. 2021), visual examination of higher spatial resolution images from the Digitized Sky Survey (DSS), and/or literature reports of spectroscopic multiplicity. We consider an object to be blended if a neighboring star within the same *TESS* pixel is brighter or no more than two *TESS* magnitudes fainter than the intended target. Blended objects were only thrown out if we were unable to selected a suitable photometric aperture (§3).

Table 1. Intermediate-mass young stars with *TESS* photometry

TIC id	2MASS id	Other name	TESS mag	Spectral type	Blend?
4206238	J05233100-0104237	HD 290380	9.9	F5-F8	N
8806247	J16271510-4839268	Hen 3-1191	12.28	B1	N
11199521	J05380526-0115216	HD 290764	9.51	A5-A7	N
11402323	J05410229-0243006	HD 37806	7.86	B8	N
12161661	J06065848-0555066	PDS 124	11.94	B8-B9	N
12876844	J22531560+6208450	IL Cep	8.53	B2	Y
13002932	J20202825+4121514	V1685 Cyg	9.59	B2-B3	N
13417240	J20213607+4047561	VOS 321	12.27	A8	N
14740791	J20253882+4019008	VOS 398	12.95	G	N
15898682	J20292692+4140439	MWC 1021	9.02	B6-B7	N
17130641	J20324553+4039366	V1478 Cyg	9.72	B5-B6	Y
24344701	J05160047-0948353	HD 34282	9.74	A0-A1	N
30243973	J08554594-4425140	SAO 220669	8.22	B4	N
31638754	J09060000-4718581	PDS 286	10.1	B0	N
35485982	J06484168-1648056	PDS 24	12.82	B9	N
45124112	J06074953+1839264	LkHa 208	10.99	A9-F0	N
46749954	J17125876-3214335	HD 155448	8.73	B8	N

Table 1 *continued*

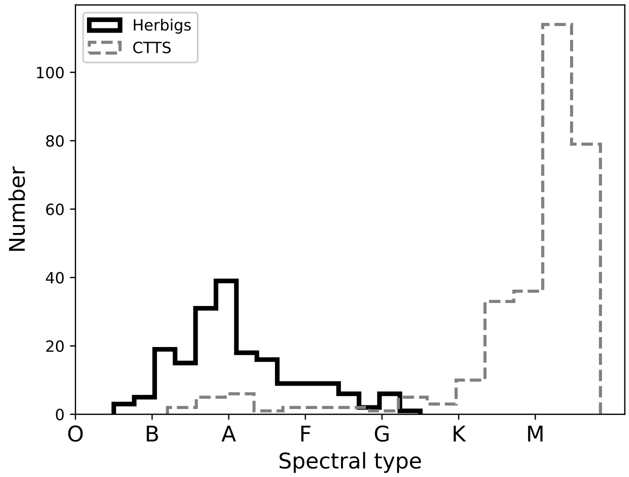

Figure 1. Spectral type distribution for the photometric sample employed in this work (Herbig Ae/Be stars), as well as those from previous works on lower mass stars ("CTTS"). Spectral types are labeled at the zero subtype (i.e., "A" is A0), and adopted from Guzmán-Díaz et al. (2021). If a range of spectral types is given, we take the subtype at the middle. As seen in the histogram, late B and early A stars comprise the most common types here, while earlier samples were dominated by late K and M types.

Table 1 *(continued)*

TIC id	2MASS id	Other name	TESS mag	Spectral type	Blend?
50656450	J05294805-0023434	HD 290500	10.75	A2-A3	N
50745417	J05320993-0249467	RY Ori	10.83	F4-F9	N
53898232	J06542787-2502158	PDS 25	12.69	A3-A6	N
54003409	J01343776-1540348	HD 9672	5.6	A1-A2	N
54185990	J05240118+2457370	HD 35187	8.22	B9-A0	Y
63705801	J21212751+5059475	HD 235495	9.46	B9	N
66918331	J05534254-1024006	V1818 Ori	9.53	B8	N
67671603	J16065795-2743094	HD 144432	7.81	A5-A7	N
72553036	J06133726-0625017	PDS 126	11.3	A5-A7	N
72780071	J05431188-0459499	HD 38120	9.06	B8	N
72781767	J05430057-0218454	HD 38087	8.05	B5-B6	N
73816033	J05302753+2519571	HD 36112	7.98	A9-F0	N
74632969	J05355845+2444542	CQ Tau	9.86	F2-F3	N
75242497	J05393051+2622269	RR Tau	11.71	B9	N
75242566	J05393048+2619552	HD 245906	10.0	A5-A7	N
81297869	J08114457-4405087	HD 68695	9.76	B9-A0	N
85100457	J04584626+2950370	HD 31648	7.55	A5-A6	N
89189882	J05585578+1639573	HD 249879	10.64	B8	N
95586779	J07092789-1212160	VOS 465	12.79	A7	N

Table 1 *continued*

Table 1 *(continued)*

TIC id	2MASS id	Other name	TESS mag	Spectral type	Blend?
96680681	J04554582+3033043	AB Aur	6.94	A1-A2	N
97638779	J06010465+1654407	VOS 131	11.86	F6-G4	N
97807159	J06015998+1630567	HD 250550	9.37	B8	N
101186168	J17332078-3234256	VOS 15	13.11	A6	N
107406463	J07241754-2616053	GSC 6546-3156	13.8	B9-A0	N
107544865	J07250495-2545496	PDS 133	13.71	B7-B8	N
110990131	J19264025+2353508	PX Vul	10.57	F3-F5	N
120751782	J06495854-0738522	PDS 130	12.65	B8-B9	N
121137860	J16590677-4242083	V921 Sco	9.24	B0-B1	N
125641610	J07034316-1133062	Z CMa	8.36	A4-A6	N
125644224	J07040669-1126084	HU CMa	11.42	B7	N
136712091	J21111906+4738476	VOS 22	11.8	B8	N
138670679	J21200323+4657466	VOS 522	12.53	F1	N
138941394	J05330479+0228096	HD 288012	9.64	A2-A3	Y
139019368	J21220592+4651406	VOS 336	12.03	F6-G4	N
139715411	J07283676-2157493	HD 59319	8.37	B7-B8	N
149542947	J05444639-6544079	HD 39014	4.14	A5-A6	N
163268072	J17310584-3508292	HD 319896	10.14	B4-B5	N
166896955	J13574395-3958471	PDS 69	10.0	B4-B5	Y
168627773	J07083879-0419048	PDS 241	11.48	B1	Y
178486401	J07143123-1129271	VOS 703	12.26	F1-F6	N
181142391	J08421727-4044096	V388 Vel	14.33	B9	Y
183658281	J08231185-3907015	PDS 277	9.57	F3-F5	N
189283710	J20384588+4207047	VOS 1331	12.51	B0.5	N
189286260	J20391272+4220546	VOS 111	13.29	A0	N
190255749	J08511143-4138500	VOS 4	12.31	A0	N
199757113	J05274279-0819386	HD 35929	7.68	A9-F0	N
199967382	J05441880+0008403	V351 Ori	8.63	A7-A9	N
200511734	J05301903+1120199	HD 244314	9.87	A2-A3	N
200517741	J05315724+1117414	HD 244604	9.23	A2-A3	N
207044437	J06310692+1026049	VY Mon	12.74	B6-B7	N
207045303	J06310363+1001133	PDS 129	11.42	F2-F3	N
213103713	J05042998-0347142	UX Ori	10.01	A3-A6	N
220322651	J06405118+0944461	HBC 222	11.47	F3-F6	N
229340364	J06330519+1019199	HD 259431	8.31	B7	N
254045303	J19014081-3652337	TY CrA	8.65	B8	N
254387071	J15404638-4229536	HD 139614	8.03	A7-A9	N
255191560	J15564188-4219232	HD 142527	7.57	F2-F3	N
261539498	J05081303+4214558	VOS 84	12.85	A8	N
264460023	J05244279+0143482	V346 Ori	9.9	A7-A9	N
265290711	J02464395+5921168	VOS 2047	12.52	B9.5	N

Table 1 *continued*

Table 1 *(continued)*

TIC id	2MASS id	Other name	TESS mag	Spectral type	Blend?
265464119	J23584164+6626126	LkHa 259	13.02	A7-A9	N
266773096	J04054937+5128348	VOS 200	12.13	A0	N
269112596	J23172558+6050436	MWC 1080	9.8	B0	N
272142683	J23422673+6337387	VOS 42	12.21	B	N
272956728	J11223166-5322114	HD 98922	6.65	B8-B9	N
272995440	J04301623+4852099	VOS 898	12.25	A0	N
276661825	J05370245-0137213	HD 290770	9.2	B8	N
280773136	J11332542-7011412	HD 100546	6.66	A0-A1	N
283096205	J06554005-0309506	PDS 229N	12.8	B7	Y
284214915	J00365177+6329300	VOS 70	11.94	A7	N
285920558	J07591156-5022468	GSC 8143-1225	12.18	F1-F4	N
286322252	J02590513+6054041	VOS 588	12.37	B8	N
287757971	J05365925-0609164	HD 37258	9.53	A0-A1	N
287840183	J05371326-0635005	BF Ori	10.07	A2-A3	N
288924907	J20590591+4805368	VOS 69	12.26	A3	N
290064548	J21035423+5015101	LkHa 324	11.39	B7-B8	N
293537745	J15580967-5351349	Hen 3-1121S	10.47	O-B0	Y
297154074	J20480478+4347258	V2019 Cyg	10.46	B8	N
299797908	J13524285-6332492	Hen 3-938	11.36	O	N
302824830	J05321413+1703292	HD 36408	6.08	B6-B7	Y
305447083	J11034056-5925590	HD 96042	8.41	B0	N
307606851	J15154894-3708558	HD 135344	7.71	F0-F2	N
309449806	J06071539+2957550	GSC 1876-0892	12.71	B4	Y
311826580	J00385008+5954101	VOS 32	13.82	G0	N
312493387	J20140898+4029502	VOS 250	12.46	A3	N
317789227	J11311339-6350120	VOS 290	10.96	B2	N
319939254	J11374699-6342562	VOS 1336	12.88	B2.5-B9.5	Y
320547523	J11394445-6010278	HD 101412	9.07	B9-A0	N
322312832	J21425018+6606351	V361 Cep	9.53	B4	N
332856261	J05374708-0642301	HD 37357	7.38	B9	N
332856968	J05380931-0649166	V1787 Ori	12.0	A3-A4	N
332914217	J05385862-0716457	V599 Ori	11.66	A4-A6	N
332970982	J05401176-0942110	V350 Ori	11.4	A1-A3	N
335623526	J22114281+6036433	VOS 48	13.15	G0	N
336518731	J14185145-6124377	VOS 1245	13.55	A0	Y
339989392	J16544485-3653185	AK Sco	8.79	F7-G5	N
341984965	J22111311+5253341	VOS 475	13.02	B9.5	Y
349354945	J03291977+3124572	BD+30 549	9.9	B8	N
355320922	J08442365-5956578	GSC 8581-2002	10.55	B9	N
355676575	J19251419+2240382	VOS 481	12.52	F6-G4	N
356608297	J20510271+4349318	HBC 705	12.34	B2	N

Table 1 *continued*

Table 1 *(continued)*

TIC id	2MASS id	Other name	TESS mag	Spectral type	Blend?
357040880	J12000511-7811346	HD 104237	6.35	A5-A7	N
358568109	J05505477+2014476	UCAC4 552-019438	12.33	B7-B8	N
358901633	J23101132+6555587	VOS 35	12.53	F	N
362789897	J19422811+2306515	VOS 105	13.48	F5	N
365776906	J05273833+1125389	CO Ori	10.84	F3-F6	N
367036276	J20473745+4347249	V1977 Cyg	10.22	B8	N
367420555	J22165406+7003450	BO Cep	10.96	F3-F5	N
369496705	J12484238-5954350	Hen 3-823	10.08	B4	N
372070676	J22014287+6944364	BH Cep	10.68	F1-F4	N
377617067	J23122637+6058129	VOS 1026	11.87	B0.5	N
377893466	J23160757+6001437	VOS 672	12.42	B1.5-B8	N
385894679	J19255874+2112313	WW Vul	10.12	A3-A4	N
386040374	J07255610-1410435	HD 58647	6.71	B8	N
387813185	J21013691+6809476	HD 200775	6.77	B4	Y
388143588	J22383182+5550052	MWC 655	8.86	B2-B3	N
388935225	J05362543-0642577	V380 Ori	9.78	B9	Y
390384783	J12174750-5943590	GSC 8645-1401	11.98	A9-F2	N
395172881	J21400313+4802106	VOS 759	11.71	A8	N
396284614	J19111124+1547155	HD 179218	7.32	B9	N
396300742	J00093755+5813106	MQ Cas	12.97	B9	N
401214336	J21380845+5726476	GSC 3975-0579	11.26	A0-A1	N
408081161	J19555428+1932354	VOS 199	12.7	F1	N
409323949	J07193593-1739180	PDS 27	11.79	B4-B5	N
409406992	J16130668-5023199	WRAY 15-1435	11.67	B2-B3	N
410736126	J03283262+5113543	VOS 934	11.94	A2	N
410951921	J16160533-5046035	VOS 911	12.03	B2-B4	N
412645923	J21590612+6040533	VOS 473	12.19	A0	N
420018149	J00431825+6154402	V594 Cas	9.73	B7-B8	N
420307432	J22585908+5918024	VOS 1126	12.59	B2	N
427352999	J05341416-0536542	HBC 442	9.65	F8-G1	N
427373765	J05344698-0534145	HD 36917	6.1	B8	N
427395300	J05350983-0527532	HD 36982	8.17	B2	N
427395473	J05353136-0533088	NV Ori	9.37	F0-F2	N
427396230	J05355043-0528349	T Ori	10.87	A0-A1	N
427577547	J03390056+2941457	PDS 4	10.3	B9-A0	N
427938329	J21523408+4713436	AS 477	9.7	B8-B9	N
428476066	J00313068+6158509	VX Cas	11.19	B9	N
430006517	J21351915+5736382	VOS 121	12.75	B9.5	N
434633379	J23022850+6316309	VOS 274	12.54	A3	N
434972921	J23050746+6215362	V374 Cep	9.58	B3-B5	N
436098606	J05350960+1001515	HD 245185	9.79	B9	N

Table 1 *continued*

Table 1 *(continued)*

TIC id	2MASS id	Other name	TESS mag	Spectral type	Blend?
437994564	J06184553+1516522	MWC 137	10.23	B1	N
441152806	J02440733-1351312	HD 17081	4.38	B7	N
441744490	J09424032-5615341	PDS 297	11.85	B8	N
444356276	J00231367+6159318	VOS 787	12.9	B1.5	N
445062554	J06045913-1629039	HD 41511	4.18	B9-A0	N
449260863	J05194140+0538428	HD 34700	8.61	F8-G1	N
452035938	J11330559-5419285	HD 100453	7.5	A9-F0	N
452248316	J19471649+2719558	VOS 104	12.28	A2	Y
454215115	J15032380-6322588	DG Cir	11.72	A2-A3	N
454274408	J15045606-6307526	HD 132947	8.91	B8-B9	N
454291762	J11080329-7739174	HD 97048	8.07	B8	N
455573060	J21541877+4712096	LkHa 257	12.51	A1-A2	N
456030854	J22411697+6302377	VOS 56	13.18	A4	Y
457231768	J05270547+0025075	HD 290409	9.88	B9	N
459571845	J10520871-5612066	PDS 322	11.82	B2	N
459699513	J10532726-5825245	HD 94509	9.15	B7	N
459990291	J05240804+0227468	HD 287823	9.58	A4-A6	N
460571412	J10330498-6019513	HD 305298	9.46	O	N
462436722	J10043028-5839521	HD 87643	8.04	B4	N
462878642	J10100032-5702073	PDS 37	11.51	B2-B3	N
463597276	J17244469-3843514	MWC 878	9.62	B0	N
465196254	J17340462-3923413	HD 323771	10.72	B5-B6	N
465790701	J10572427-6253132	PDS 324	13.62	B2-B3	N
467356861	J22213319+7340270	SV Cep	10.03	A3-A4	N
469534433	J21361422+5721309	AS 470	11.49	A4-A7	Y
642035133	J03493638+3858556	XY Per A	9.12	B9	Y
709004859	J06033705-1453025	PDS 22	10.72	B9	Y
816058534	J08550867-4327596	HD 76534	8.2	B2	Y
1139218134	J15542182-5519443	HD 141926	8.21	B0	Y

NOTE—The sample of stars observed with *TESS* as part of this work. Alternate names and spectral types are taken from Guzmán-Díaz et al. (2021), whereas magnitudes, TIC ids, and 2MASS ids are based on cross matching with the TESS Input Catalog. The final column indicates whether a target is deemed to be blended, as explained in the text.

3. *TESS* OBSERVATIONS AND LIGHT CURVE PRODUCTION

The *TESS* mission has been underway since mid-2018, with new regions of sky ("sectors") observed approximately every 27 days. Many stars have been observed in multiple sectors, as camera fields overlap and *TESS's* extended mission campaigns have also revisited sky regions. During the primary mission (2018-2020; sectors 1-26), so-called Full Frame Images (FFIs) were acquired every 30 minutes during each sector. For the first extended mission (2020-2022; sectors 27-55), the FFI cadence was raised to once every 10 minutes. While *TESS* has continued with further extended missions, for the purposes of this work, we only consider FFI data taken through sector 45 (i.e., from 25 July 2018 through 2 December 2021).

From the initial list of 318 HArchiBe members, we checked which stars were observed by *TESS* in any of the sectors 1–45 and removed 39 objects with no data.

For the remaining stars, we downloaded FFI data in the form of 11×11 target pixel files (TPFs), as produced by the `astrocut` Python package. Many of the targets did not have publicly available light curves, so we ran several custom pipelines to create our own.

The first pipeline consisted of circular aperture photometry with radii of one, two, three, and four pixels. The aperture was centered on the known coordinates of each star, with no shifts. Upon summing the enclosed flux, we subtracted background, as determined from the median flux level of the TPF after an iterative five-sigma cut to remove point sources.

The second pipeline employed the `lightkurve` package to measure fluxes using non-circular aperture masks. We again created several versions, included 1-pixel and 2×2-pixel masks centered on the target, as well as asymmetric masks defined by all pixels exceeding an eight or 12-sigma threshold relative to the median flux level. Upon summing the flux within these apertures, the background was estimated based on the median flux of pixels exterior to the mask, minus the fifth percentile of values over those regions. Background subtraction corrected most of the artificial time variability due to, e.g., scattered Earth light, but did not necessarily remove such trends completely. To further correct systematic effects, we applied the `lightcurve` RegressionCorrector function to subtract off up to four orders of principal component vectors associated with the background. For cases where this was unsuccessful in reducing pronounced systematic trends, we instead applied `lightkurve's` pixel-level decorrelation corrector function, again with up to four principle components.

For stars included in the public TESS-SPOC reduction (Caldwell et al. 2020), we considered both the simple aperture photometry (SAP) and pre-search data conditioning (PDC) products. The latter includes a prescription for removing common trends among neighboring stars, and thus typically displays a reduction in artificial systematics, similar to the `lightkurve` RegressionCorrector and PLDCorrector methods.

Finally, for one star (TIC 460571412) for which we were unable to mitigate systematics with the above pipelines, we created a light curve using the `eleanor` package (Feinstein et al. 2019). Upon creation of all light curves for each star and in each sector, we selected the option with the lowest random and systematic noise levels on visual comparison. Most HAeBes are relatively bright, but some of the more distant ones fall outside of *TESS's* optimal range of magnitude 7-16. If a light curve was consistent with background noise and no star was visible in the TPF, we removed it from consideration. Likewise, if there was a clear blend and the aperture could not be centered, we also discarded the object. In some cases, a light curve version had large (multi-day) gaps, such that the variability pattern could not be inferred; we removed these sectors from the set.

These procedures resulted in a set of 188 Herbig Ae/Be stars with a viable light curve in at least one *TESS* sector. This includes a total of 452 final light curves, all of which are displayed in the Appendix. Those that were not derived directly from the TESS-SPOC pipeline ("SAP" and "PDC" apertures in Table 2) are made publicly available at MAST as a High Level Science Product via 10.17909/fkzx-2z29. The corresponding list of observed TIC identification numbers, sectors, and chosen photometric method, is provided in Table 2. For each light curve, we retained data quality flags from the originating *TESS* TPF; all flagged points are included in the light curve files at MAST, but nonzero (i.e., bad) quality points are omitted from the light curve plots here.

Table 2. Properties of the *TESS* Herbig light curve sample

TIC id	Sector	Phot ap	Vartype	Amplitude	Timescale [d]	Q	M
4206238	6	sap	APD	0.0367	17.42	1.0	0.76
4206238	32	sap	APD	0.0303	26.92	1.0	1.07
8806247	12	1a	SC	0.035	24.29	1.0	0.14
8806247	39	1a	SC	0.0369	19.54	1.0	0.08
11199521	6	sap	SC	1.1557	16.6	1.0	-0.12
11199521	32	sap	N	0.021	7.94	0.88	0.07

Table 2 *continued*

Table 2 *(continued)*

TIC id	Sector	Phot ap	Vartype	Amplitude	Timescale [d]	Q	M
11402323	6	3a	S	0.0344	3.62	0.74	0.02
12161661	6	sap	SC	0.0432	19.75	1.0	0.04
12161661	33	sap	SC	0.0381	31.39	1.0	-0.26
12876844	24	3a	EB	0.0417	7.14	0.08	1.44
13002932	14	3a	S	0.1245	26.54	1.0	0.35
13002932	15	3a	S	0.0885	24.52	1.0	-0.25
13002932	41	3a	S	0.0455	5.33	1.0	0.04
13417240	41	2m	L	0.0856	25.17	1.0	0.58
14740791	14	1a	EB	0.3339	0.29	0.13	0.19
14740791	15	1a	EB	0.3808	0.29	0.1	0.26
14740791	41	1a	EB	0.2986	0.29	0.06	0.58
15898682	14	8m	S	0.0244	14.83	1.0	0.38
15898682	15	8m	S	0.0253	16.96	1.0	-0.26
15898682	41	8m	S	0.0311	23.49	1.0	0.45
17130641	14	8m	SC	0.0076	22.96	1.0	-0.45
17130641	15	8m	SC	0.0061	6.33	1.0	-0.19
17130641	41	8m	SC	0.0102	12.63	1.0	0.29
24344701	5	2a	L	0.1298	7.17	1.0	0.3
24344701	32	2a	APDC	0.1435	18.22	1.0	0.54
30243973	8	pdc	MP	0.0125	1.45	0.43	0.46
30243973	9	pdc	MP	0.0166	1.46	0.69	-0.28
30243973	35	pdc	MP	0.0132	1.47	0.38	-0.21
30243973	36	pdc	MP	0.0112	1.46	0.39	0.34
31638754	9	3a	SC	0.0167	7.81	0.38	0.02
31638754	35	3a	SC	0.0197	19.81	0.93	0.2
31638754	36	3a	SC	0.0179	3.51	0.86	-0.19
35485982	6	2m	S	0.0176	5.54	1.0	0.26
35485982	7	2m	S	0.0104	2.19	0.8	0.06
35485982	33	2m	APDC	0.0232	9.47	1.0	0.47
45124112	43	8m	QPSC	0.0068	0.55	0.82	-0.06
45124112	44	8m	QPSC	0.0048	0.55	0.83	0.21
46749954	12	8m	QPS	0.0068	5.1	0.47	-0.07
46749954	39	8m	QPS	0.0086	5.44	0.64	0.27
50656450	6	pdc	MP	0.0044	10.87	0.96	0.08
50656450	32	pdc	MP	0.0103	1.61	1.0	0.19
50745417	6	3a	S	0.6238	22.75	1.0	0.35
50745417	32	3a	S	0.3894	21.29	1.0	0.0
53898232	6	2a	APDC	0.6157	16.63	1.0	0.38
53898232	7	2a	APDC	0.7859	15.17	1.0	0.77
53898232	33	2a	APDC	0.5644	30.56	1.0	0.81

Table 2 *continued*

Table 2 *(continued)*

TIC id	Sector	Phot ap	Vartype	Amplitude	Timescale [d]	Q	M
54003409	3	pdc	N	0.0001	3.33	0.86	0.11
54185990	43	sap	APDC	0.0569	12.19	1.0	0.67
54185990	44	sap	SC	0.0476	24.09	1.0	-0.38
54185990	45	sap	LC	0.0277	28.25	1.0	-0.12
63705801	15	3a	S	0.0342	20.79	1.0	0.54
63705801	16	3a	S	0.0255	4.17	1.0	0.48
66918331	6	2a	L	0.2724	31.0	1.0	-0.99
66918331	33	2a	L	2.7715	0.35	1.0	-1.14
67671603	12	sap	QPS	0.0152	1.12	0.74	0.12
72553036	6	pdc	S	0.0083	3.96	0.92	0.1
72780071	6	3a	QPS	0.0091	2.36	0.67	-0.19
72781767	6	sap	MPC	0.0118	2.36	0.69	-0.01
73816033	43	3a	MP	0.0264	18.71	1.0	-0.04
73816033	44	3a	APDC	0.0512	17.94	0.99	0.96
73816033	45	3a	MP	0.0176	11.72	1.0	0.09
74632969	43	2a	S	1.0786	8.25	0.98	-0.24
74632969	44	2a	S	0.6052	8.65	0.89	0.12
74632969	45	2a	S	0.7232	6.67	0.88	-0.64
75242497	43	2a	LC	1.2832	7.64	1.0	-1.1
75242497	44	2a	SC	1.0612	19.02	1.0	-0.21
75242497	45	2a	SC	0.7765	8.1	1.0	-0.26
75242566	43	8m	QPS	0.0107	2.08	0.58	0.1
75242566	44	8m	QPS	0.0107	2.1	0.44	0.19
75242566	45	8m	QPS	0.0125	2.38	0.64	0.02
81297869	7	8m	MP	0.0057	17.9	0.98	0.08
81297869	8	8m	MP	0.0071	0.06	0.8	0.16
81297869	34	8m	MP	0.0145	25.31	0.99	0.06
81297869	35	8m	MP	0.0171	33.82	0.9	0.04
85100457	19	4a	S	0.035	5.17	1.0	0.56
85100457	43	4a	S	0.0304	23.47	1.0	-0.19
85100457	44	4a	S	0.0406	4.31	1.0	0.1
89189882	6	2m	QPS	0.0108	0.75	0.61	0.06
89189882	33	2m	QPS	0.01	0.75	0.57	-0.22
89189882	43	2m	QPS	0.0112	0.76	0.47	-0.09
89189882	45	2m	QPS	0.0118	0.75	0.56	-0.01
95586779	7	1a	EB	0.0384	2.32	0.63	0.36
95586779	33	1a	EB	0.0595	2.32	0.37	0.56
96680681	19	4a	S	0.0354	13.56	1.0	-0.36
96680681	43	4a	S	0.017	18.8	1.0	-0.18
96680681	44	4a	S	0.025	20.13	1.0	0.21

Table 2 *continued*

Table 2 *(continued)*

TIC id	Sector	Phot ap	Vartype	Amplitude	Timescale [d]	Q	M
97638779	6	2a	QPS	0.1455	1.63	0.73	0.54
97638779	33	2a	S	0.1565	13.75	1.0	-0.03
97638779	43	2a	QPS	0.3268	1.63	0.71	0.46
97638779	44	2a	QPS	0.2225	1.63	0.34	0.07
97638779	45	2a	QPS	0.1204	1.63	0.19	0.2
97807159	6	3a	S	0.0593	12.67	0.815	0.19
97807159	33	3a	B	0.0408	9.91	0.85	-0.33
97807159	43	3a	S	0.0574	8.51	0.91	-0.01
97807159	44	3a	B	0.0562	6.97	1.0	-0.3
97807159	45	3a	B	0.0488	5.1	0.6	-0.54
101186168	12	2m	APDC	0.0495	20.79	1.0	0.78
101186168	39	2m	APDC	0.0516	16.01	1.0	0.27
107406463	7	1m	QPSC	0.011	6.41	0.27	0.12
107406463	34	1m	QPSC	0.0123	11.9	0.61	0.11
107544865	7	1a	S	0.5542	23.79	1.0	0.12
107544865	34	1a	S	0.3246	29.36	1.0	-0.31
110990131	40	8m	S	0.0179	32.0	1.0	0.17
110990131	41	8m	QPDC	0.1187	5.92	0.36	0.34
120751782	6	2a	LC	0.096	10.33	1.0	-0.55
120751782	33	2a	NC	0.0477	18.96	1.0	0.06
121137860	12	2m	QPSC	0.0417	1.89	0.6	0.31
121137860	39	2m	QPSC	0.1048	1.88	0.65	0.38
125641610	7	2a	S	0.0872	9.37	0.83	-0.36
125641610	33	2a	L	0.2231	8.13	1.0	-0.27
125644224	7	1m	S	0.0271	6.4	1.0	-0.11
125644224	33	1m	S	0.0382	6.27	1.0	-0.12
136712091	15	2m	LC	0.1735	33.29	1.0	0.72
136712091	16	2m	SC	0.0657	23.04	1.0	0.27
138670679	15	2m	QPSC	0.0124	2.08	0.71	-0.06
138670679	16	2m	QPSC	0.0212	19.37	1.0	0.66
138941394	6	sap	APDC	0.0834	16.71	1.0	0.34
138941394	32	sap	APDC	0.0626	12.93	1.0	0.33
139019368	16	2m	SC	0.0575	21.06	1.0	0.05
139715411	7	pdc	P	0.0083	0.73	0.05	-0.03
139715411	34	pdc	P	0.0134	0.73	0.02	0.12
149542947	2	8m	MP	0.0015	0.11	0.65	0.15
149542947	3	8m	MP	0.0014	0.11	0.34	0.04
149542947	5	8m	MP	0.0014	0.11	0.53	0.03
149542947	6	8m	MP	0.0013	0.11	0.48	0.01
149542947	9	8m	MP	0.0016	0.11	0.39	0.05

Table 2 *continued*

Table 2 *(continued)*

TIC id	Sector	Phot ap	Vartype	Amplitude	Timescale [d]	Q	M
149542947	11	8m	MP	0.0013	0.11	0.27	0.01
149542947	12	8m	MP	0.0013	0.11	0.45	0.05
149542947	13	8m	MP	0.0014	0.11	0.47	0.02
149542947	28	8m	MP	0.0016	0.11	0.72	0.09
149542947	29	8m	MP	0.0014	0.11	0.66	-0.03
149542947	30	8m	MP	0.0015	0.11	0.69	-0.01
149542947	31	8m	MP	0.0014	0.11	0.61	-0.01
149542947	32	8m	MP	0.0017	0.11	0.78	-0.11
149542947	33	8m	MP	0.0014	0.11	0.65	0.03
149542947	35	8m	MP	0.0015	0.11	0.79	0.04
149542947	36	8m	MP	0.0016	0.11	0.59	0.0
149542947	38	8m	MP	0.0015	0.11	0.66	-0.04
149542947	39	8m	MP	0.0014	0.11	0.6	-0.05
163268072	12	8m	MP	0.0084	0.66	0.57	-0.2
163268072	39	8m	MP	0.0119	0.66	0.83	-0.13
166896955	11	3a	S	0.0349	5.12	1.0	0.31
166896955	38	3a	S	0.0471	28.53	1.0	-0.59
168627773	7	8m	EB	0.0163	3.57	0.06	1.36
168627773	33	8m	EB	0.0199	3.57	0.16	1.41
178486401	7	2m	APDC	0.0404	23.33	1.0	0.77
178486401	33	2m	APDC	0.0235	8.97	0.84	0.45
181142391	9	8m	QPSC	0.0146	6.41	0.23	0.28
181142391	35	8m	QPSC	0.0132	6.41	0.52	-0.16
183658281	8	pdc	APDC	0.006	3.54	1.0	0.78
183658281	34	pdc	QPSC	0.002	6.1	0.63	0.01
183658281	35	pdc	QPSC	0.0073	4.81	0.52	0.23
189283710	15	1a	S	0.1034	8.06	1.0	0.19
189283710	41	1a	S	0.1108	14.67	1.0	-0.31
189286260	15	2m	LC	0.1295	21.83	1.0	0.84
189286260	41	2m	SC	0.0315	16.51	1.0	0.28
190255749	8	1m	APDC	0.0883	3.96	0.85	0.41
190255749	9	1m	SC	0.1125	23.19	1.0	-0.2
199757113	6	pdc	P	0.0039	1.37	0.09	0.08
199757113	32	pdc	P	0.003	1.37	0.2	-0.03
199967382	6	3a	APDC	0.1017	14.44	1.0	0.8
200511734	6	sap	S	0.0236	16.21	1.0	-0.7
200511734	32	sap	S	0.0195	0.02	0.64	-0.04
200517741	6	pdc	QPSC	0.0047	3.29	0.69	-0.09
200517741	32	pdc	QPSC	0.0037	3.05	0.79	0.18
207044437	6	2a	L	0.072	20.42	1.0	0.1

Table 2 *continued*

Table 2 *(continued)*

TIC id	Sector	Phot ap	Vartype	Amplitude	Timescale [d]	Q	M
207044437	33	2a	L	0.1602	28.75	1.0	-0.36
207045303	6	pdc	N	0.0027	11.5	1.0	-0.05
207045303	33	pdc	N	0.0056	8.88	1.0	0.02
213103713	5	3a	SC	1.1527	12.75	1.0	-0.22
213103713	32	3a	APDC	0.7898	11.17	1.0	0.0
220322651	6	pdc	QPSC	0.0198	6.58	0.55	0.12
220322651	33	pdc	QPSC	0.0266	10.87	0.19	-0.12
229340364	6	3a	S	0.0445	2.96	1.0	-0.09
229340364	33	3a	BC	0.0219	3.57	0.82	0.12
254045303	13	sap	EB	0.1282	2.87	0.14	1.24
254387071	12	sap	MP	0.0042	0.05	0.35	0.1
254387071	38	sap	MP	0.0054	0.05	0.78	0.04
255191560	12	sap	L	0.0187	10.5	1.0	-0.49
261539498	19	2a	APD	0.1095	13.25	1.0	0.44
264460023	6	pdc	MP	0.0068	5.73	0.98	0.05
264460023	32	pdc	MP	0.0059	0.03	0.8	0.02
265290711	18	8m	EB	0.0074	0.32	0.56	0.65
265464119	17	2a	S	0.0621	10.19	1.0	-0.08
265464119	18	2a	S	0.0653	11.79	1.0	-0.36
265464119	24	2a	S	0.0606	10.75	0.91	-0.2
266773096	19	2a	S	0.1174	32.46	0.79	-0.13
269112596	17	3a	QPS	0.1348	1.44	0.74	-0.16
269112596	24	3a	QPS	0.1505	1.44	0.72	0.12
272142683	17	1a	L	1.6777	11.08	1.0	-0.91
272142683	18	1a	LC	0.5175	6.04	1.0	0.05
272142683	24	1a	S	0.3147	16.42	1.0	0.0
272956728	10	3a	QPSC	0.0189	5.95	0.63	0.24
272956728	37	3a	SC	0.0296	16.03	1.0	-0.21
272995440	19	8m	SC	0.0103	5.83	1.0	-0.22
276661825	6	sap	B	0.0132	20.81	1.0	-0.25
276661825	32	sap	B	0.0214	15.06	1.0	-0.07
280773136	11	3a	B	0.0141	15.17	1.0	-0.34
280773136	37	3a	APD	0.0623	24.61	1.0	1.17
280773136	38	3a	APD	0.0631	2.33	1.0	0.31
283096205	6	2m	S	0.0164	7.17	1.0	-0.44
283096205	33	2m	S	0.0125	5.11	1.0	0.15
284214915	17	2m	APDC	0.0434	8.33	0.56	0.51
284214915	18	2m	APDC	0.1889	9.79	1.0	0.9
285920558	7	sap	APD	0.3656	15.65	1.0	0.76
285920558	8	sap	APD	0.187	5.04	1.0	0.28

Table 2 *continued*

Table 2 *(continued)*

TIC id	Sector	Phot ap	Vartype	Amplitude	Timescale [d]	Q	M
285920558	9	sap	APD	0.3248	16.06	1.0	0.61
285920558	34	sap	APD	0.2403	9.99	1.0	0.28
285920558	35	sap	APD	0.3486	14.67	1.0	0.27
285920558	36	sap	APD	0.4845	7.64	0.86	0.48
286322252	19	1m	S	0.0205	8.08	1.0	0.06
287757971	6	3a	APDC	0.0498	6.37	1.0	0.33
287840183	6	pdc	QPDC	0.1403	4.46	0.68	0.71
287840183	32	pdc	QPDC	0.2515	3.91	0.66	0.32
288924907	15	sap	APDC	0.4023	24.67	1.0	-0.18
288924907	16	sap	LC	0.7486	14.5	1.0	-0.2
290064548	15	sap	SC	0.018	33.83	1.0	-0.13
290064548	16	sap	SC	0.0204	30.37	1.0	0.12
293537745	12	3a	QPS	0.0257	4.39	0.17	-0.2
293537745	39	2a	QPS	0.034	4.46	0.32	0.01
297154074	15	2a	S	0.0835	5.67	1.0	0.2
297154074	41	2a	S	0.0585	5.68	0.81	-0.19
299797908	11	1m	QPS	0.0323	1.69	0.6	0.28
299797908	38	1m	QPS	0.0184	1.8	0.79	-0.34
302824830	6	8m	QPSC	0.0005	2.98	0.52	0.43
302824830	43	8m	P	0.0004	1.19	0.61	-0.0
302824830	44	8m	P	0.0003	1.19	0.68	0.01
302824830	45	8m	PC	0.0005	1.19	0.83	0.08
305447083	10	8m	MP	0.0099	0.49	0.36	-0.17
305447083	11	8m	MP	0.0101	0.49	0.52	-0.04
307606851	11	3a	LC	0.03	17.88	1.0	0.53
307606851	38	3a	APDC	0.0071	10.35	1.0	0.1
309449806	44	1a	EBC	0.0289	0.39	0.49	0.02
311826580	17	pld	QPSC	0.0936	5.91	0.62	-0.24
311826580	18	pld	LC	0.2096	10.92	1.0	-0.57
311826580	24	pld	LC	0.1666	11.33	1.0	0.2
312493387	15	2m	APDC	0.0204	11.19	1.0	0.74
312493387	41	2m	APD	0.0443	11.78	1.0	0.52
317789227	10	2a	QPS	0.035	0.16	0.06	-0.09
317789227	11	2a	S	0.0473	22.54	1.0	-0.12
317789227	37	2a	QPS	0.0245	0.16	0.76	-0.12
317789227	38	2a	SC	0.0349	6.41	1.0	0.3
319939254	10	1a	QPSC	0.0509	6.41	0.69	-0.05
319939254	11	1a	SC	0.0381	6.58	0.75	0.2
319939254	37	1a	LC	0.0457	24.77	1.0	0.42
319939254	38	1a	LC	0.0364	22.06	1.0	-0.27

Table 2 *continued*

Table 2 *(continued)*

TIC id	Sector	Phot ap	Vartype	Amplitude	Timescale [d]	Q	M
320547523	10	pdc	N	0.0011	8.17	1.0	-0.11
320547523	11	pdc	N	0.0019	4.75	1.0	-0.31
320547523	37	pdc	N	0.0022	7.12	1.0	-0.0
320547523	38	pdc	N	0.0019	11.81	1.0	-0.13
322312832	16	pdc	MP	0.0069	5.54	0.9	0.12
322312832	17	pdc	MP	0.0069	13.25	0.94	0.01
322312832	18	pdc	MP	0.007	0.32	0.84	-0.06
322312832	24	pdc	MP	0.0055	5.88	1.0	0.26
332856261	6	pdc	S	0.0101	17.79	1.0	-0.05
332856261	32	pdc	N	0.0082	10.24	1.0	-0.14
332856968	6	2a	LC	0.0262	20.83	1.0	0.18
332856968	32	2a	N	0.0138	6.36	1.0	0.03
332914217	6	3a	LC	0.3852	18.12	1.0	0.77
332914217	32	3a	MP	0.0624	29.21	0.98	-0.13
332970982	6	2a	L	0.9485	16.25	1.0	0.15
332970982	32	2a	S	0.6188	12.3	1.0	-0.55
335623526	16	1a	APD	0.3295	2.91	0.84	1.02
335623526	17	1a	APD	0.1548	8.54	0.92	0.85
335623526	24	1a	APDC	0.2592	14.4	1.0	0.51
336518731	11	1m	P	0.0086	0.24	0.08	0.17
336518731	12	1m	P	0.0145	0.24	0.13	0.28
336518731	38	1m	P	0.0083	0.24	0.12	-0.04
339989392	12	sap	APD	0.3583	12.58	1.0	0.32
339989392	39	sap	APD	0.5934	18.53	1.0	0.52
341984965	16	2m	P	0.0044	0.09	0.06	0.08
341984965	17	2m	P	0.0024	0.09	0.4	-0.02
349354945	42	pld	N	0.0158	26.28	1.0	-0.1
349354945	43	pld	N	0.0341	24.71	1.0	-0.1
349354945	44	pld	N	0.0055	25.86	1.0	0.05
355320922	8	12m	MP	0.0017	4.48	0.99	-0.1
355320922	9	12m	MP	0.0016	17.0	0.95	0.16
355320922	10	12m	MP	0.0015	14.12	0.94	0.16
355320922	35	12m	MP	0.0023	10.82	0.87	0.05
355320922	37	12m	MP	0.0022	0.06	0.63	-0.01
355676575	14	1m	SC	0.0191	18.98	1.0	0.07
355676575	40	1m	SC	0.0366	13.25	1.0	-0.06
355676575	41	1m	S	0.0152	5.1	0.81	-0.13
356608297	15	8m	MPC	0.0331	29.0	0.94	0.32
357040880	11	3a	APDC	0.0685	5.56	0.82	0.39
357040880	12	3a	BC	0.0508	15.62	0.35	-0.46

Table 2 *continued*

Table 2 *(continued)*

TIC id	Sector	Phot ap	Vartype	Amplitude	Timescale [d]	Q	M
357040880	38	3a	SC	0.0405	13.89	0.43	0.17
357040880	39	3a	BC	0.0485	14.71	0.33	-0.28
358568109	44	2a	QPSC	0.0791	6.41	0.47	-0.1
358568109	45	2a	S	0.064	3.92	0.94	0.06
358901633	17	1a	QPS	0.0487	2.32	0.26	0.08
358901633	18	1a	APD	0.3326	18.77	1.0	1.02
358901633	24	1a	QPSC	0.2347	2.27	0.76	0.63
362789897	40	2m	APDC	0.042	9.0	1.0	0.18
362789897	41	2m	APDC	0.0309	4.08	1.0	0.64
365776906	6	3a	L	1.3834	13.92	1.0	-0.25
365776906	32	3a	L	0.7687	14.89	1.0	0.14
367036276	15	2a	S	0.1165	15.42	1.0	0.0
367036276	41	2a	S	0.0932	10.67	1.0	0.38
367420555	17	sap	QPD	0.1083	10.0	0.34	1.26
367420555	18	sap	QPD	0.1188	11.36	0.23	1.24
367420555	24	sap	QPD	0.0539	10.87	0.41	1.13
367420555	25	sap	QPD	0.0807	10.42	0.5	1.18
369496705	11	2m	MPC	0.0482	6.21	0.99	-0.2
369496705	37	2m	MPC	0.0402	10.47	0.96	-0.12
369496705	38	2m	MPC	0.0765	6.81	0.89	-0.53
372070676	17	2a	APD	0.319	8.75	0.85	0.87
372070676	18	2a	S	0.0967	9.62	1.0	0.75
372070676	24	2a	SC	0.2533	6.52	1.0	0.54
377617067	17	2m	QPSC	0.0043	4.33	0.86	0.08
377617067	24	2m	QPSC	0.0042	14.0	1.0	-0.06
377893466	17	2m	MPC	0.0075	0.59	0.71	0.42
377893466	24	2m	MPC	0.0069	11.42	0.95	-0.03
385894679	14	sap	APD	0.1369	21.79	1.0	0.48
386040374	7	12m	QPS	0.0007	0.52	0.82	-0.06
386040374	34	12m	QPS	0.0012	1.04	0.56	0.02
387813185	16	4a	S	0.0159	4.33	1.0	-0.01
387813185	18	4a	S	0.0237	20.58	1.0	-0.29
387813185	24	4a	S	0.0227	4.31	0.83	0.15
387813185	25	4a	S	0.0183	34.88	1.0	-0.03
388143588	16	2m	MPC	0.0556	1.06	0.75	0.08
388143588	17	2m	MPC	0.0568	21.85	0.93	-0.08
388935225	32	pdc	B	0.0547	4.54	0.73	-0.35
390384783	10	2a	APDC	0.0968	17.1	1.0	0.5
390384783	11	sap	SC	0.0505	26.67	1.0	0.77
390384783	37	2a	APDC	0.2239	3.74	1.0	1.09

Table 2 *continued*

Table 2 *(continued)*

TIC id	Sector	Phot ap	Vartype	Amplitude	Timescale [d]	Q	M
390384783	38	2a	QPSC	0.1849	3.79	0.81	0.19
395172881	15	2m	MP	0.0134	0.04	0.36	0.1
395172881	16	2m	MP	0.012	0.04	0.28	0.05
396284614	40	8m	BC	0.0029	4.68	1.0	-0.31
396300742	17	2a	SC	1.3896	22.96	1.0	-0.09
396300742	18	2a	SC	1.8148	15.98	1.0	-1.14
396300742	24	2a	SC	1.3655	5.79	1.0	-0.46
401214336	16	pdc	MPC	0.0026	1.71	0.7	0.06
401214336	17	pdc	P	0.0037	1.7	0.38	-0.04
408081161	41	2m	APDC	0.0321	6.06	1.0	0.61
409323949	7	2a	QPS	0.884	1.91	0.64	-0.18
409323949	33	2a	QPS	0.2566	1.88	0.32	-0.12
409323949	34	2a	QPS	0.204	1.89	0.25	0.14
409406992	12	pld	EB	0.0439	2.36	0.06	1.1
409406992	39	pld	EB	0.052	2.36	0.06	1.27
410736126	18	8m	N	0.0038	3.68	0.78	0.35
410951921	12	1a	PC	0.0051	0.56	0.69	0.06
410951921	39	1a	PC	0.0058	0.56	0.46	0.03
412645923	16	sap	S	0.0113	16.83	1.0	-0.1
412645923	17	sap	S	0.0114	19.96	1.0	-0.05
420018149	17	sap	S	0.1546	32.96	1.0	-0.03
420018149	18	sap	S	0.1584	18.69	1.0	-0.41
420018149	24	sap	S	0.0966	11.83	1.0	-0.22
420307432	17	1m	QPSC	0.0087	16.44	0.95	-0.24
420307432	24	1m	QPSC	0.0096	25.77	0.92	-0.22
427352999	6	4a	APDC	0.0652	11.29	1.0	0.1
427352999	32	4a	SC	0.1069	17.36	0.92	0.72
427373765	6	3a	S	0.005	17.94	1.0	-0.33
427373765	32	3a	S	0.0061	11.62	1.0	0.09
427395300	32	pdc	MP	0.002	0.74	0.77	0.03
427395473	6	3a	QPD	0.0317	3.91	0.66	0.42
427395473	32	3a	APD	0.0497	3.79	0.62	0.32
427396230	6	2a	L	0.0783	32.29	1.0	-0.32
427396230	32	2a	SC	0.6767	16.48	1.0	-0.04
427577547	42	8m	MP	0.0126	5.07	0.94	-0.04
427577547	43	8m	MP	0.0129	9.14	0.73	0.01
427577547	44	8m	MP	0.0147	8.48	0.94	-0.03
427938329	16	8m	S	0.041	20.4	0.89	-0.03
428476066	17	sap	APD	0.292	7.25	1.0	1.23
428476066	18	sap	APD	0.2169	6.87	1.0	0.3

Table 2 *continued*

Table 2 *(continued)*

TIC id	Sector	Phot ap	Vartype	Amplitude	Timescale [d]	Q	M
428476066	24	sap	APD	0.3425	10.08	1.0	0.72
430006517	16	1a	APDC	0.1225	9.5	1.0	0.67
430006517	17	1a	APDC	0.222	7.35	0.54	0.58
434633379	17	2m	S	0.0346	21.92	1.0	0.18
434633379	18	2m	S	0.0376	10.42	1.0	-0.22
434633379	24	2m	S	0.0279	22.1	1.0	-0.06
434972921	17	8m	QPS	0.0075	0.08	0.84	-0.04
434972921	18	8m	QPSC	0.0092	17.1	0.88	0.09
434972921	24	8m	QPSC	0.0103	3.0	0.95	-0.06
436098606	6	2a	APDC	0.0218	11.65	1.0	0.45
437994564	6	2a	QPS	0.0468	1.94	0.54	-0.26
437994564	33	2a	QPS	0.0446	1.94	0.74	-0.05
437994564	43	2a	QPS	0.0589	1.94	0.67	-0.25
437994564	44	2a	QPS	0.065	1.92	0.63	-0.25
437994564	45	2a	QPS	0.0384	1.95	0.61	-0.26
441152806	4	sap	QPS	0.0028	2.58	0.67	0.28
441152806	31	sap	QPS	0.0035	2.55	0.51	-0.17
441744490	9	pld	QPS	0.0098	0.9	0.65	0.16
441744490	10	pld	QPS	0.0222	0.89	0.54	-0.04
441744490	36	pld	QPS	0.0347	0.9	0.79	-0.29
444356276	17	2m	QPSC	0.0164	7.83	0.94	-0.42
444356276	18	2m	QPSC	0.0233	14.21	0.98	0.03
444356276	24	2m	QPSC	0.0147	21.37	0.9	-0.26
445062554	6	pdc	QPSC	0.0076	3.01	0.66	0.01
445062554	33	pdc	QPSC	0.01	2.81	0.59	-0.26
449260863	32	pdc	QPS	0.0025	4.54	0.72	0.05
452035938	10	sap	MP	0.0071	0.55	0.58	0.06
452035938	37	sap	MP	0.0059	0.55	0.54	-0.14
452248316	41	2m	S	0.0829	26.05	1.0	-0.21
454215115	12	1a	B	0.0997	4.72	0.74	-0.31
454215115	38	1a	S	0.1796	13.07	0.97	-0.06
454215115	39	1a	B	0.1119	7.58	0.67	-0.31
454274408	12	8m	QPSC	0.0016	13.38	0.86	0.34
454274408	38	8m	N	0.0026	26.27	1.0	0.21
454274408	39	8m	QPSC	0.0032	6.25	0.61	0.4
454291762	11	3a	S	0.0357	27.25	1.0	0.51
454291762	12	3a	S	0.0256	14.79	1.0	0.39
454291762	38	3a	S	0.0125	3.47	0.68	0.43
454291762	39	3a	S	0.02	6.25	0.61	0.15
455573060	16	1a	N	0.0138	3.29	1.0	-0.01

Table 2 *continued*

Table 2 *(continued)*

TIC id	Sector	Phot ap	Vartype	Amplitude	Timescale [d]	Q	M
456030854	18	1a	S	0.4398	11.73	1.0	-0.26
456030854	24	1a	S	0.7016	20.67	1.0	0.72
457231768	6	sap	APDC	0.0542	17.96	1.0	0.45
457231768	32	sap	APDC	0.0489	13.68	0.86	0.66
459571845	36	1m	EB	0.0077	7.65	0.13	0.71
459571845	37	1m	EB	0.0055	7.65	0.26	0.6
459699513	10	8m	QPS	0.0037	1.52	0.43	0.06
459699513	36	8m	QPS	0.0032	1.51	0.54	-0.04
459699513	37	8m	QPS	0.0035	1.52	0.27	-0.11
459990291	6	pdc	MP	0.0014	4.9	1.0	-0.02
459990291	32	pdc	MP	0.0031	9.58	1.0	-0.02
460571412	10	eleanor	N	0.0025	11.71	1.0	0.14
460571412	11	eleanor	N	0.0066	2.29	1.0	0.31
460571412	36	eleanor	N	0.0049	13.2	1.0	0.03
460571412	37	eleanor	N	0.0062	4.08	1.0	-0.08
462436722	9	3a	S	0.0728	13.58	1.0	0.05
462436722	10	3a	S	0.0819	18.31	1.0	-0.25
462436722	36	3a	S	0.0815	4.72	0.79	-0.5
462436722	37	3a	S	0.0691	21.44	1.0	0.14
462878642	9	2a	S	0.0993	7.67	0.88	0.08
462878642	10	2a	S	0.1394	24.29	1.0	0.3
462878642	36	2a	S	0.159	5.18	0.93	-0.48
462878642	37	2a	S	0.1033	7.83	0.9	-0.25
463597276	12	8m	MPC	0.0073	6.54	0.89	0.27
463597276	39	8m	QMP	0.0094	5.81	0.88	-0.12
465196254	12	2a	S	0.1041	8.25	1.0	-0.28
465196254	39	2a	S	0.1456	13.47	1.0	0.14
465790701	11	1a	EB	0.0883	6.8	0.4	0.55
465790701	37	1a	EB	0.0487	6.8	0.18	0.62
465790701	38	1a	EB	0.049	6.8	0.33	0.46
467356861	17	3a	S	0.0653	17.5	1.0	0.22
467356861	18	3a	S	0.071	5.95	0.81	0.37
467356861	19	3a	APDC	0.0705	17.83	1.0	0.45
467356861	24	3a	APDC	0.0744	25.54	1.0	0.49
467356861	25	3a	L	0.0997	21.71	1.0	0.36
469534433	16	2a	P	0.0559	1.11	0.06	0.16
469534433	17	2a	P	0.0486	1.11	0.1	0.08
642035133	18	4a	SC	0.2452	19.38	1.0	0.41
709004859	6	2a	SC	0.0044	21.25	1.0	0.26
709004859	33	2a	N	0.006	25.42	1.0	0.09

Table 2 *continued*

Table 2 *(continued)*

TIC id	Sector	Phot ap	Vartype	Amplitude	Timescale [d]	Q	M
816058534	8	pdc	MPC	0.0105	0.38	0.48	0.06
816058534	9	pdc	MPC	0.0109	0.39	0.72	0.12
816058534	35	pdc	MPC	0.0108	1.47	0.89	-0.01
816058534	36	pdc	MPC	0.0101	0.39	0.83	0.02
1139218134	12	sap	QPS	0.0445	0.9	0.44	0.38
1139218134	39	sap	QPS	0.0404	0.91	0.42	0.29

NOTE—We provide here photometric data and variability metrics for each star and light curve derived from *TESS* FFI images in sectors 1–45. The information is listed separately for each sector, as shown in the second column. The "phot ap" code refers to the selected photometric method and aperture, and is defined as follows: "1m" and "2m" are 1-pixel and 2×2-pixel masks, respectively, centered on the target. "8m" and "12m" also employ masks, as determined by the collection of pixels eight and 12 standard deviations above the median flux level. Codes with "a" in them are circular apertures, with the number in front denoting the aperture radius. "SAP," "PDC," and "PLD" are as described in the text (§3). Variability types (column "vartype") are encoded following the descriptions in §4.1. Finally, the listed peak-to-peak normalized flux amplitudes, timescales, and Q/M values are derived as described in §4.

4. VARIABILITY ANALYSIS

Upon production and selection of *TESS* light curves for each target, we assessed variability behavior on a sector-by-sector basis. In general, a light curve was considered to be variable if its standard deviation exceeded the median photometric uncertainty, as determined by the chosen photometric pipeline.

4.1. *Variability categories*

The first step in variability analysis was visual classification, following the same comprehensive light curve morphology categories developed for CTTSs in our previous work (Cody et al. 2014).

In brief, we placed each light curve into one of nine categories according to the dominant behavior, or otherwise designated it as non-variable ("N" in Table 2). A light curve was considered periodic ("P") if it was comprised of a repeating trend with little change in shape or amplitude. If, instead, there were modulations in amplitude that repeated on longer timescales (i.e., a "beating" pattern), then we considered a light curve to be multiperiodic ("MP"). Light curves that only displayed a single dominant repetition timescale, but had significant variations in shape or amplitude were designated quasi-periodic symmetric ("QPS"). When a quasi-periodic pattern was present but predominantly as fading events, then we classified the behavior as quasi-periodic dipping ("QPD"). Likewise, if fading events were present but no pattern was discernable, we labeled it as aperiodic dipper ("APD"). Perfectly periodic light curves with fading events were exclusively classified as eclipsing binary systems ("EB"). For light curves dominated by brightening events (whether quasi-periodic or aperiodic), we used the burster classificaton ("B"). Variable behavior that favored neither bursting nor dipping but showed significant variations on timescales less than the 27-day sector duration was labeled stochastic ("S"). On the other hand, if a light curve displayed undulations but the dominant feature was a trend on timescales *longer* than the full sector, then we classified it as a long-timescale variable ("L").

Since light curve behavior may change over time, we classified light curves separately in each sector. In a number of cases, the variability type was difficult to select, particularly when a longer-term trend or noise-like features were present. When we were not confident in the classification, we still chose a type but appended a "C" for "candidate" to the end of the label. Variability morphology types are provided in Table 2 under the "vartype" column. These same classifications are used throughout the rest of this paper, e.g., to color code the plots in Figures 3–9 and 11. Typical examples of each type are also provided in Figure 2.

Taking the set of light curves that have well determined variability behavior (i.e., no "C" on the end in Table 2), we can obtain an approximate distribution of morphology types. For stars that were observed multiple times, we randomly selected a single sector for each, tabulating the variability type therein. We find the most common variability type is stochastic, comprising roughly 32% of the sample. The next most common type are the quasi-periodic variables, at ∼15%. Periodic and multi-periodic behavior makes up ∼5% and ∼13% of the sample, respectively, while long-timescale variables and aperiodic dippers are present at levels of ∼6% and ∼7%. Bursters make up ∼3% of the sample, while quasi-periodic dippers are the most rare at ∼2%.

4.2. *Statistical metrics*

To evaluate the behavior of the HAeBes in our sample on a more quantitative basis, we calculated several statistical metrics on each light curve. Since the distribution of available sectors varies across the stellar sample, we calculated the metrics independently for each sector.

The first metric is a version of peak-to-peak amplitude, which involves first determining the fifth and 95th percentile of normalized flux values. The difference between these two numbers is then calculated, and normalized by the median flux value.

Next, we calculated the metrics "Q" and "M" as described in Cody et al. (2014) and Cody & Hillenbrand (2018), again on a sector-by-sector basis. In brief, M is a measure of a light curve's tendency toward either fading ($M > 0.25$) or brightening ($M < -0.25$) events. It involves taking the difference of the median flux value and the mean of the tenth and 90th percentiles. This value is then normalized by the photometric noise level. M values close to zero indicate relatively symmetric light curves, for which neither fading nor brightening dominates.

The Q metric, on the other hand, provides a measure of a light curve's degree of periodicity. Periodic signals are drawn from an autocorrelation function and verified with a Fourier transform periodogram. Once a periodicity is found, the light curve is phased up, and the phased pattern subtracted from the original time series. Q is then the ratio of the residual variance to the original variance, after both have had the variance due to photometric noise subtracted off. This metric was designed such that perfectly periodic light curves attain $Q = 0$ while those with little periodicity have Q closer to 1 (i.e., subtracting off a phased pattern does not reduce variance much). In previous work with space-based monitoring facilities (e.g., Cody et al. 2014), we established an empirical cut-off between periodic and quasi-periodic at $Q = 0.15$. Upon cross-checking with visually-based variability classifications, this boundary value appears to remain suitable for the *TESS* data analyzed here. Likewise, the value $Q = 0.8$ separates well quasi-periodic and aperiodic behavior. Light curves for which no periodicity was detected are automatically assigned $Q = 1$. Additionally, if a long-timescale trend was suspected to be present, we fit it using a 15-day window filter and subtracted the result before computing Q and M.

For lower mass T Tauri stars, the diagnostic Q-M diagram has proven useful in demonstrating correlation between visual light curve morphology classifications and statistical behavior, for both space and ground-based time series photometry (Cody et al. 2014; Hillenbrand et al. 2022). The corresponding plot for our HAeBe sample is displayed in Figure 3, along with our previously established boundaries between different variability morphologies. In general, there is good correspondence between a light curve's position on this diagram and its visually assigned variability type (as indicated by color on the diagram). However, the parameter space is not nearly as well populated as is typical for lower-mass YSOs. In particular, we find a dearth of "dipper" and "burster" variables. Potential reasons for this finding are provided in §6.

4.3. *Timescales*

Timescale is another metric of interest for young variable stars, and it is easiest to quantify in the case of a clear periodicity. For light curves that are periodic or quasi-periodic (i.e., $Q < 0.8$), we directly adopt the dominant timescale that was identified in the autocorrelation function and periodogram analysis as part of computing Q. For light curves that do not show clear periods, there may still exist a characteristic timescale of stochasticity. In Cody et al. (2014) we developed a way to estimate this timescale, by first identifying all peaks differing by an amplitude threshold. For each such threshold, we calculate the median timescale separating the peaks. We then plot the sequence of timescales against changing amplitude threshold. The largest amplitude difference is similar to the full amplitude of the light curve. We adopt the characteristic timescale as being the one that corresponds to an amplitude difference that is 70% of this. For aperiodic light curves, the resulting timescales are presented in Table 2, alongside the aforementioned peak-to-peak amplitudes and Q-M metrics. We assess these measures of variability in the context of (circum-)stellar properties in §5.

In addition, a plot of variability amplitude versus timescale is shown in the top of Figure 4. Here, points correspond to individual sectors, so stars may appear multiple times in the plot. We find that periodic and multi-periodic light curves (assumed to be associated with cool spot modulation and/or pulsation) dominate the low-amplitude space over the entire range of timescales. Quasi-periodic sources cover a narrower

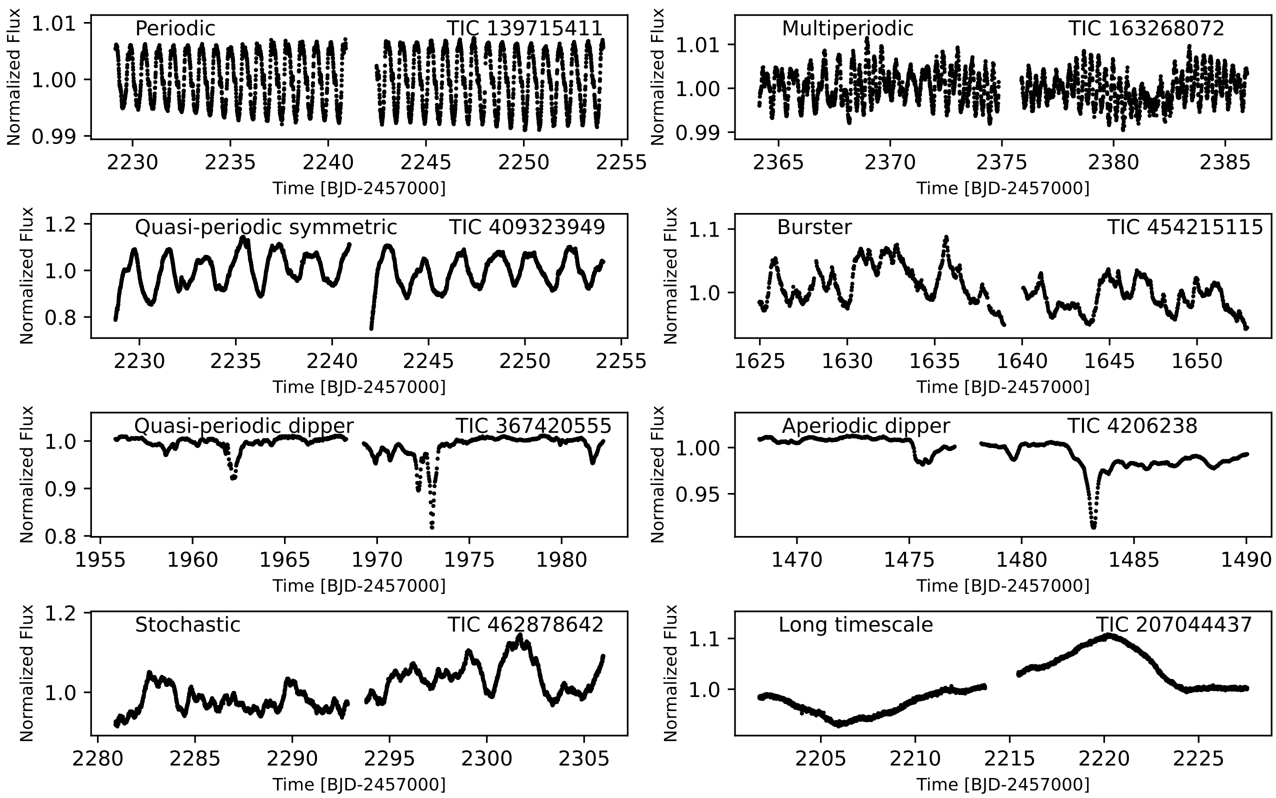

Figure 2. Representative examples of light curve morphology types from our Herbig Ae/Be sample observed by *TESS*. We omit eclipsing binaries and non-variable objects.

range, from primarily half a day to a few days duration. Longer timescales are associated with dippers, bursters, stochastic variables and, not surprisingly, the long-timescale variables. Bursters have moderate amplitudes in single sectors, from 1–10%, while other forms of disk or accretion-dominated variables fluctuate from 1% to over 100%.

At the bottom of Figure 4 are analogous data for low-mass classical T Tauri stars in Taurus, ρ Ophiuchus, and the Upper Scorpius association, presented in Cody & Hillenbrand (2018) and Cody et al. (2022). Several features stand out in the comparison of this plot with that of the HAeBes. First, the Herbig Ae/Be star sample extends to much lower timescale and amplitude for the periodic, multiperiodic, and some quasi-periodic stars. This is likely a combination of pulsation (particularly for the multiperiodic objects) and potentially short-timescale rotational modulation of spot patterns (see §6.2). The pulsation instability strip crosses the H-R diagram at intermediate masses, and hence the presence of short-timescale oscillations among HAeBes but not CTTS is not surprising.

The photometric precision of *TESS* light curves is generally similar to or slightly less than that of the *K2* light curves. There, the extension of Herbig Ae/Be stars toward short timescale should not be biased by the data quality. At longer timescales, the CTTS appear to better populate the diagram, but this is a consequence of the total time baseline of photoemtric monitoring, which was close to 90 days for the *K2* mission-derived light curves. In contrast, timescales for HAeBes were based on the 27-day extent of available *TESS* sectors, and hence cannot extend much beyond that.

Within the range of timescales probed by both datasets, we do see a shift in the dippers toward longer timescales. Whereas for the CTTS, both quasi-periodic and aperiodic dipper light curves are present with timescales of less than ∼3 days, this is rare among HAeBe light curves. A logical explanation is the larger dust sublimation radii at play (see Figure 8) and correspondingly longer orbital timescales associated with circumstellar material that may occult the central star.

4.4. *Multi-sector variability*

While we computed variability metrics only on single-sector light curves, additional information lies in longer timescale data for stars that were observed over multiple *TESS* sectors. Due to the difficulty in stitching together different sectors and calibrating the relative photometric zero point, we do not consider amplitudes on these

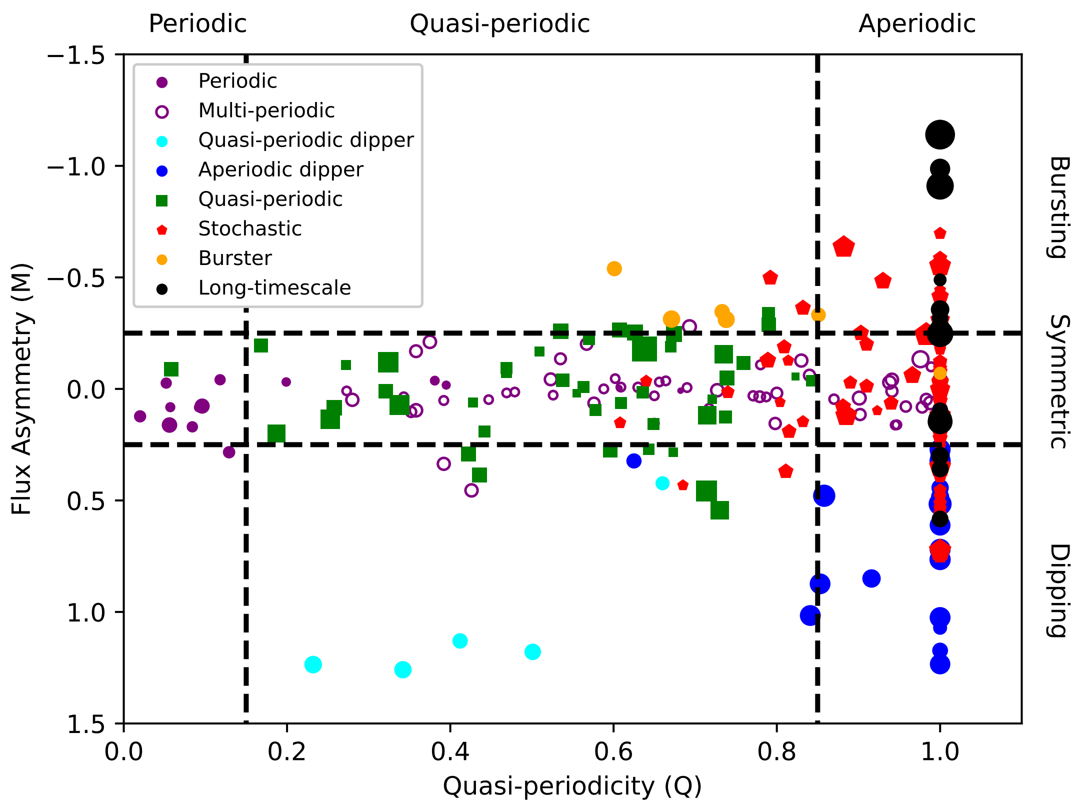

Figure 3. Q-M diagram for the portion of the Herbig Ae/Be star sample with more certain variable types, as shown by the color coding. Point size represents a scaling of variability amplitude to the one third power. Data for objects with more than one sector of data appear as multiple points in this plot. The pile-up of points at $Q = 1$ illustrates the sequence of objects with no discernible period.

longer timescales. However, we can assess changes in light curve morphology.

Considering the sample of stars with well-defined variability types (i.e., not preceded by a "C" in Table 2), 81 display the same morphological classification across multiple sectors, while 13 changed behaviors (the remaining 94 stars have either a single sector or some uncertainty in variability type). The total durations under consideration here range from 78 days (two sectors) to two years (39 sectors).

Among the most notable changes in behavior, TIC 11199521 switches from clearly variable at the 200% level in sector 6, to non-variable in sector 32, some 700 days later. Interestingly, the total flux that we measure in the same TESS aperture increases about 50% over this timespan. In addition, TIC 200511734 appears to have developed a short-timescale periodicity (∼31 minutes) between sector 6 and 32. However, the observing cadence changed from 30 minutes to 10 minutes in that timespan, so the short period may have simply been impossible to detect in the earlier sector.

TIC 280773136 appears as a burster in sector 11, but is classified as a dipper in sectors 37, 38 (i.e., two years later). The flux level from sector 11 to 37 decreases about 4%, and remains stable into sector 38. While not considered as part of this dataset, a check of sectors available two years later reveals a potential reversion to bursting in sector 64, and then two prominent dips in sector 65. Finally, TIC 125641610 is stochastic in sector 7, but changes to a more steady long-term increase with higher amplitudes in sector 33 (timespan again about two years). Light curves for both TIC 11199521 and TIC 280773136 are shown as examples in Figure 5.

5. VARIABILITY AS RELATED TO (CIRCUM-)STELLAR PROPERTIES

5.1. *Correlations with stellar parameters*

We retrieved masses, luminosities, accretion rates, disk properties, and their uncertainties from the HArchiBe. One way to assess variability in the context of stellar properties is via the Hertzsprung-Russell diagram. We present one version of this, color coded by

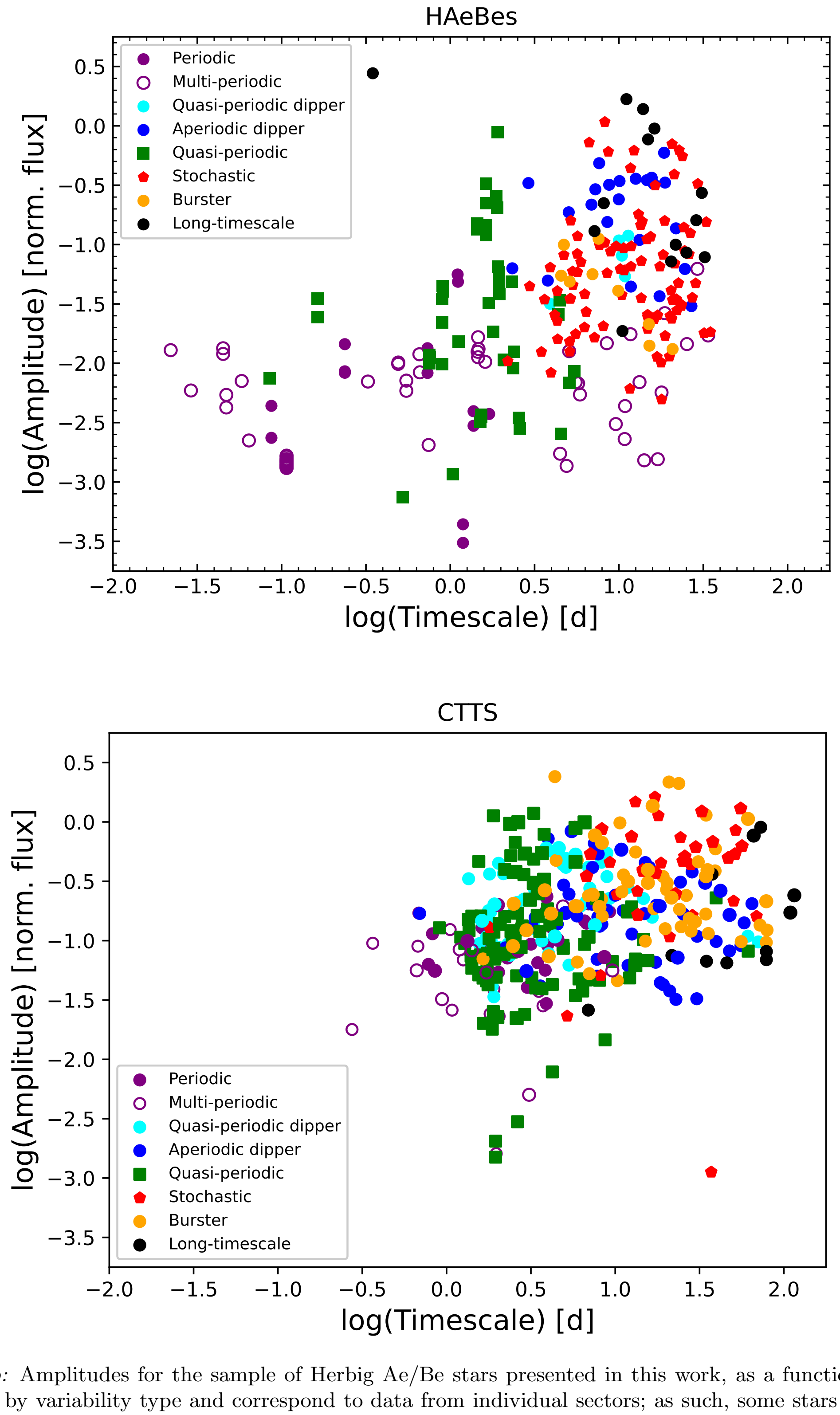

Figure 4. *Top:* Amplitudes for the sample of Herbig Ae/Be stars presented in this work, as a function of timescale. Points are color-coded by variability type and correspond to data from individual sectors; as such, some stars appear multiple times. *Bottom:* We show the sample quantities, but for the low-mass T Tauri stars from Cody & Hillenbrand (2018) and Cody et al. (2022).

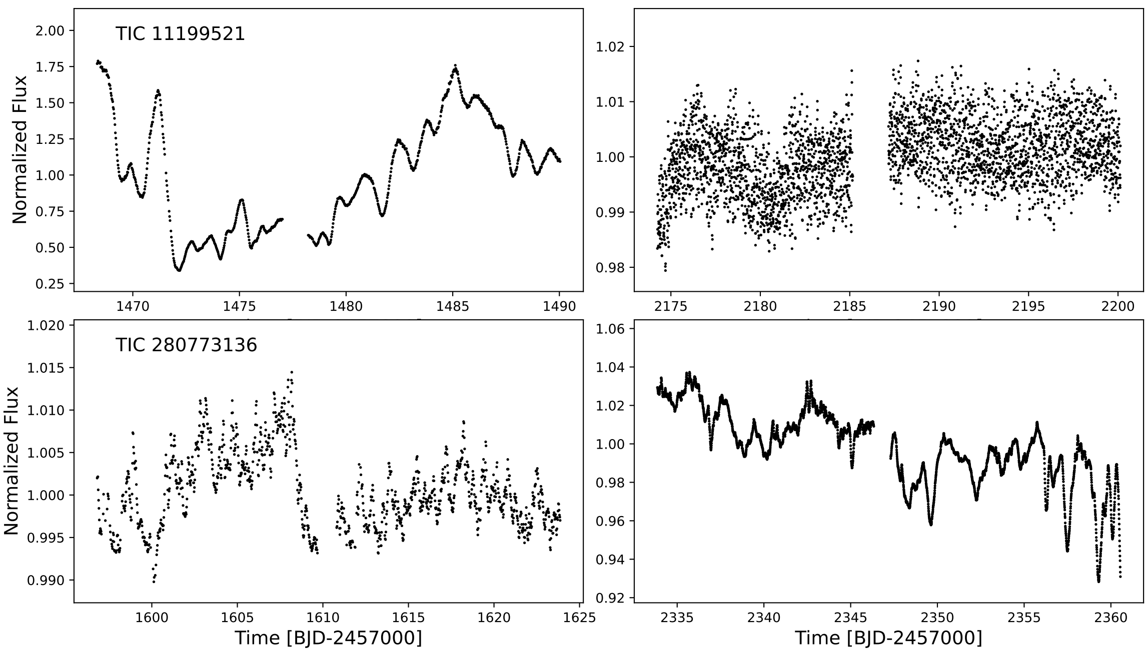

Figure 5. Light curves for two stars with pronounced changes in variability morphology and amplitude over a couple years. While relatively rare, these cases highlight the possibility that HAeBe variability drivers may shift dramatically on relatively short astronomical timescales.

variability type, in Figure 6. Mass tracks and isochrones are included, based on PARSEC V2.0 stellar models (Nguyen et al. 2022; Costa et al. 2025). Stars that change variability morphology or have unclear types are included in gray, while those with stable behavior across all available TESS sectors are shown in color.

Several features stand out on this H-R diagram. First, the few dipper stars in the sample are confined to effective temperatures less than about 10,000 K. The only stable quasi-periodic dipper (TIC 287840183, otherwise known as BF Ori) is even cooler at 8,750 K. Thus the dipper phenomenon appears to be mass-dependent, at least on the roughly month timescales under consideration here. We suspect this is directly related to the increasing orbital periods of inner disk dust around hotter stars (see §6.1 for more discussion).

With one exception, the non-variable stars are also confined in effective temperature, to $T_{\rm eff}$ <14000 K. On the other hand, multi-periodic, stochastic, and quasi-periodic sources span the entire mass/temperature range. The same goes for objects with unstable and/or unknown variability types. Mass dependencies for bursters or periodic stars are less clear due to small number statistics.

To further explore trends with stellar parameters, we also plot the median variability amplitude across available sectors (peak-to-peak normalized flux, in log space) versus mass in Figure 7. Again, points are color coded by variability type; objects with uncertain or changing light curve morphology are again shown in gray. Where multiple *TESS* sectors were available, we show the median of all amplitudes for each object. In addition to the confinement of various variability types as mentioned above, there is at first glance a gradual decline in amplitude with mass. However, this is likely an effect of the sample size being lower for stars over 10 $M_\odot$.

The predominant variable types at high mass are quasi-periodic (QPS) and stochastic types. A distinct jump in the typical amplitude of QPS variability appears around 10 $M_\odot$. Stochastic stars, on the other hand do not exhibit a statistically significant change in amplitude with mass.

5.2. *Correlations with accretion and the inner disk*

To test associations of variability with circumstellar properties, we consider the accretion rates and inner disk dust radii estimated by Guzmán-Díaz et al. (2021) for stars in the sample. The dust radius, $R_{\rm in}$, corresponds to the location in the spectral energy distribution where an infrared excess begins, while accretion rate was derived based on empirical relations between accretion luminosity and stellar luminosity (Wichittanakom et al. 2020). These quantities are plotted in Fig. 8 according to variability type and amplitude. There is a correlation in accretion rate and inner disk dust radius, which is due to the connection of both quantities to the stellar mass. However, there are a number of outliers from this general trend. These outliers all have lower estimated accretion rates than expected for their relatively large radii ($R_{\rm in} > 2$ AU). Furthermore, all of these outliers have some level of periodicity, suggestive of either starspot modulation at the stellar rotation period or pulsation at shorter periods. Our interpretation of this phenomenon is that in cases for which the accretion rate is low relative to the dust destruction radius (and correspondingly, stellar mass/luminosity), accretion-related stochastic variability is no longer present in time series photometry, at least on the roughly month sector timescales available from *TESS* monitoring. This may happen if, e.g., the inner disk has been cleared out well beyond the point of dust sublimation.

To probe further connections between variability and inner disk size, we calculate the Keplerian orbital period associated with the estimated inner disk dust radius ($R_{\rm in}$; see §5.2), from the SED analysis of Guzmán-Díaz et al. (2021), and for stars where they provide mass estimates. In some cases, it is consistent with sublimation, whereas for others it lies farther out. We plot the associated period against the variability timescales determined in §4.3 in Figure 9. It is clear that the vast majority of the variability timescales are much shorter than the expected orbital period of the inner disk. The exceptions are mainly dippers, for which the two timescales are similar. This is not surprising, as the leading theory for explaining dipper variability is occultation of the central star by material at the inner disk edge. Remaining variability types involve fluctuations on shorter timescales, suggesting that they originate either at the stellar surface (e.g., starspots) or in the circumstellar gas accreting through an inner disk hole.

For many stars in our sample, the HArchiBe also provides classifications of inner disks via spectral energy distribution (SED) analysis, in terms of the wavelength where the infrared excess begins. As discussed in Guzmán-Díaz et al. (2021), SEDs are tagged with a J, H, Ks, or $> Ks$, after the band associated with that wavelength. Excesses starting at Ks band or redward are considered to reflect "transitional" disk status, with those systems having inner dust cavities. To check whether variability behavior correlates with the status of inner disk dust, we show in Fig. 10 the breakdown of light curve morphology type with the so-called JHK category. We find that the majority of variabil-

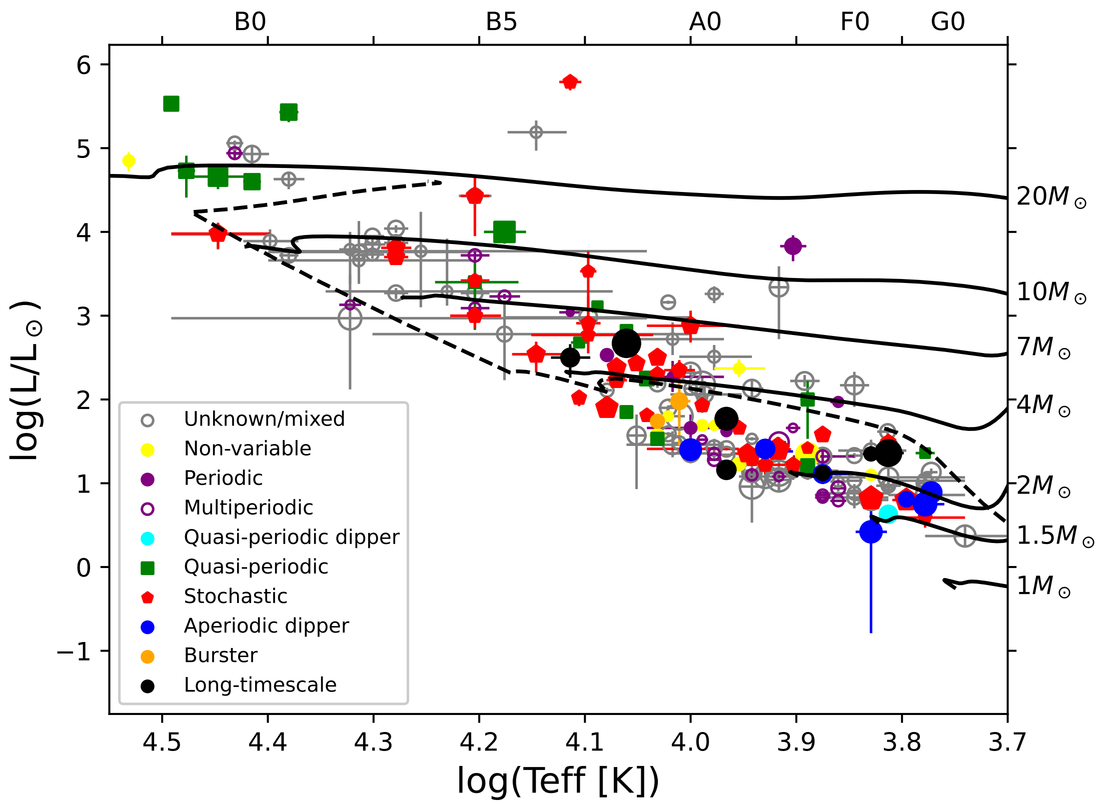

Figure 6. Hertzsprung-Russell diagram for the sample, color coded by variability type. We display theoretical solar metallicity mass tracks (solid black curves) as well as a 2 Myr isochrone from Nguyen et al. (2022) and Costa et al. (2025). Spectral types are shown at the top, based on effective temperatures of stars in the HarchiBe sample. Point size represents a scaling of variability amplitude to the one third power.

ity types have infrared excesses beginning at or close to the J band, indicating relatively small inner disk holes. This is somewhat expected, as the majority (89/188) of the stars in our *TESS* dataset have excesses starting here. The periodic and multi-periodic variables stand out as exceptions, with roughly equal distributions of JHK types. This suggests that starspot modulation and pulsation are easier to observe when the disk rim lies farther out from the central star. However, the small total number of such sources makes this result a tentative one. We find that none of the variability types are dominated by infrared excesses that are exclusively long-wavelength (">Ks"). In particular, several of the classes (bursters, dippers, long-timescale variables) are completely devoid of such transitional disks.

In addition to disk types via spectral energy distributions, we can search for connections between HAeBe variability and circumstellar properties via a 2MASS color-color diagram. In Fig. 11, we display the sequence of $(J-H)_0$ versus $(H-K_S)_0$ after correcting for extinction using the A_V values reported in the HarchiBe and the wavelength dependence of Cardelli et al. (1989) for $R_V = 3.1$. The locus of HAeBes defined by Hernández et al. (2005) is shown as a dashed quadrilateral. We find that the majority of the highly variable stars (in terms of amplitude) lie within the HAeBe locus, predominantly with redder colors than that of an extincted A or B dwarf. Several light curve types, including the aperiodic dippers and bursters, appear exclusively within this region. In contrast, a number of stars with periodic or quasi-periodic patterns appear on the bluer area of the diagram, which may be more consistent with contamination by main sequence classical Be stars (Hernández et al. 2005).

6. DISCUSSION

6.1. *A paucity of dipper variables*

As mentioned in §4.3, there is a lack of dipper variables in our sample, relative to previously observed populations of CTTS. This finding applies to both the quasi-periodic and aperiodic types. Among the former, TIC 367420555 (BO Cep) is perhaps the most prominent. With a spectral type of F3, it is on the border be-

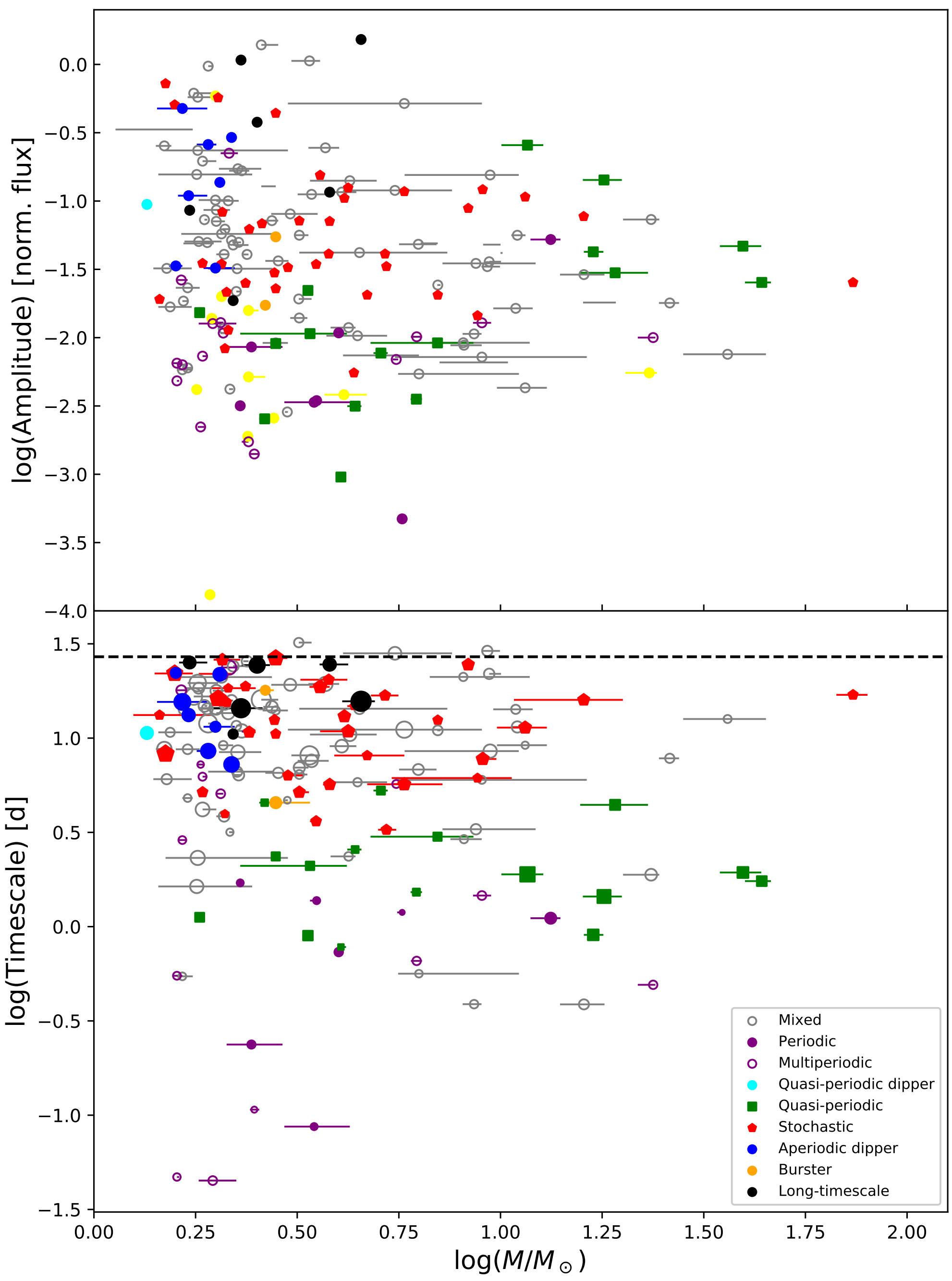

Figure 7. At top, we plot amplitudes of variability versus mass, color coded by variability type. The amplitude values are taken as medians across available sectors. In the bottom panel, timescales of variability are shown versus mass, sized by amplitude to the one-third power. Amplitude and timescale values are taken as medians across available sectors. The TESS 27-day sector duration is shown as a dashed horizontal line.

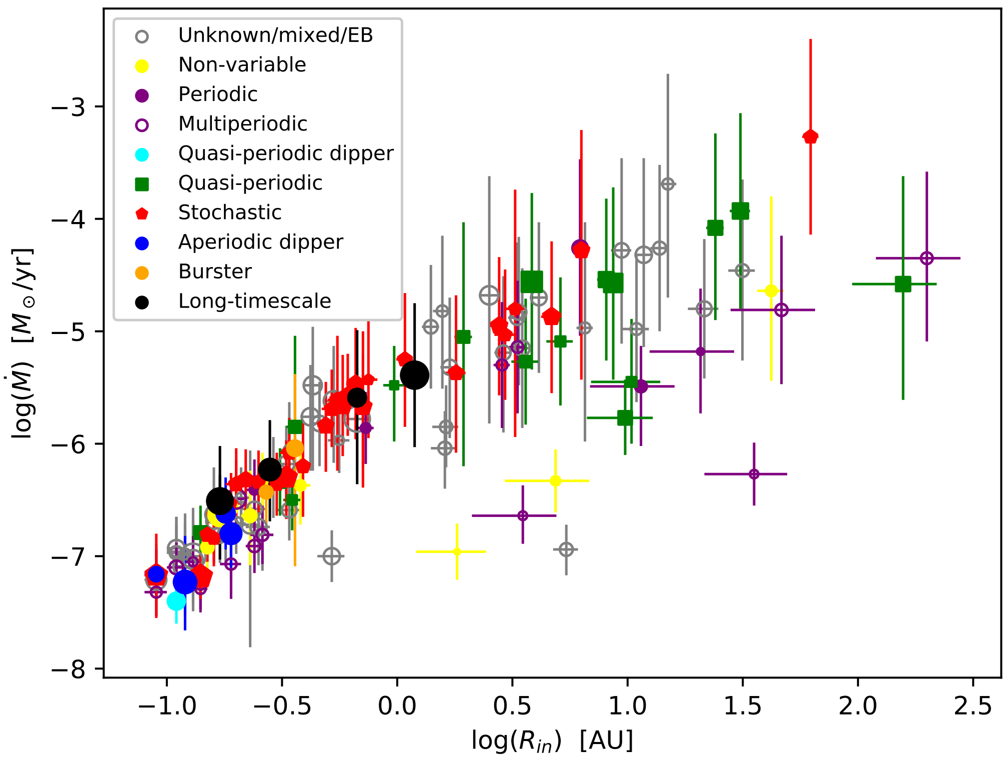

Figure 8. Accretion rate versus estimated inner disk dust radius, color coded by variability type, as in Fig. 7. Point size scales with the amplitude of variability to the one-third power.

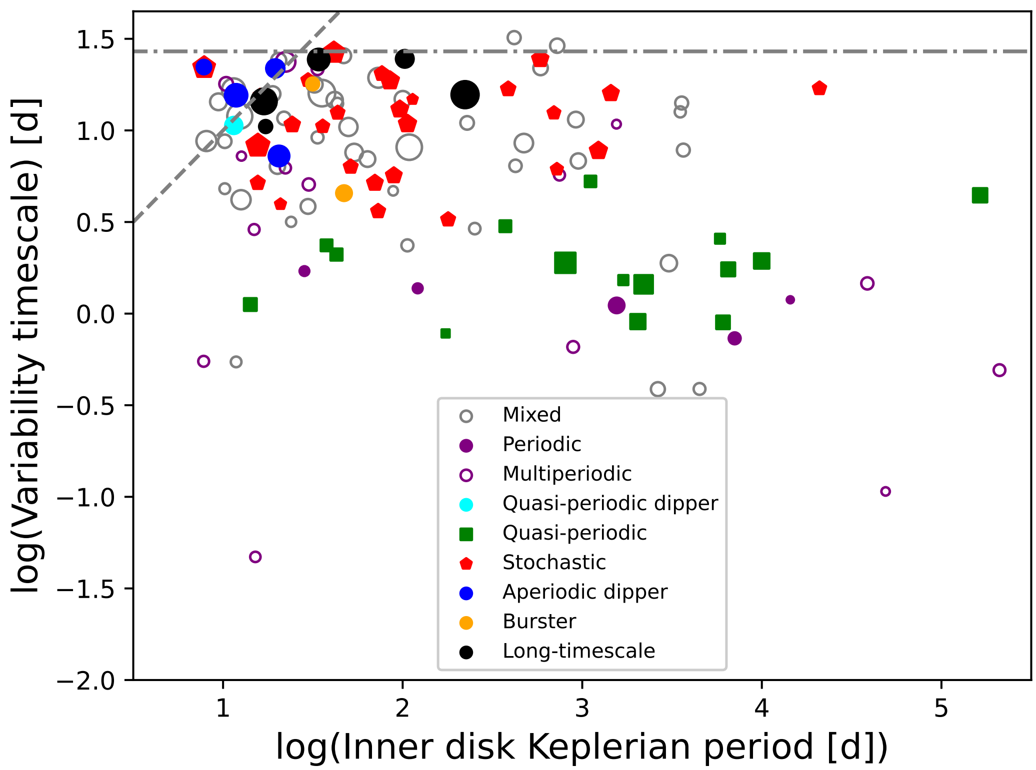

Figure 9. Keplerian orbital period of the inner dust disk versus variability timescale, scaled and color coded by variability type, as in Fig. 8. Non-variable objects and unknown types are excluded since they do not have a well-definied variability timescale. Eclipsing binaries are also omitted. The gray dot-dashed line indicates the duration of a single *TESS* sector, while the dashed line indicates equality of the two timescales. We find that the vast majority of Herbig Ae/Be star variability observed here is dominated by timescales shorter than the inner disk orbital period.

tween the HAeBes and lower mass CTTS. Poxon (2015) found it to be a UX Orionis star ("UXor"), and earlier, Gürtler et al. (1999) found a period of 10.7 d. This is consistent with the timescales that we have derived, in the 10.0-11.4 d range, depending on sector. The only other quasi-periodic variable is TIC 427395473 (NV Ori) in sector 6. This star likewise has an F spectral type (F0-F2). TIC 287840183 (BF Ori) remains a candidate quasi-periodic dipper in the early A spectral type range.

There are a handful more aperiodic dippers and candidates, as listed under the "APD" category in Table 2. These include TIC 261539498 (spectral type A8), TIC 280773136 (A0-A1), TIC 285920558 (F1-F4), TIC 312493387 (A3), TIC 335623526 (G0), TIC 339989392 (F7-G5), TIC 358901633 (F), TIC 372070676 (F1-F4), TIC 385894679 (A3-A4), TIC 4206238 (F5-F8), TIC 427395473 (F0-F2), and TIC 428476066 (B9). What stands out about this subset is that more than half have spectral types of G or F. This is in stark contrast to the overall distribution shown in Fig. 1, for which only 15% of our sample falls at these types.

A simple explanation for these findings is that, as proposed by others (Bouvier et al. 2003; Bodman et al. 2017, and references therein), dipper variability is caused by inner disk dust warps or other structures occulting the central star along the line of sight. Higher mass stars have larger dust sublimation radii, and hence the minimum inner disk Keplerian orbital period (assumed equivalent to timescale of quasi-periodic dippers) eventually becomes longer than the *TESS* single sector observing duration for stars hotter than a late F spectral type (see Venuti et al. 2021). Where inner disk radius estimates are available, this conclusion is borne out by the data in Fig. 9. Here, the dashed line shows that most of the dipper variables have variability timescales similar to the inner disk Keplerian period.

Aperiodic dippers are slightly more challenging to explain, but may be associated with dusty material at or beyond the inner disk edge. For higher mass stars, single-sector *TESS* observations could encompass a sin-

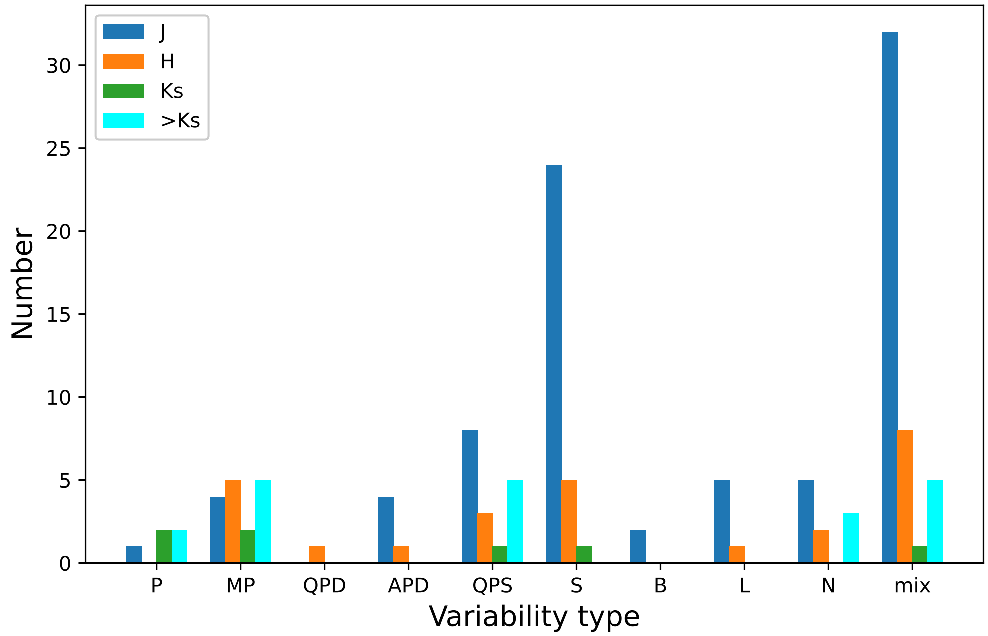

Figure 10. Histogram of disk SED types, according to Guzmán-Díaz et al. (2021). In brief, the J/H/Ks label is an indication of the shortest wavelength at which an infrared excess appears. These types are broken down by variability class, as shown in the labels.

gle occultation event, but would be increasingly unlikely to do so for the larger sublimation radii, if just one or two inner disk warps were responsible for such occultations. Overall, the picture of both quasi-periodic and aperiodic dippers is consistent with variability arising from stuctures at or just beyond the dust sublimation radius. It explains why the UXor variables, many of which have timescales of weeks to months (The 1994; Herbst & Shevchenko 1999), would only be identified in photometric observing campaigns with durations longer than the *TESS* sectors analyzed here.

6.2. *The meaning of periodic modulations*

Sinusoidal variability in young stars is typically attributed to starspots (either chemically peculiar or lower in temperature relative to the surrounding photosphere), which is in turn thought to originate in magnetic activity. It is estimated that 7% of HAeBes are magnetic (Hubrig et al. 2019, and reference therein), but the origin of such fields remain controversial due to the lack of a convective envelope. They may be fossil relics of an earlier convective phase (Donati & Landstreet 2009), or the result of mergers (Ferrario et al. 2009) or representative of a dynamo generated by sub-surface turbulence (Boehm & Catala 1995). In the pre-main sequence cluster NGC 2264, Fossati et al. (2014) identified a connection between sinusoidal photometric modulations and large-scale magnetic fields (∼400 G) in two early B-type stars. However, they could not pinpoint the origin of the observed fields. Given that we have also detected a handful of periodic stars among our Herbig sample, it is natural to ask whether their variability may also be the result of magnetic effects.

The two most prominent periodic HAeBe stars with *TESS* light curves are TIC 469534433 (AS 470) and TIC 139715411 (HD 59319). The light curve of TIC 469534433 displays clear sinusoidal modulations with a period of 1.1 days and normalized flux semi-amplitude of ∼0.025 in *TESS* sectors 16 and 17. It is categorized as an A4–A7 star in Guzmán-Díaz et al. (2021), but its listed mass of 13.3 $M_\odot$ is at odds with that. Based on the spectral type range, we suspect that the mass is closer to 2–4 $M_\odot$ (i.e., in line with the data on other stars in the HArchiBe). Of additional concern, the light curve of TIC 469534433 (TESS magnitude 11.5) is blended with neighboring star TIC 469534429 (magnitude 13.1). No literature information is available on this neighbor, but if it were at the same distance, it would be ∼23% of the brightness of our Herbig target. If brightness variations originate here, then the semi-amplitude would instead be 13%. Thus without higher resolution observations, we cannot rule out that these modulations are caused by spots on a lower mass neighbor.

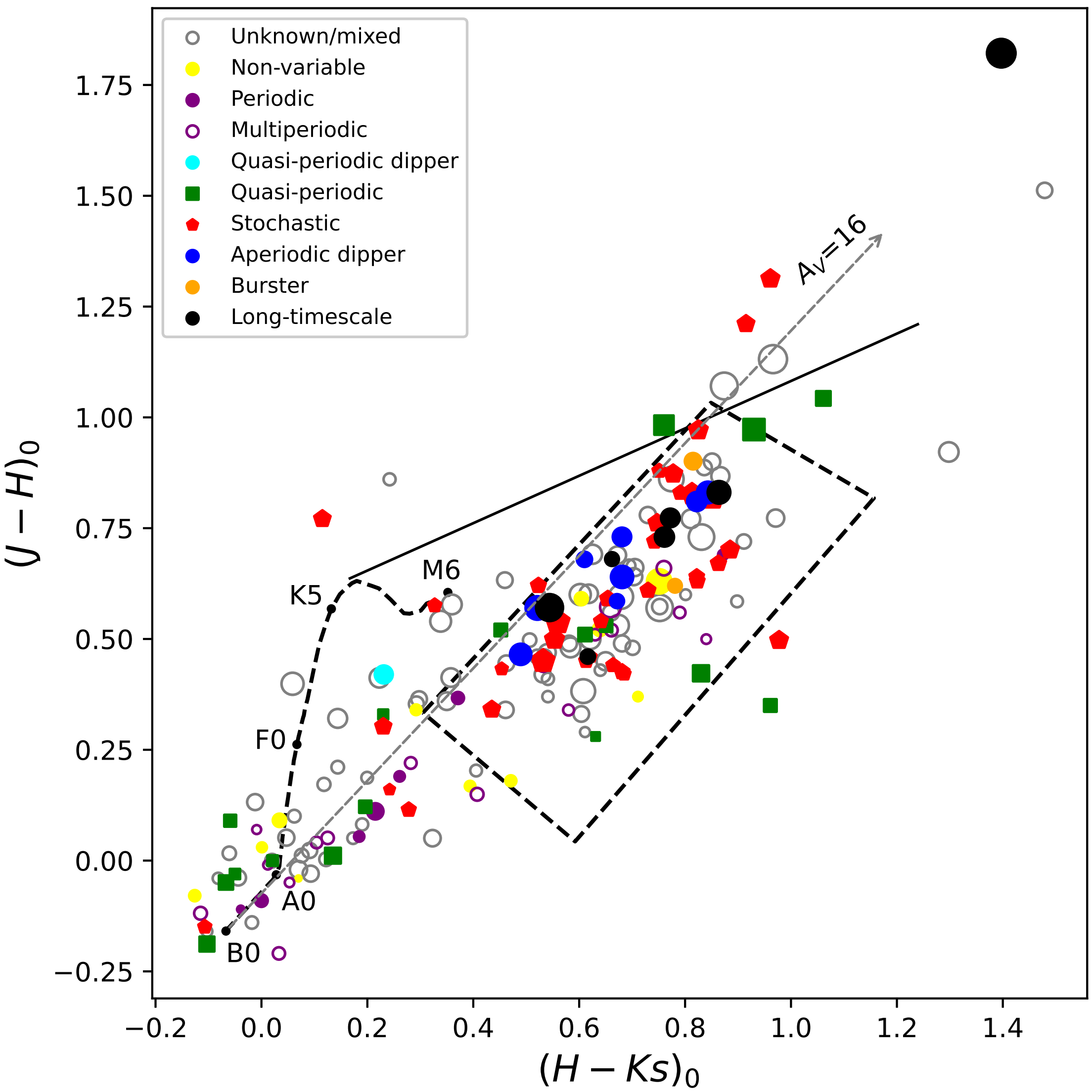

Figure 11. Dereddened $J-H$ versus $H-Ks$ for our sources. The dashed quadrilateral region indicates the locus of HAeBes defined by Hernández et al. (2005). The corresponding locus for CTTS (Meyer et al. 1997) is shown as a solid line, while the sequence of dwarf stars from Pecaut & Mamajek (2013) is included as a dashed curve. A gray dashed vector marks the colors of an extincted B0 dwarf with various values of A_V up to 16. All colors have been transformed to the 2MASS system.

Our second periodic star, TIC 139715411, is of spectral type B7–B8 and TESS magnitude 8.4. All other stars in the photometric aperture are at minimum five magnitudes fainter. We conclude that the ∼0.5% sinusoidal photometric fluctuations in the light curve of TIC 139715411 are from this star. The period is 0.73 days, and no additional signals other than harmonics appear in the periodogram. The variability is thus consistent with stellar spot modulation. With an estimated radius of 4.26 $R_\odot$, the associated equatorial rotational velocity would be 295 km s^{-1}. In an analysis of $v \sin i$ distributions, Alecian et al. (2013) found that magnetic Herbig Ae/Be stars tend to rotate slower (<100 km s^{-1}) on average than their non-magnetic counterparts (up to 350 km s^{-1}). If the variability of TIC 139715411 is magnetic in origin, then it is in tension with their finding. Follow-up studies of this object would be beneficial, as we find no prior information on magnetic field status.

Additional stars in the periodic category are TIC 199757113 (sectors 6 and 32), TIC 336518731 (sectors 11, 12, and 38), TIC 302824830 (sectors 43 and 44), and TIC 341984965 (sectors 16 and 17). However, the first was previously classified as a delta Scuti pulsator (Marconi et al. 2000). The latter three have relatively low amplitudes and are listed as blends in Table 1, so we cannot be confident that the signals are coming from these Herbig Ae/Be stars themselves.

One may also ask the question of whether magnetic field hosting stars necessarily show spot-dominated variability. There is a correlation for main sequence A- and B-type stars (i.e., an association of magnetism with chemical peculiarities), but the same pattern has not been borne out on the pre-main sequence (Folsom et al. 2012).

We can test this idea for the few stars in our sample reported to host significant magnetic fields: TIC 388935225 (V380 Ori; Alecian et al. 2007), TIC 427395300 (LP Ori; Alecian et al. (2013)), and TIC 254387071 (HD 139614; Hubrig et al. (2004)). An additional potential magnetic star, TIC 387813185 (HD 200775), is discounted since it has been found to be a spectroscopic binary, with the magnetic field *not* originating in the disk-bearing Herbig B3 component (Benisty et al. 2013). The A7-A9 star TIC 254387071 has both a 450 G longitudinal magnetic field strength (Hubrig et al. 2004) and multiperiodic variability in two sectors of *TESS* data. However, the very short dominant period of ∼1.2 h in our light curves is more suggestive of a pulsation mechanism than starspots. For the remaining two objects (each with one sector available), the variability that we observe is definitively aperiodic; TIC 388935225 shows bursting behavior, while the pattern for TIC 427395300 is tentatively stochastic. Furthermore, the star TIC 320547523 (HD 101412) was previously detected as having chemical spots (presumably of magnetic origin), modulating the light at a stellar rotation period of 13.86 d (Hubrig et al. 2010). We do not detect variability in any of the *TESS* light curves available for this HAeBe.

Thus while a small portion of our sample is known to host magnetic fields, and overall, approximately 7% (i.e., ∼13 magnetic stars of the 188) is expected, the fraction that appears spotted in our available *TESS* light curves is much smaller. It is possible that a number of our targets do host spots, but the associated variability is drowned out by accretion effects. Alternatively, magnetic fields may not necessarily generate spots at these early stages of stellar evolution. At the very least, we expect that spectroscopic and spectropolarimetric studies of the two relatively unusual periodic stars TIC 469534433 and TIC 139715411 could illuminate whether their variability may be attributed to large-scale magnetic fields.

6.3. *Timescales of variability*

In this study, we are somewhat limited to the 27-day timescales of each *TESS* sector, although we have assessed variability morphology changes over longer periods where multiple sectors are available. In contrast, previous photometric monitoring studies have covered over a decade, albeit with much sparser time sampling. Previous work (e.g., Herbst & Shevchenko 1999) has suggested that HAeBe variability timescales are longer than those observed for CTTS. We do not recover this finding, although it is potentially due to the aforementioned *TESS* sector baseline. In Figure 7, we see divisions between different light curve morphology types, with the periodic, multiperiodic, and quasiperiodic variables at the short end (sub-hour to a few days). This is likely a reflection of stellar rotation and pulsation periods. The stochastic, burster, and dipper variables span a larger range of timescales from several days to nearly a month. Not surprisingly, the long-timescale variables are at the upper end of this range.

To understand the distribution of timescales, we have plotted the inner dust disk Keplerian orbital period in Fig. 9. Apart from the few dippers, most of the variability that we observe in individual *TESS* sectors is significantly faster than this orbital timescale (but again limited by our observing duration). We suspected that the physical drivers here are not only stellar rotation and pulsation, but also short-timescale fluctuations in the accretion flow well within the disk sublimation radius. In Fig. 4, we see similar behavior among the bursters and stochastic sources when comparing the HAeBes monitored here against CTTS previously observed with the *K2* mission. Thus, on day to month timescales, there is no appreciable evidence for a change in variability properties in going from CTTS (e.g., GKM spectral types) to HAeBes. As discussed below, however, there may be a transition at higher masses.

6.4. *Mass dependence of variability*

There is previous evidence for a transition in variability behavior, and associated accretion dynamics, in the B spectral type range (e.g., Fairlamb et al. 2015). In a study undertaken with Gaia DR2 data, Vioque et al. (2018) found ∼25% of HAeBes to be variable at at least the 0.5-magnitude level on a 22-month timescale. They noted lower amplitudes for stars of mass greater than 7 $M_{\odot}$.

To look for a similar transition in our own dataset, we have plotted normalized variability amplitude versus stellar mass compiled from Guzmán-Díaz et al. (2021) in Figure 7. Among the stars with definitive and stable variability morphologies, we see that dipper stars are confined to a mass range less than 2.2 $M_{\odot}$, bursters have $M < 2.8\ M_{\odot}$, and the long-timescale variables do not exceed masses of 4.5 $M_{\odot}$. Likewise, periodic behavior only persists up to 5.7 $M_\odot$, with the exception of TIC 469534433, which may have an erroneously high mass as discussed above in §6.2. We therefore split the sample into two mass regimes, with a boundary at ∼6–7 $M_\odot$.

Of the stars reportedly more massive than 6 $M_\odot$, there are a number that either change variability types across the sectors or could not be confidently classified ("C" types in Table 2). These objects are represented by gray circles in Figure 7). In taking a closer look at this set, we find that none of the variability classes in any sector are dippers ("QPD" or "APD" in Table 2), bursters, or candidates thereof ("CAPD" or "CQPD"). In addition, only one object (TIC 125641610) in this putative higher mass set shows long-timescale variability, but its listed mass of 9.43 $M_\odot$ may be too high given the A4–A6 spectral type.

In terms of amplitudes, there is a distinct jump at 7 $M_\odot$ for the quasi-periodic symmetric variables (i.e., green in Figure 7), with values exclusively less than 1% for the lower-mass stars and values exclusively greater than 2% for higher mass stars. The stochastic variables, on the other hand, span the 7 $M_\odot$ boundary, and no clear amplitude trends are visible.

Our conclusion from this analysis is that dipper, burster, periodic, or long-timescale variability in HAeBes appears to be limited to relatively lower masses, at least when considered on timescales shorter than one month. Based on the disappearance of these variability types at higher masses and the jump in amplitude of quasi-periodic sources around 7 $M_\odot$, we concur that there is evidence for a change in accretion and/or inner disk structure at this mass boundary, which corresponds to early or mid-B spectral types.

7. CONCLUSIONS

With the high photometric precision and continuous mnonitoring of the *TESS* mission, we found that a large fraction (roughly 95% according to Table 2) of Herbig Ae/Be stars are variable on timescales of hours to months. Overall, this is an increase over the proportion of HAeBes identified as "strongly" variable ($\gtrsim$ 50%) in longer term studies (∼ 25% Vioque et al. 2018). Part of this difference can be attributed to *TESS's* sensitivity to low-amplitude variability down to 0.1%.

To assign variability categories to the Herbig star sample, we employed the same classification scheme as developed by Cody et al. (2014) for lower mass young disk-bearing stars. Many of the stars were readily classifiable by eye, although roughly 40% presented challenges due to longer timescale or more unusual behavior (i.e., those marked with "C" in front of the variability type Table 2). For light curves that were confidently classified, the Q-M diagram (Fig. 3) offered insights into differences in variability subtype prevalence among HAeBes versus CTTS. The most prominent change was a paucity of dipper stars at higher masses. We explained this by invoking the larger radius to which dust sublimination extends around hotter stars. With our extensive 188-star sample we also identified tentative mass dependences for the burster, periodic, and long-timescale subsets of HAeBe variables, uncovering further evidence for a change in the accretion structure of young stars beyond 7 $M_\odot$.

TESS observed many stars in our HAeBe sample over multiple sectors, offering a window into the longer term photometric behavior of these stars. Among the stars with clear variability subtype, 86% displayed the same light curve morphology in all available sectors. While the timescales in question vary from star to star, this result points to a tendency toward consistency over months to years.

In general, connecting variability to circumstellar properties is a challenge, with no clear correlations appearing in light curve morphology versus near-infrared colors (as shown in Fig. 11). The majority of disks in the HAeBe sample appear with excesses starting in the J band, particularly for bursters, dippers, and long-timescale variables. Periodic and multi-periodic variables, on the other hand, are associated with relatively higher numbers of H and K-band excesses. This is reminiscent of the division between classical and weak-lined T Tauri stars, the latter of which have low or no detectable accretion and tend to display periodic behavior associated with the stellar surface.

Finally, we speculated on the origin of periodicities observed in several Herbig Ae/Be stars observed with *TESS*. In particular, we identified two targets with single photometric periods that are most consistent with spot modulation. Such behavior is unusual among the A and B spectral type, and warrants follow-up to determine whether spots are indeed present, and if so, whether they are generated by large-scale magnetic fields.

We thank the referee for helpful comments. This work was supported by the National Aeronautics and Space Administration (NASA) under grants No. 80NSSC18K0141 and 80NSSC19K0670 issued through the TESS Guest Observer Program, as well as NASA SMD grant No. 80NSSC21K2077. This research made use of Lightkurve, a Python package for Kepler and TESS data analysis (Lightkurve Collaboration et al. 2018).

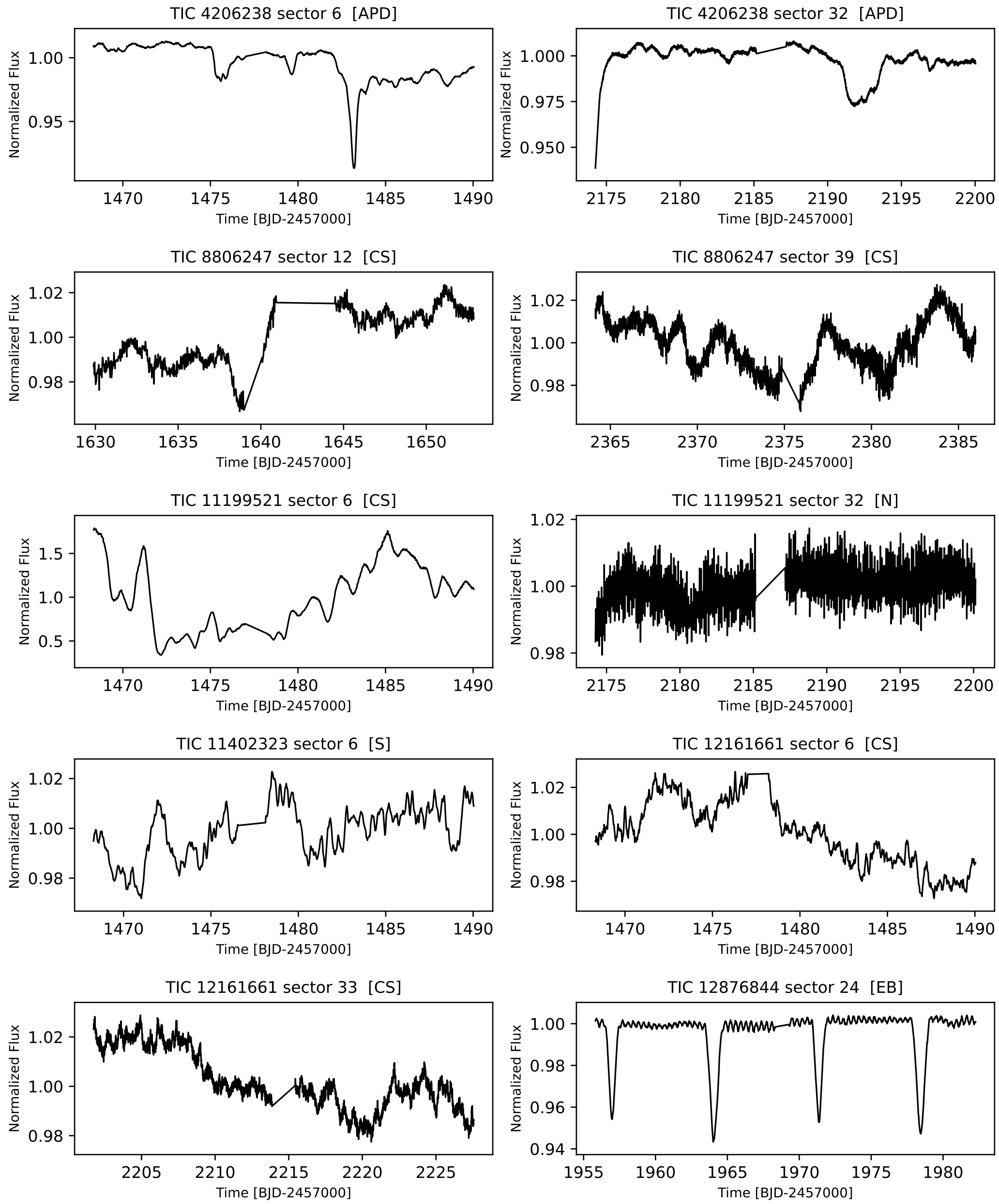

Figure 12. Median-normalized light curves of intermediate-mass stars observed with *TESS*, in order of TIC identifier. Figure labels include in brackets the variability type from Table 2, namely "P" = strictly periodic behavior, "MP" = multiple distinct periods, "QPD" = quasi-periodic dippers, "QPS" = quasi-periodic symmetric, "APD" = aperiodic dippers, "B" = bursters, "S" = stochastic stars, "L" = long-timescale behavior that doesn't fall into the other categories. The complete figure set is available in the online journal.

Facilities: TESS

Software: Matplotlib (Hunter 2007), NumPy (Harris et al. 2020), astrocut (Brasseur et al. 2019), lightkurve (Lightkurve Collaboration et al. 2018)

APPENDIX

We plot here the *TESS* light curves created for each target from sectors 1–45.

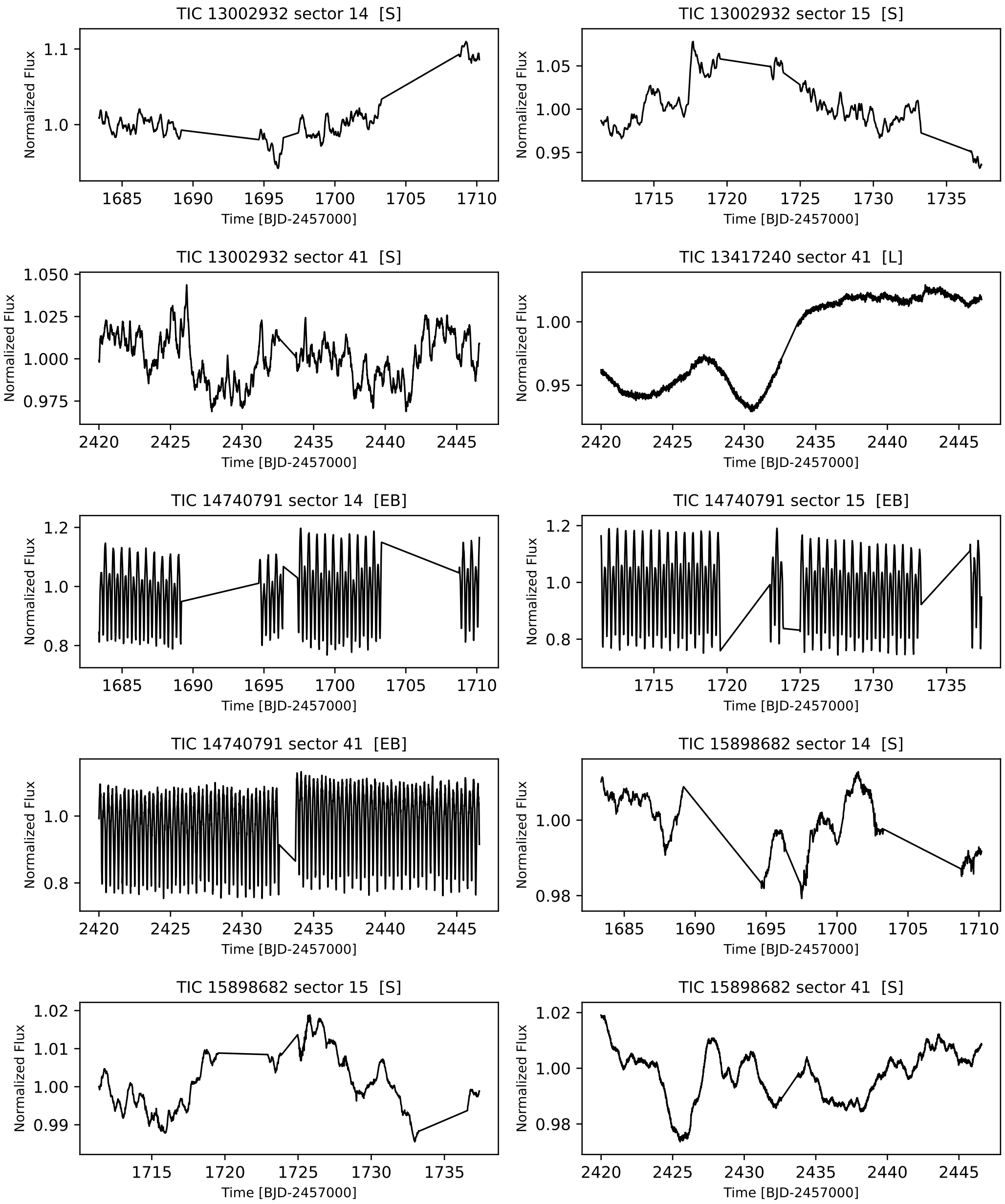

Figure 12. Cont.

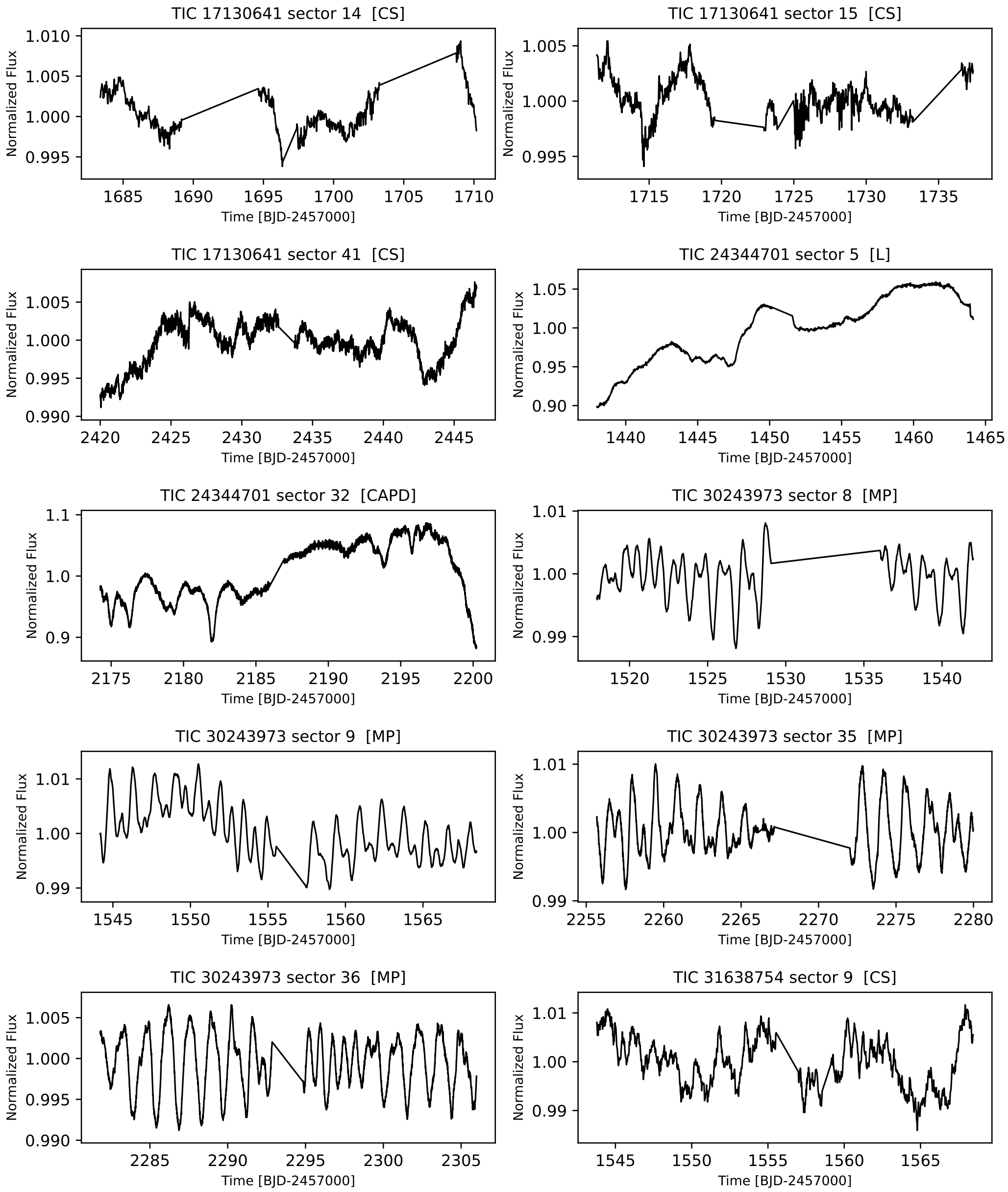

Figure 12. Cont.

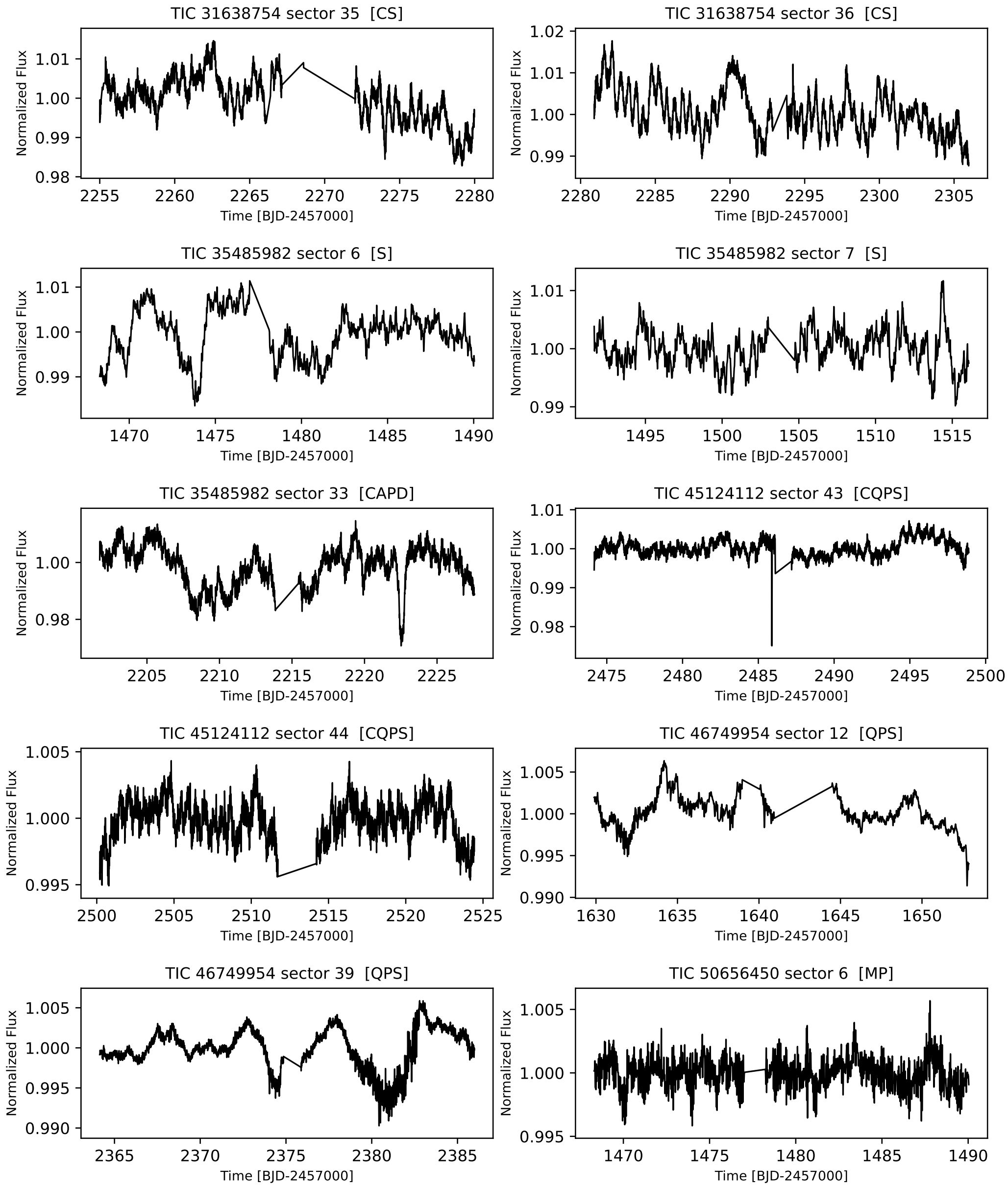

Figure 12. Cont.

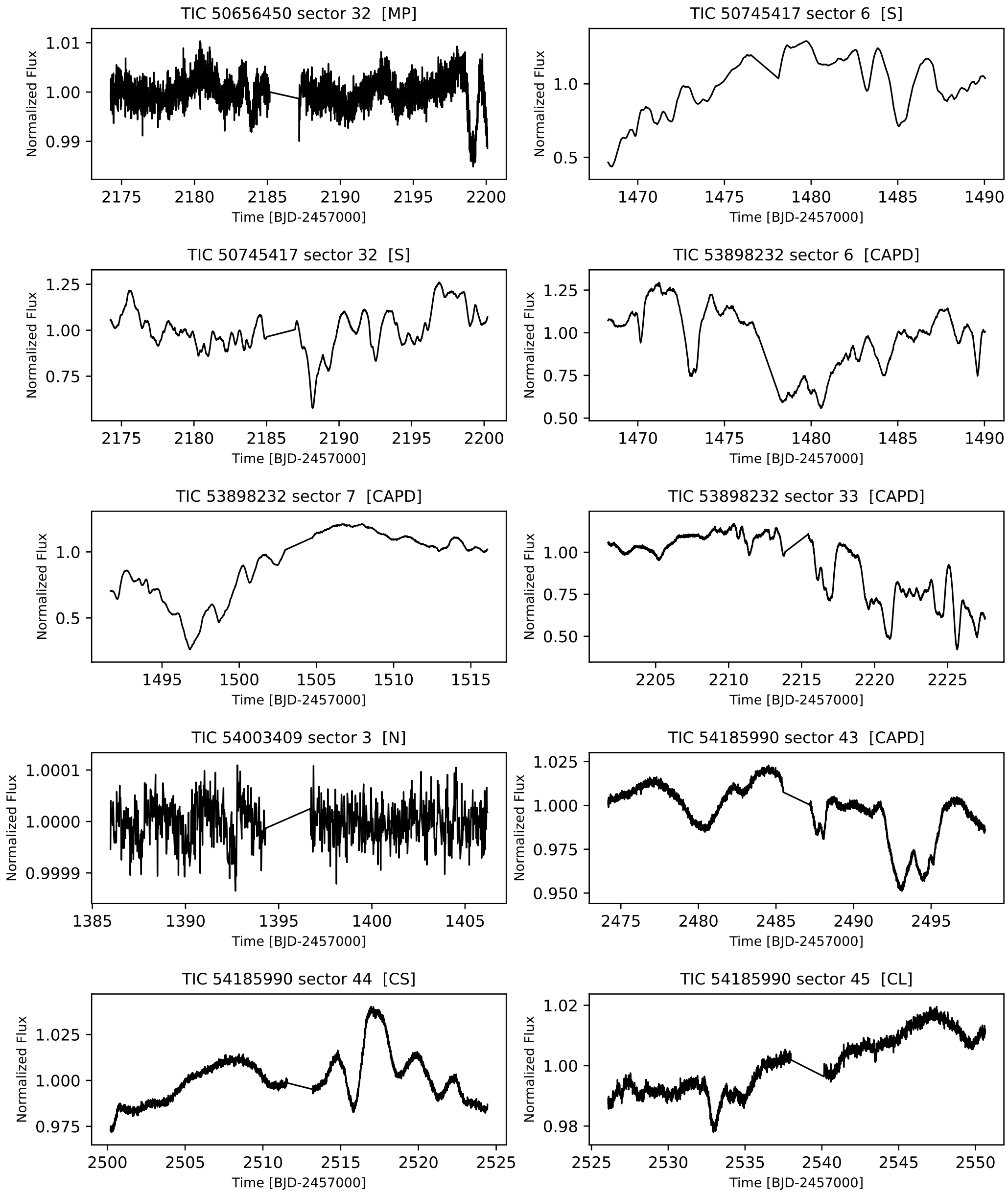

Figure 12. Cont.

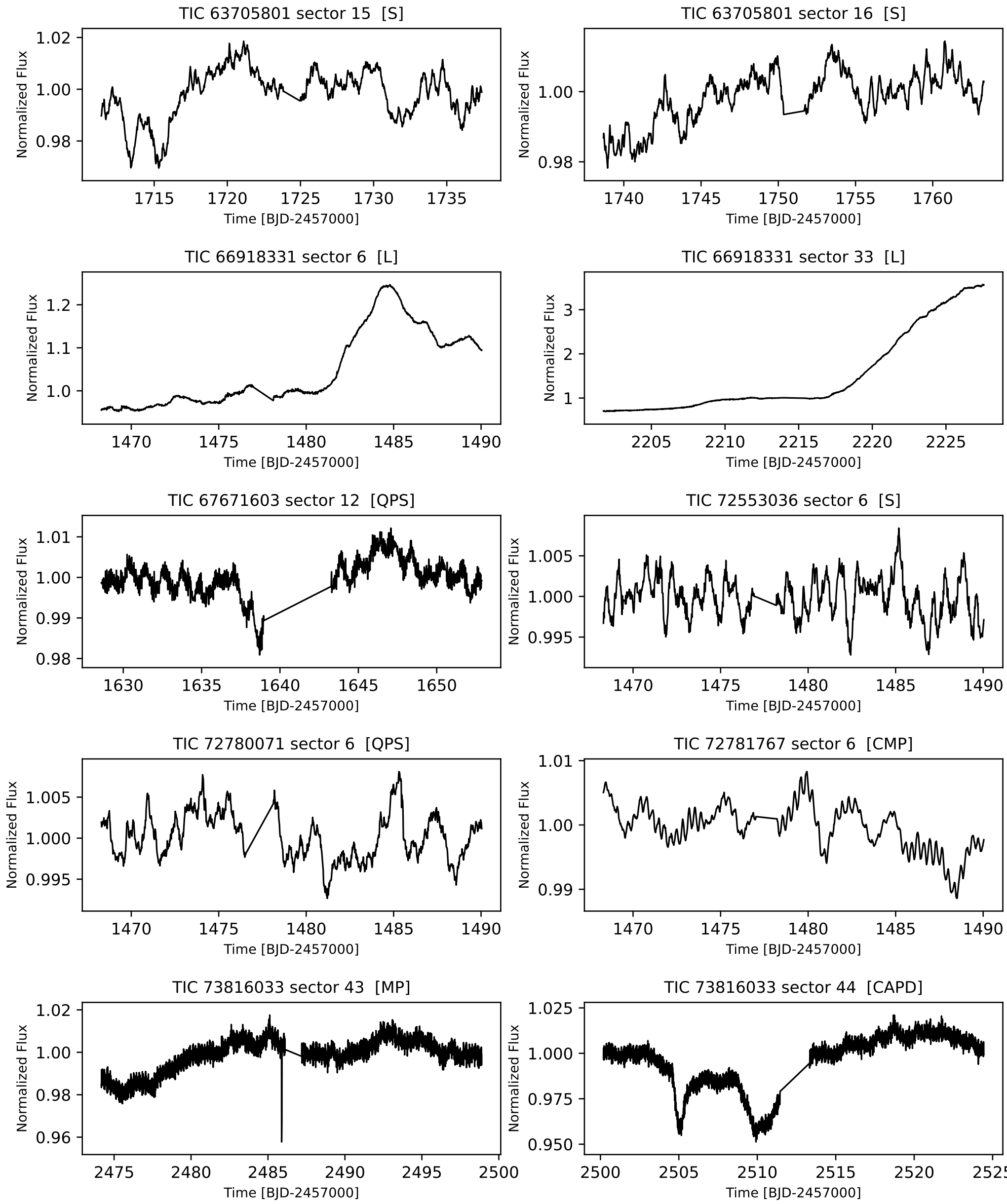

Figure 12. Cont.

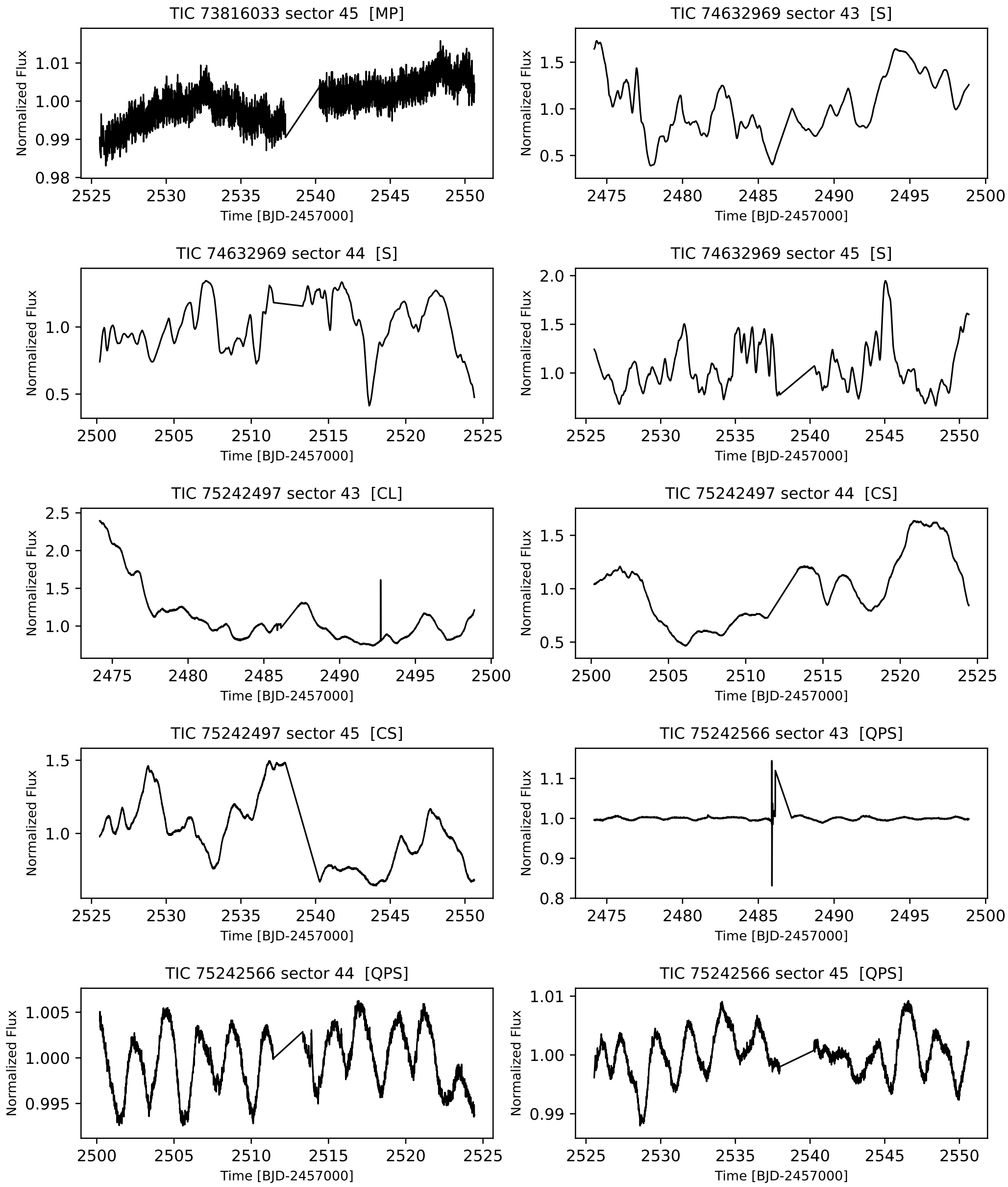

Figure 12. Cont.

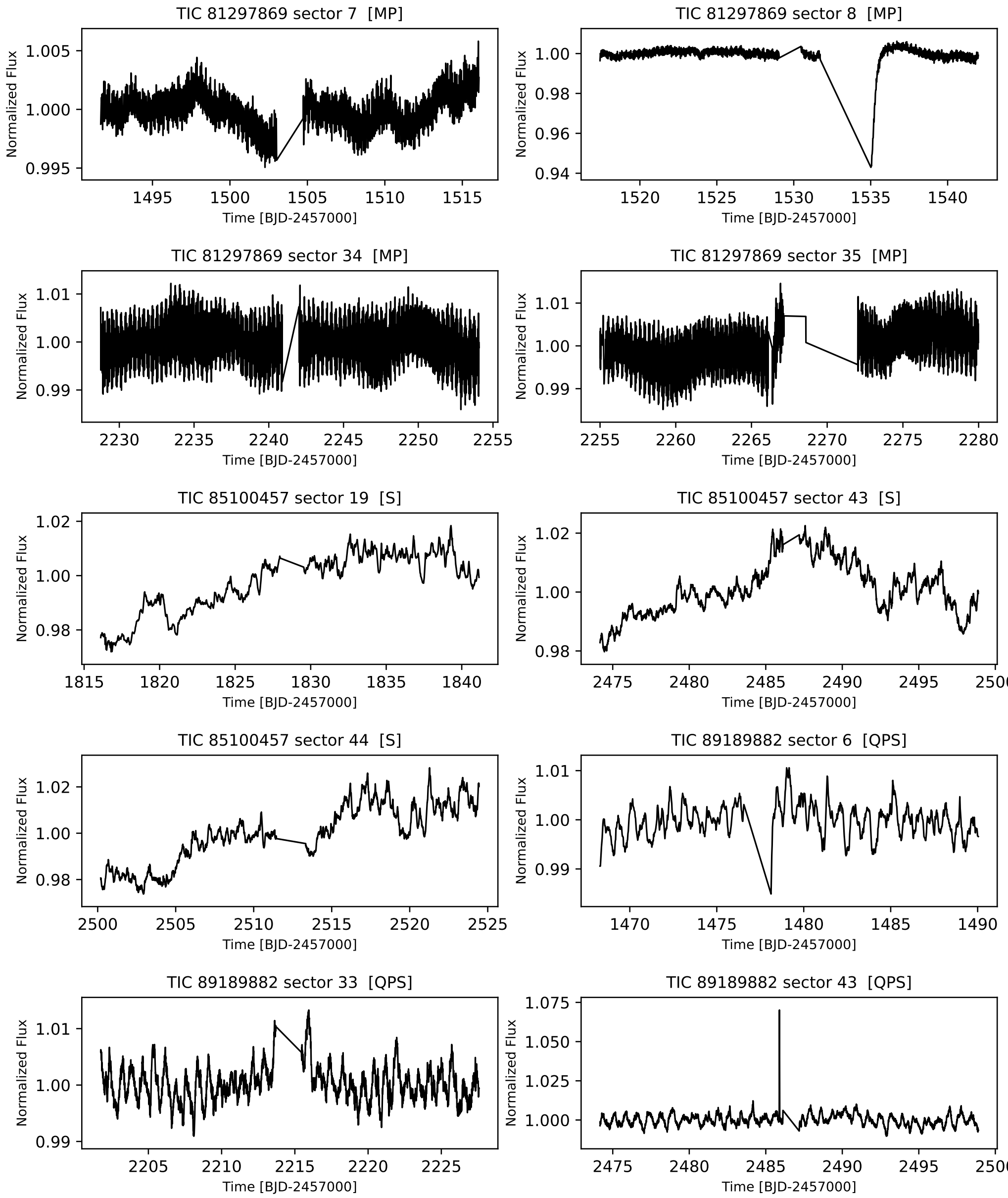

Figure 12. Cont.

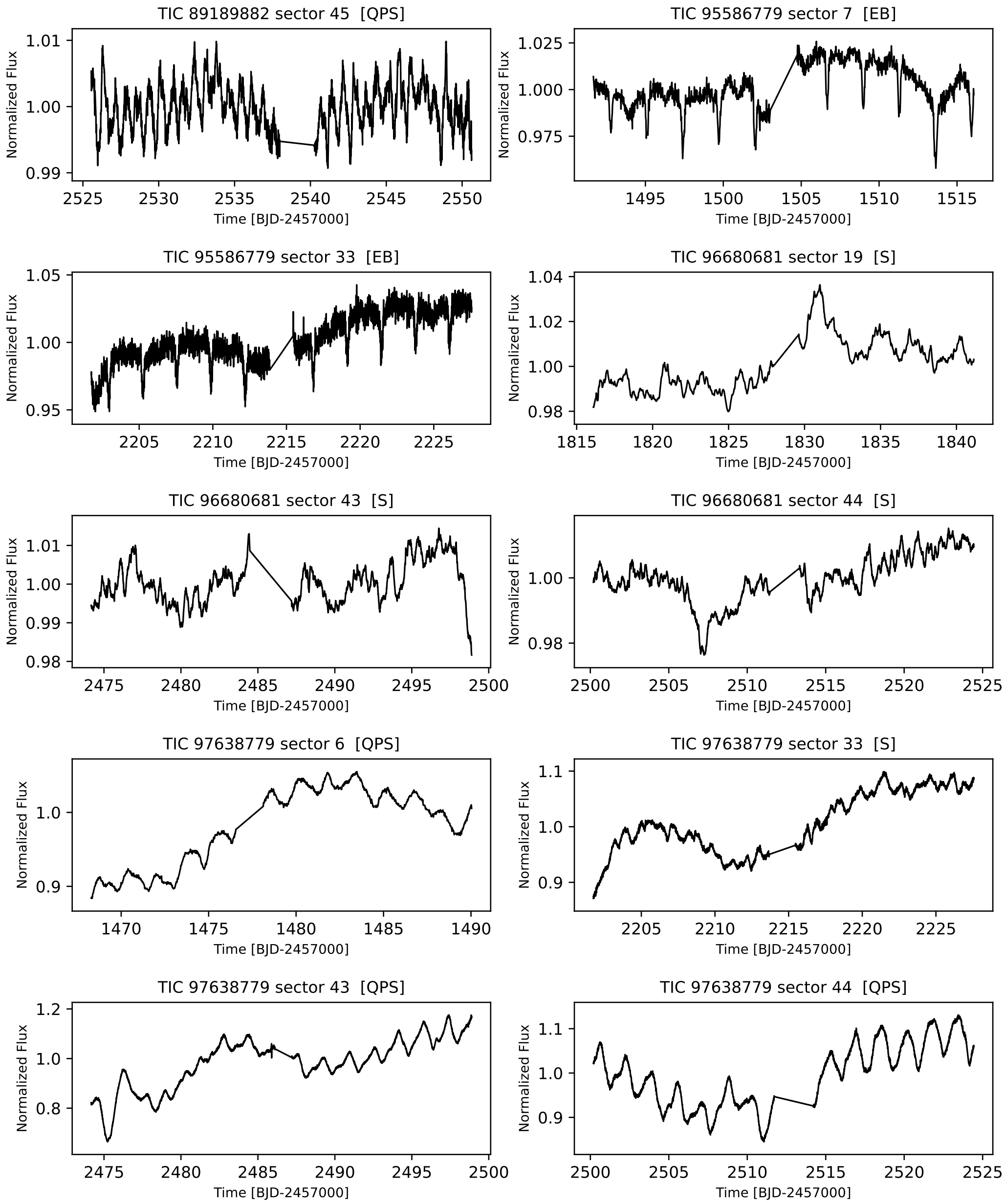

Figure 12. Cont.

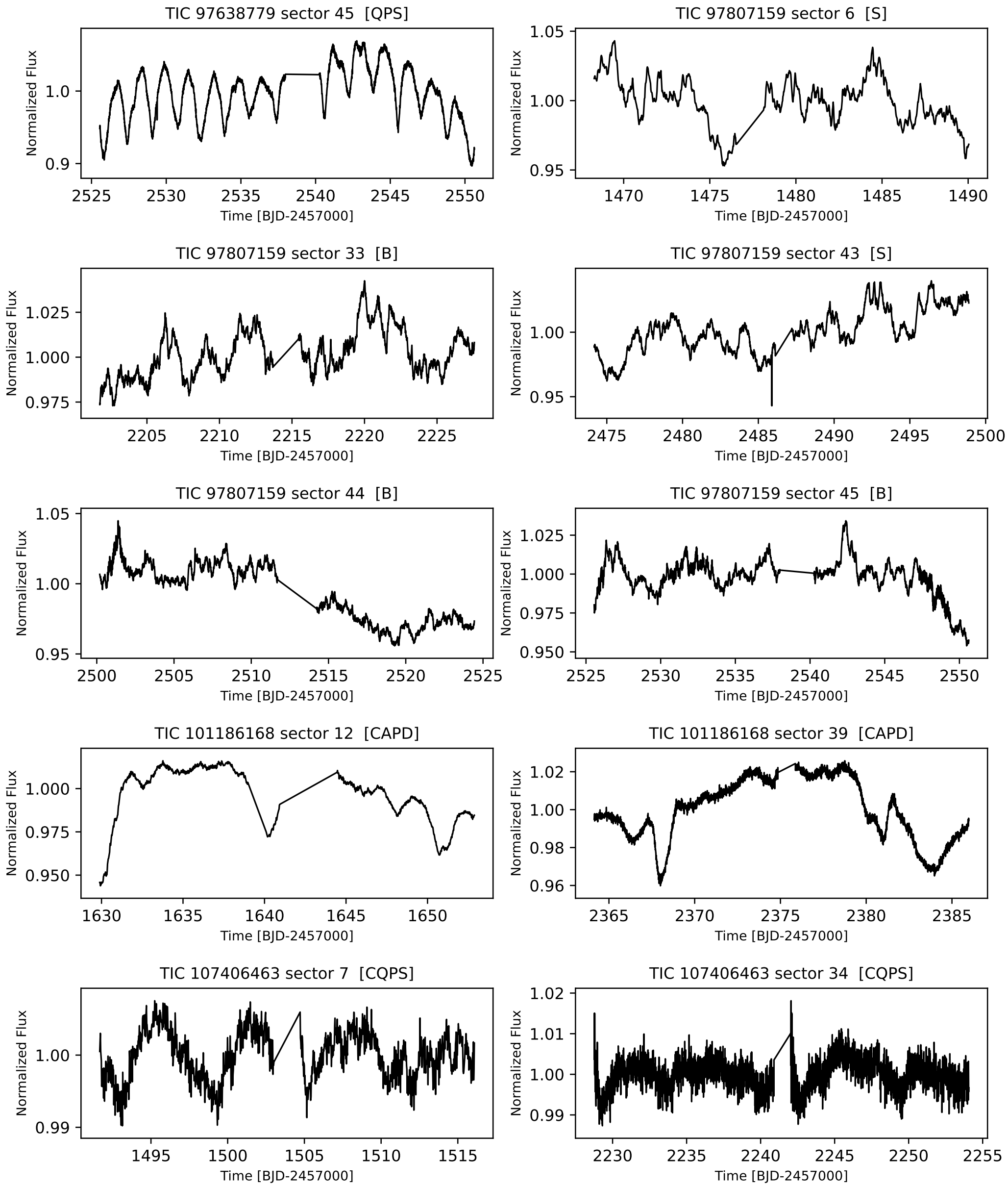

Figure 12. Cont.

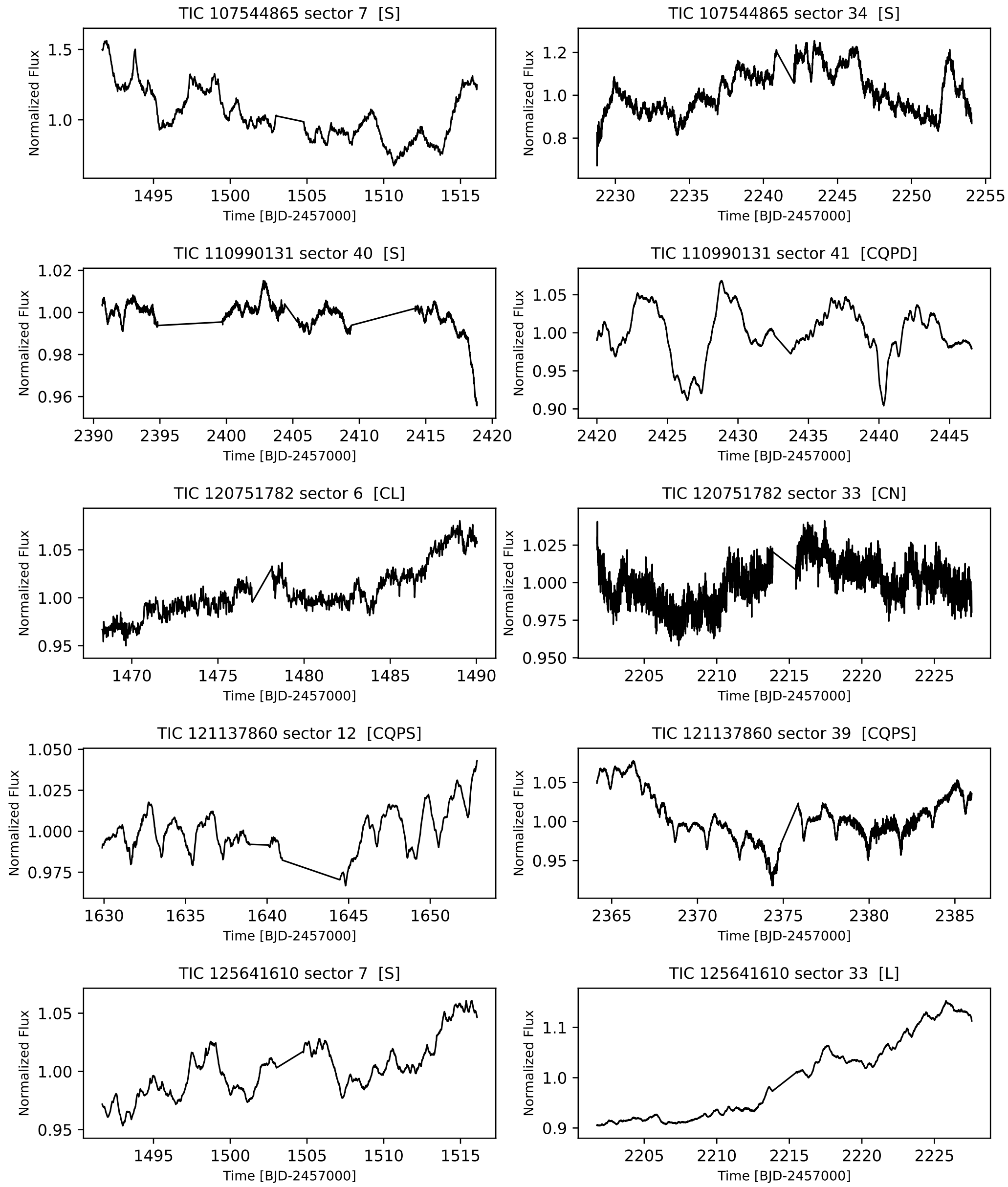

Figure 12. Cont.

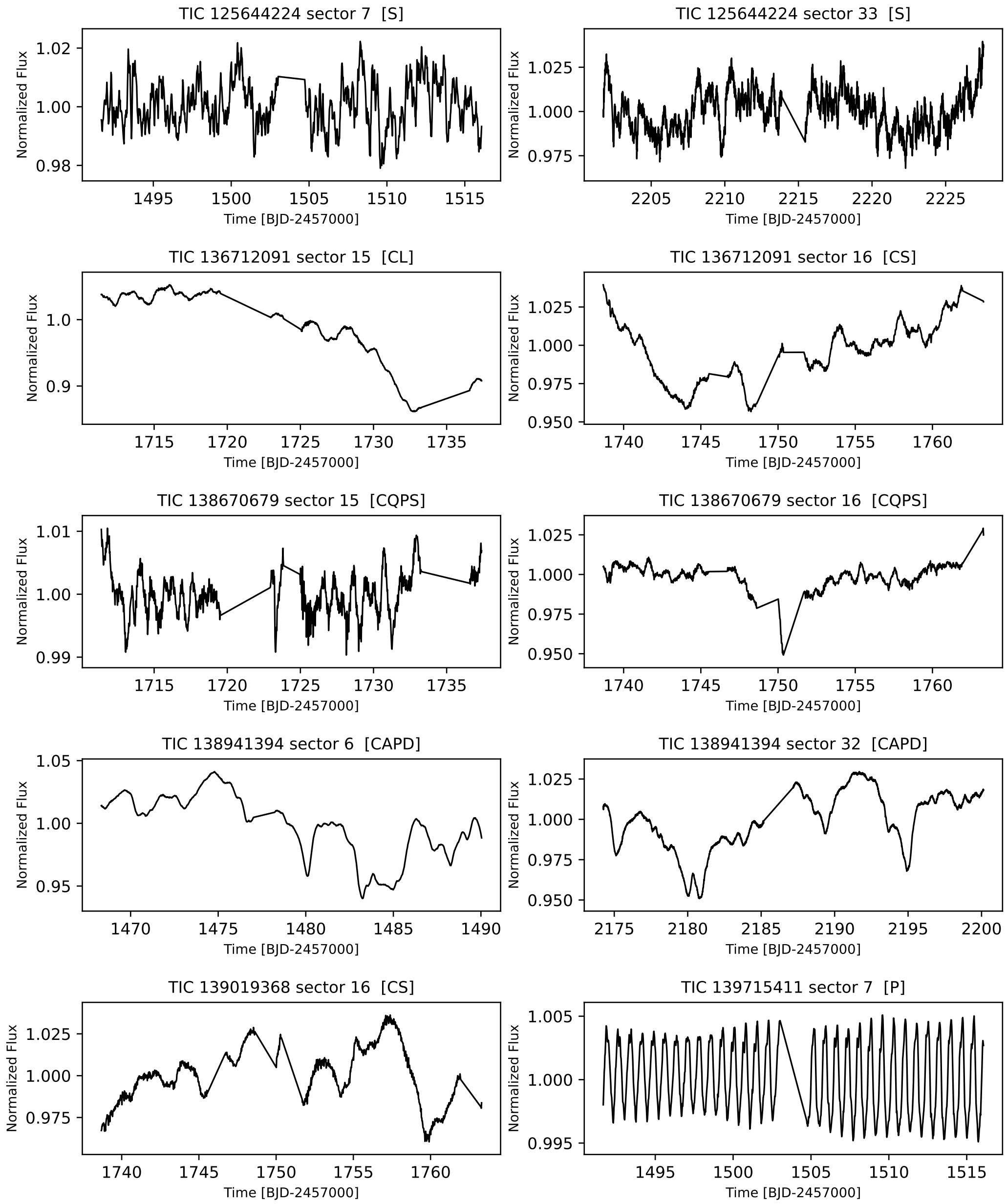

Figure 12. Cont.

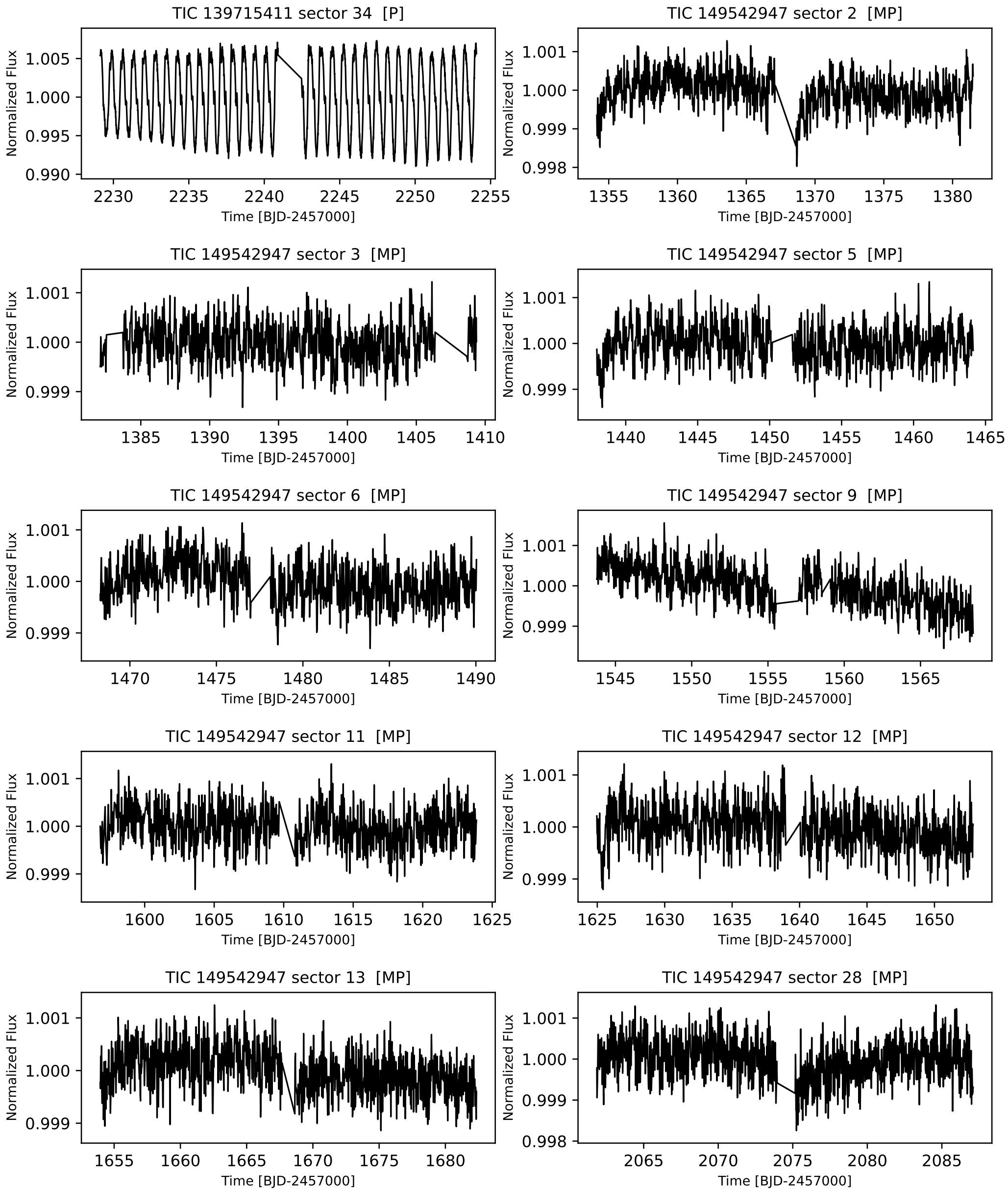

Figure 12. Cont.

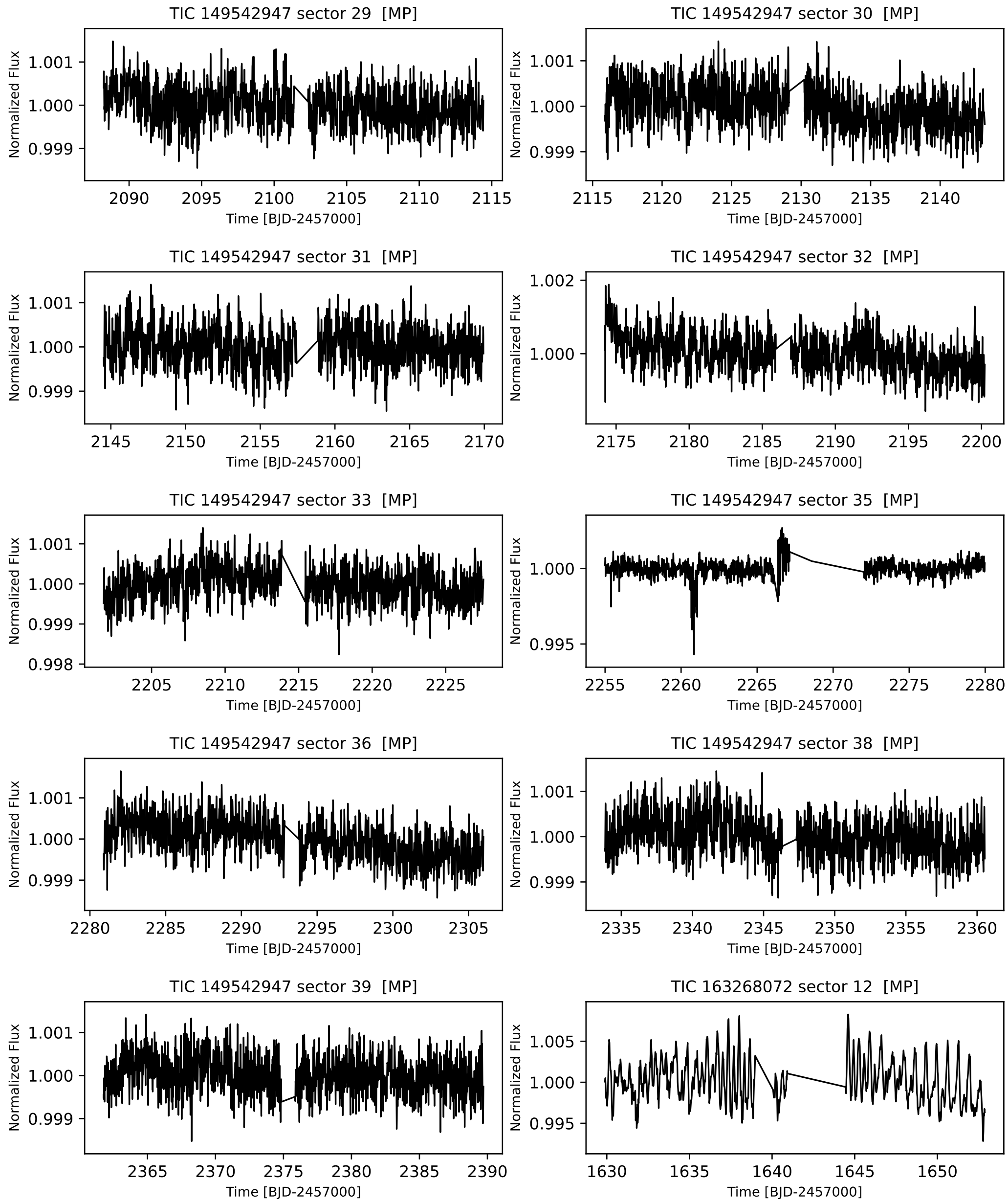

Figure 12. Cont.

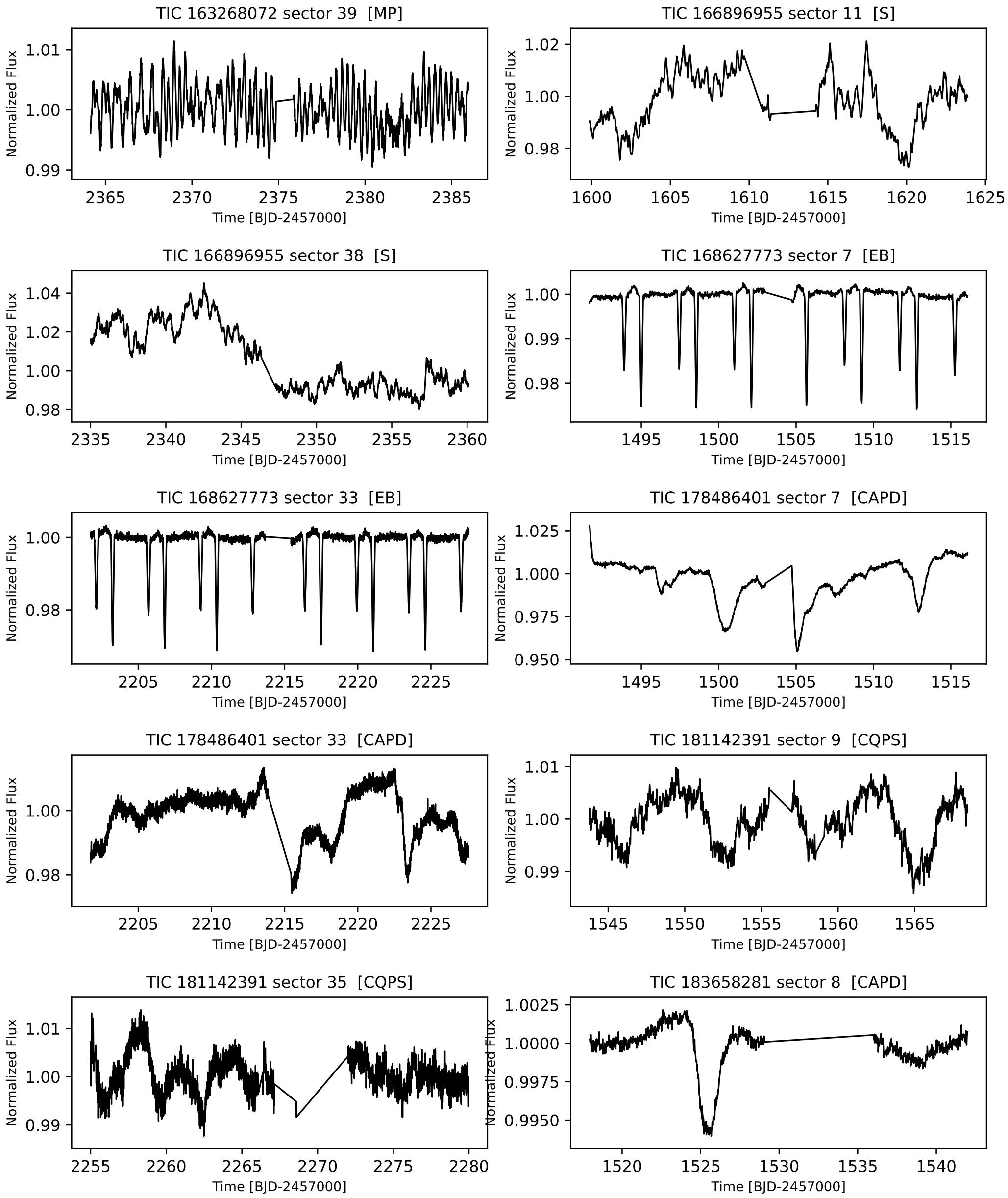

Figure 12. Cont.

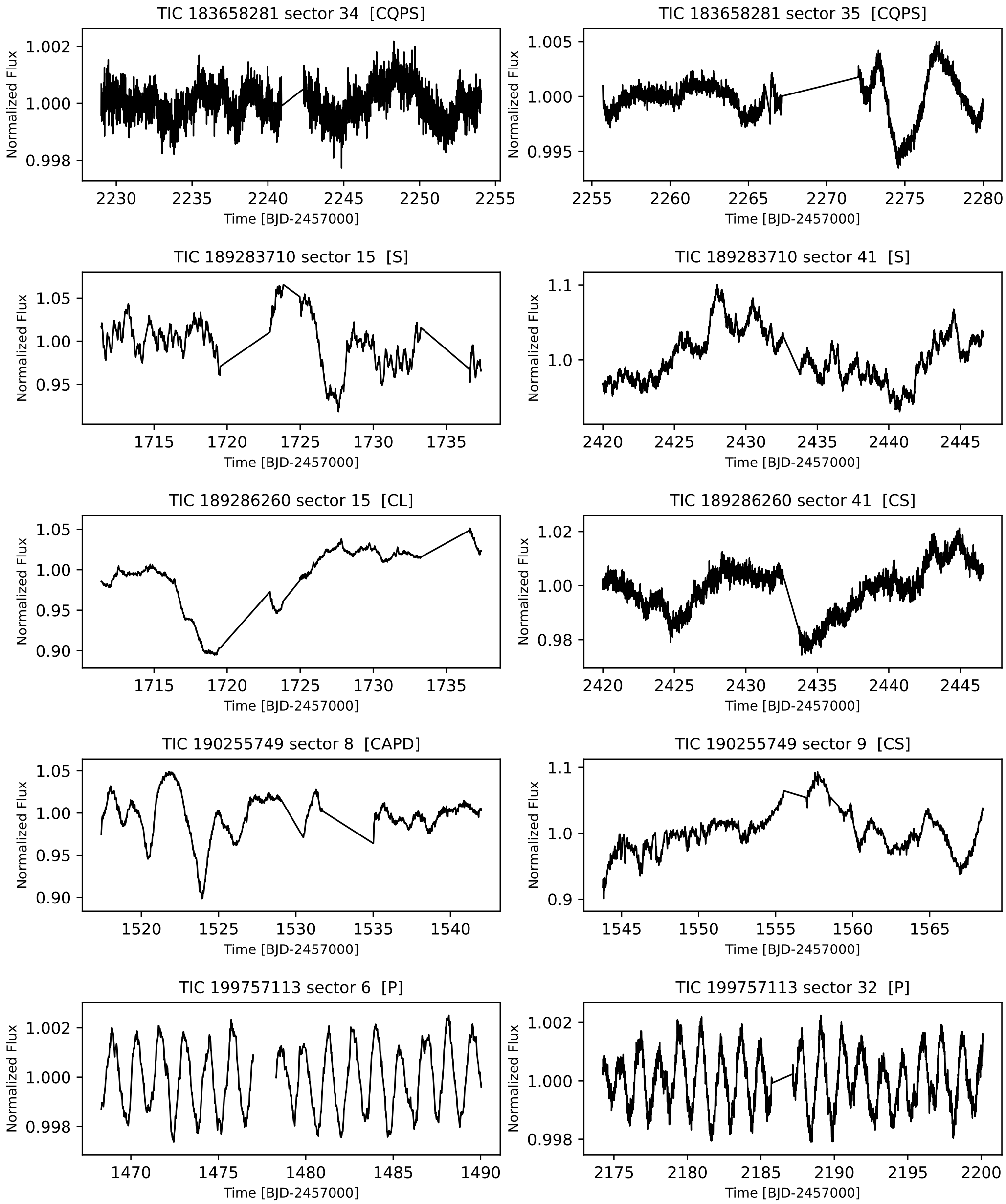

Figure 12. Cont.

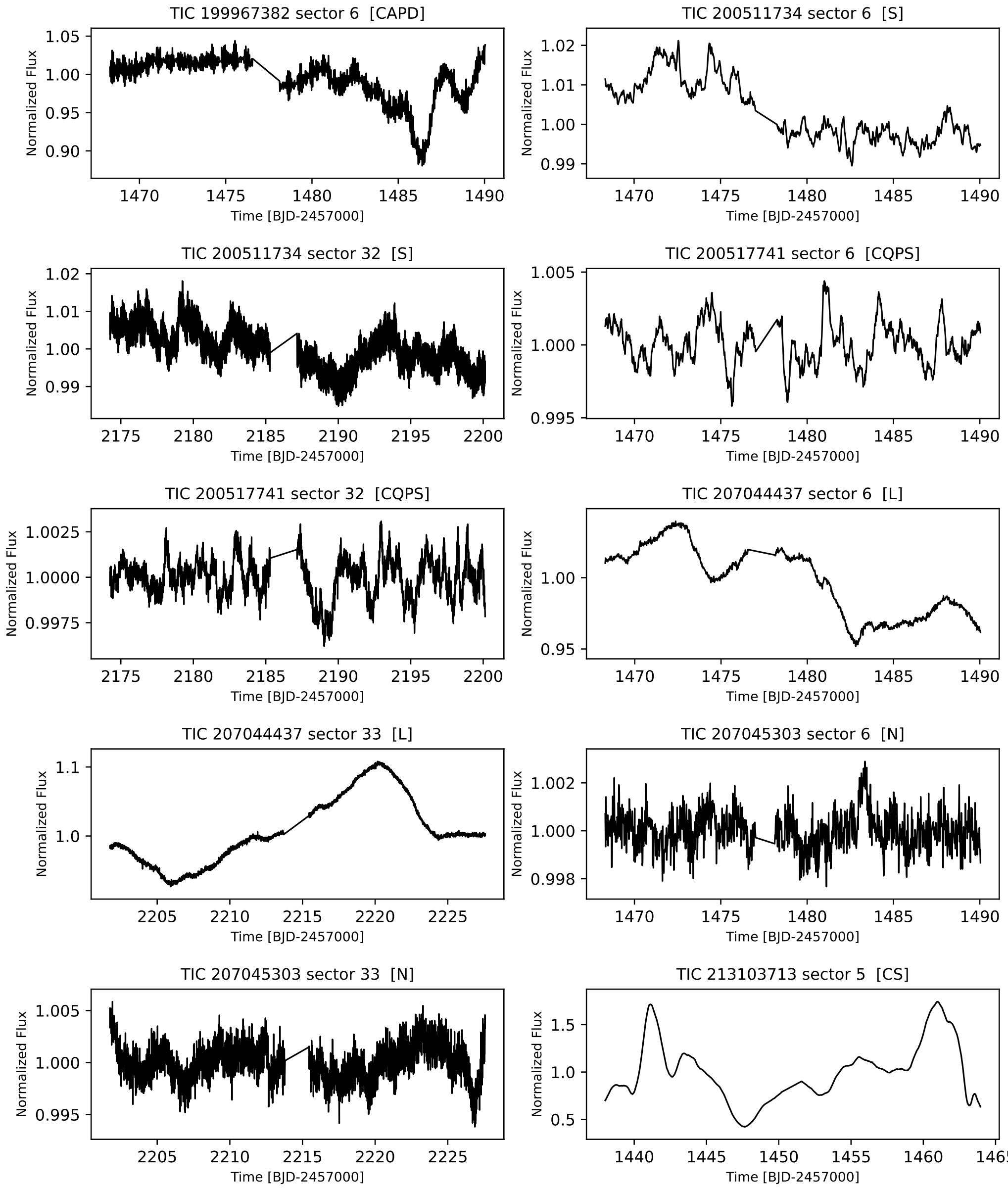

Figure 12. Cont.

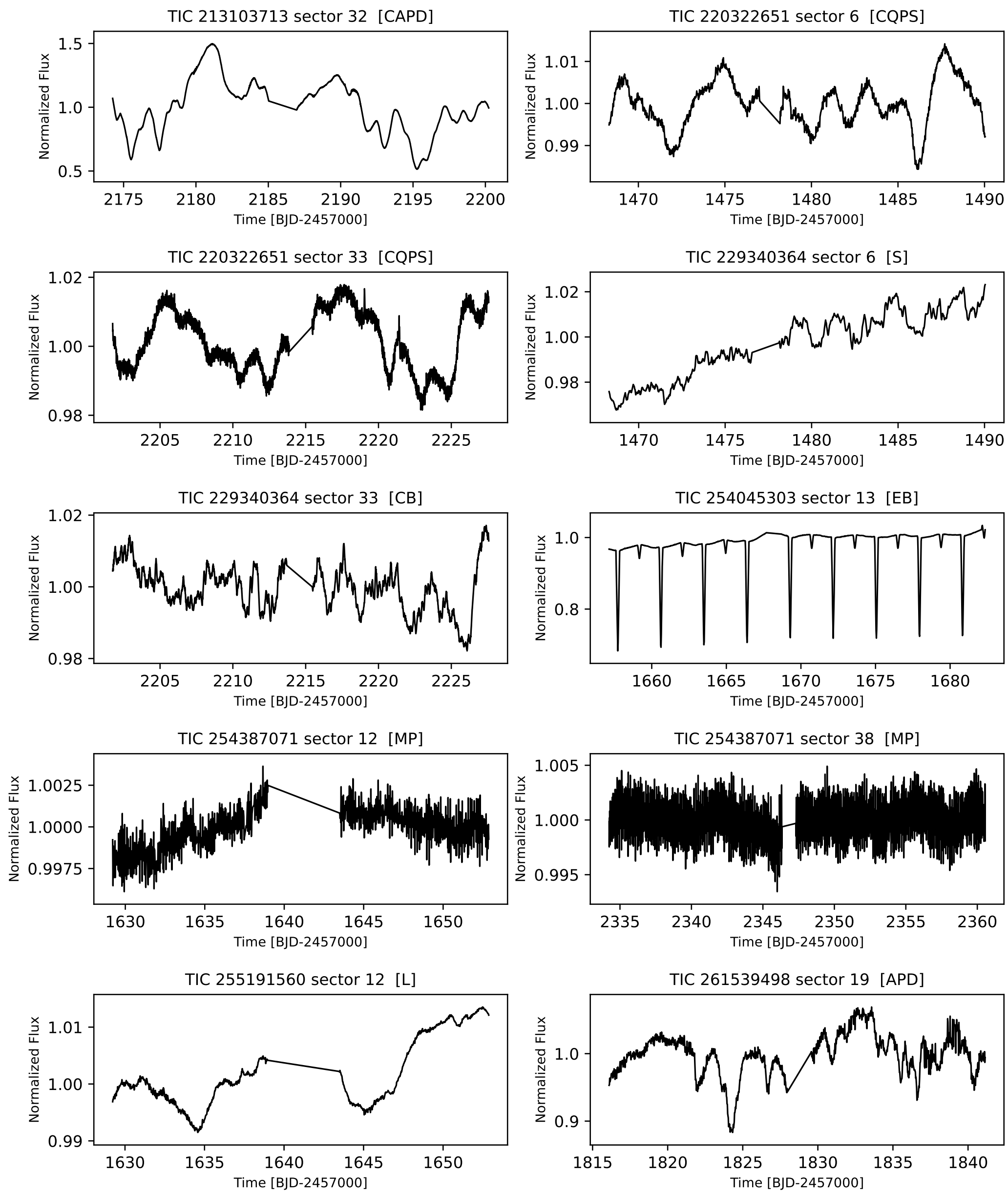

Figure 12. Cont.

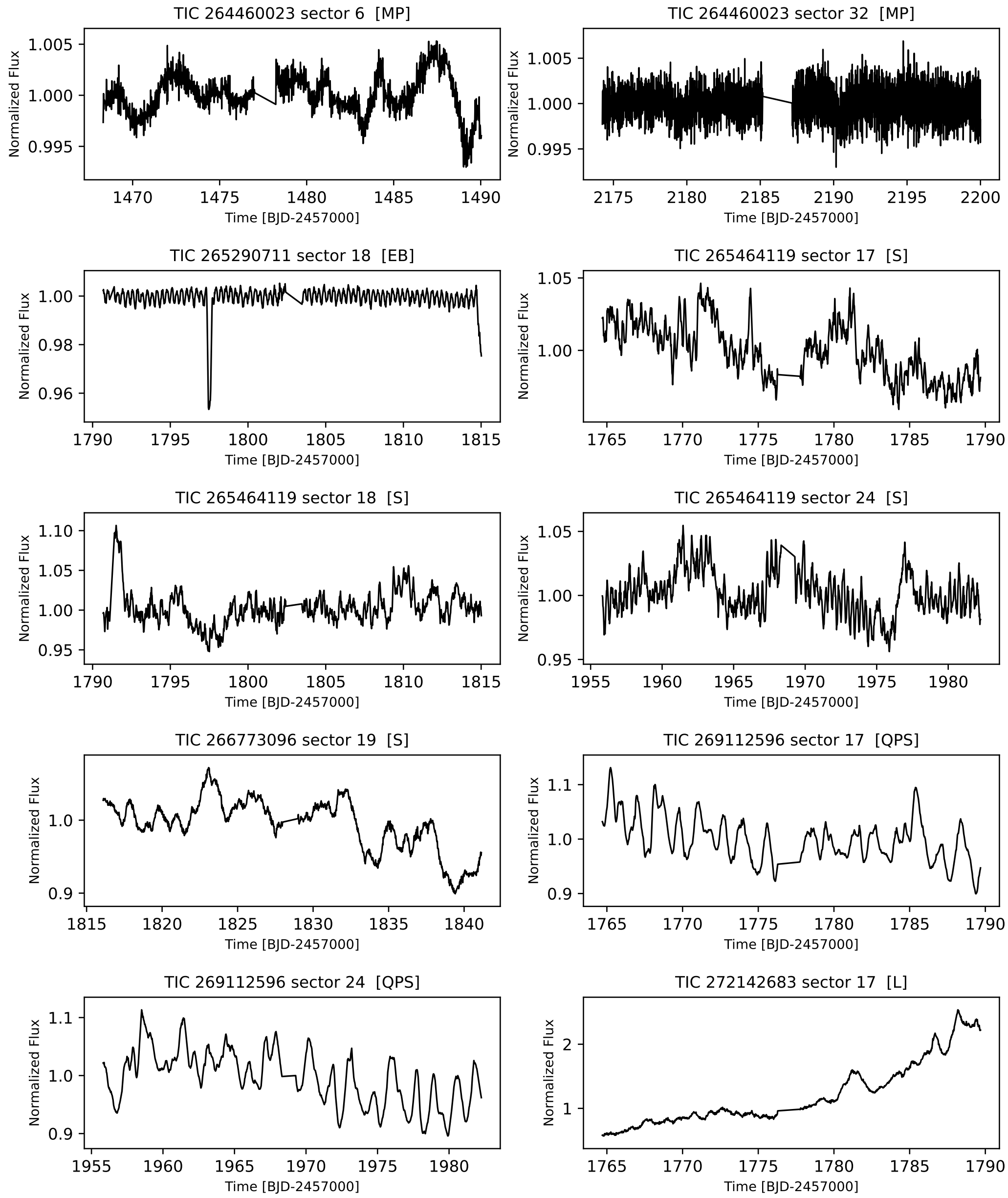

Figure 12. Cont.

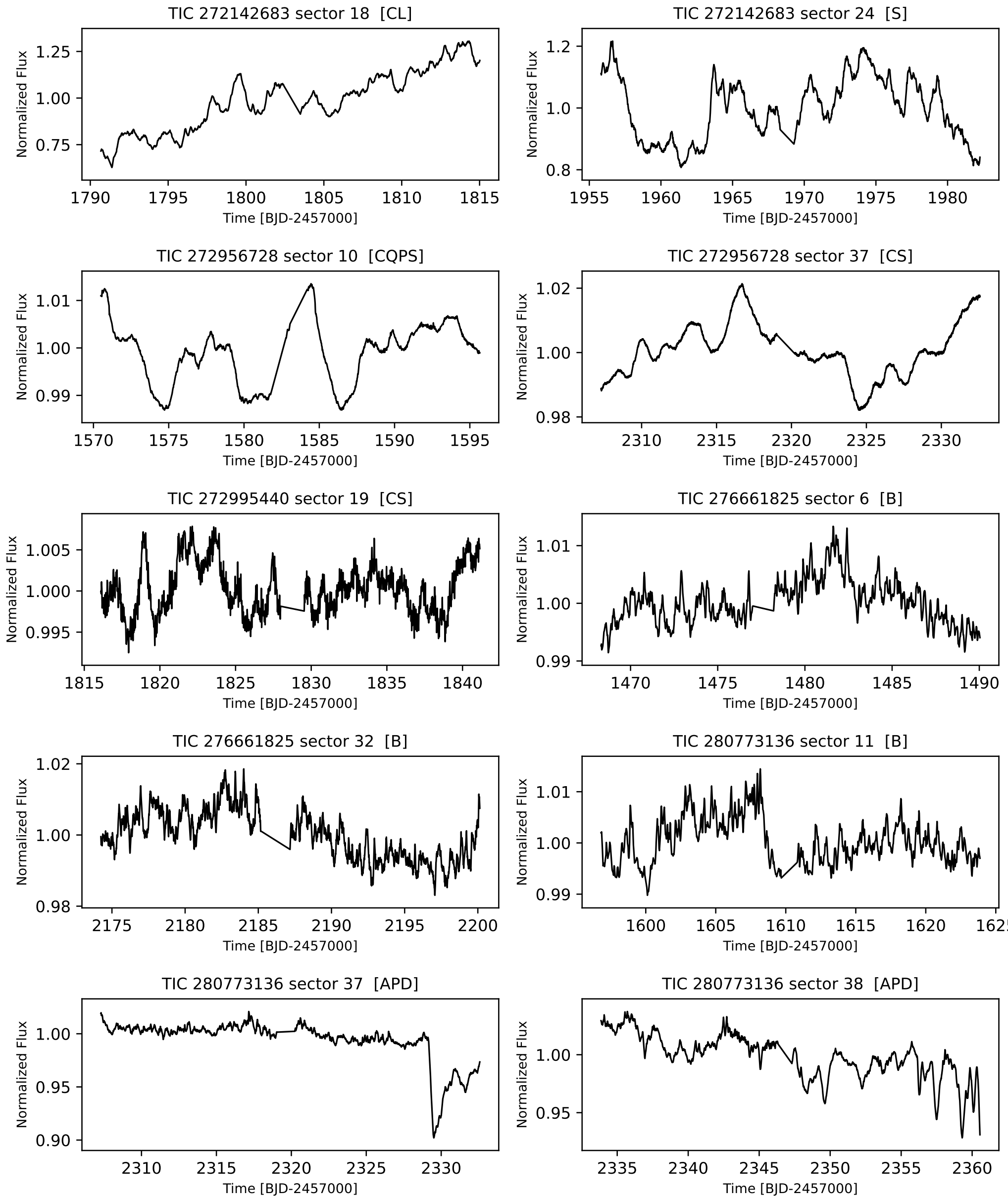

Figure 12. Cont.

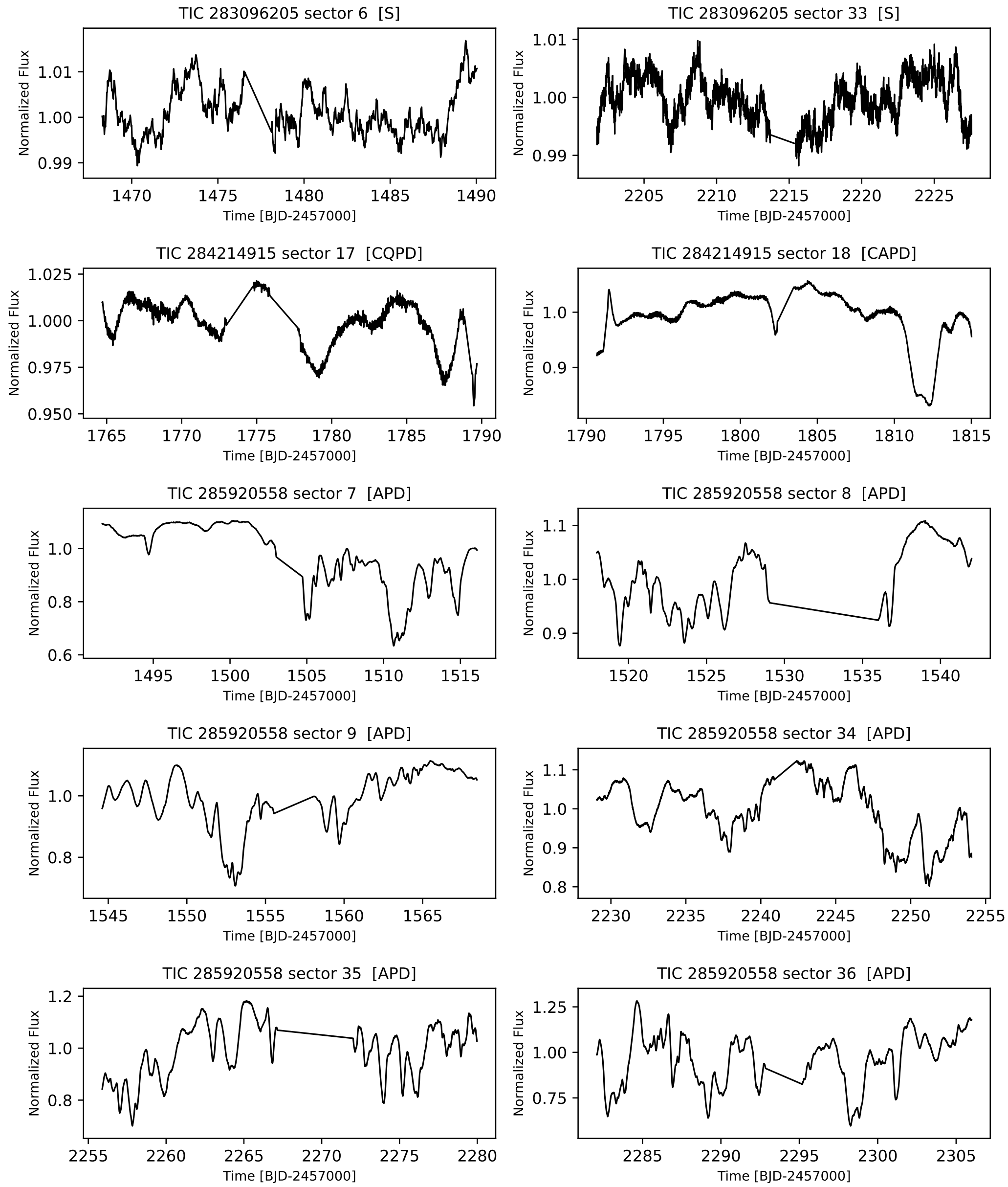

Figure 12. Cont.

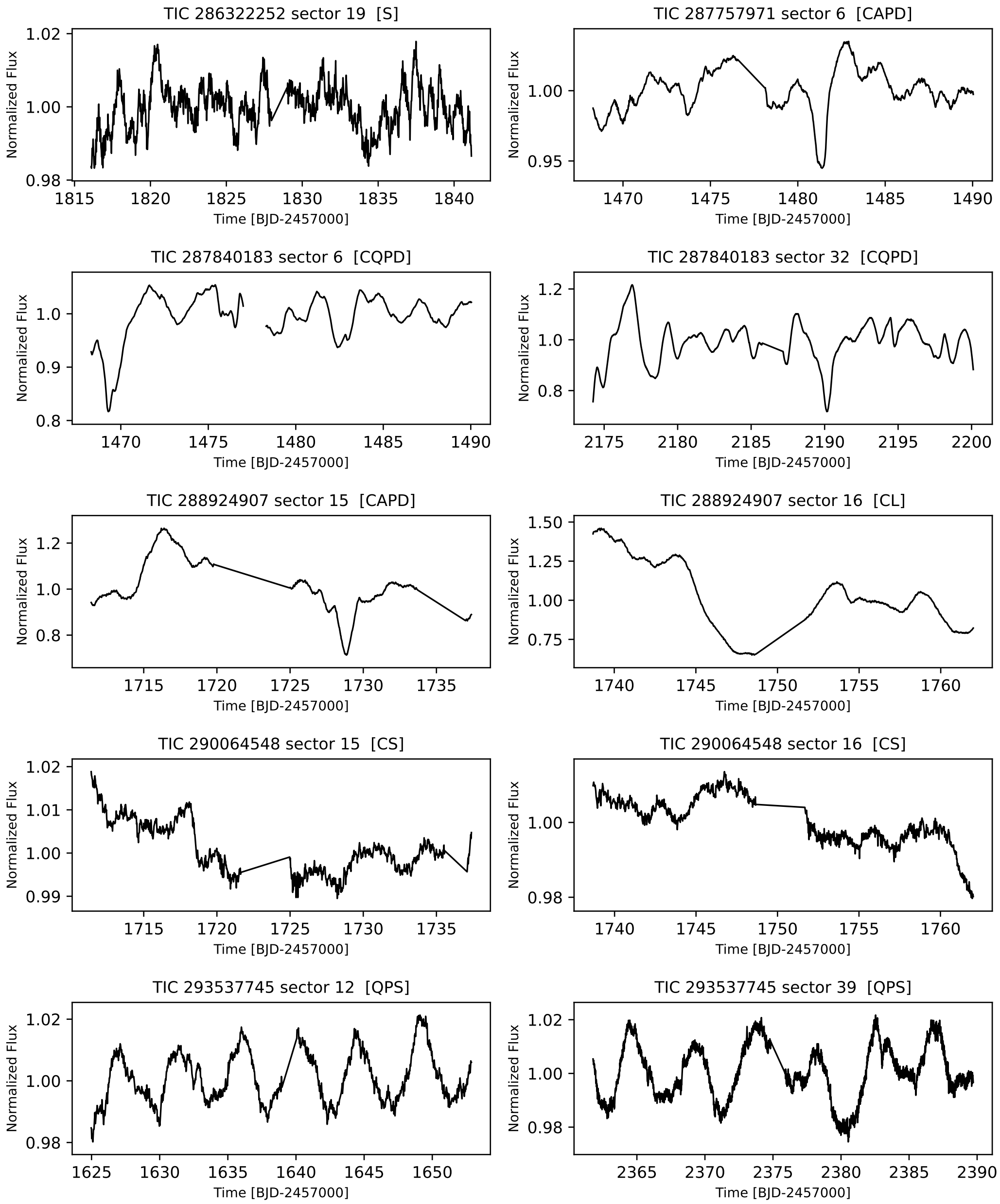

Figure 12. Cont.

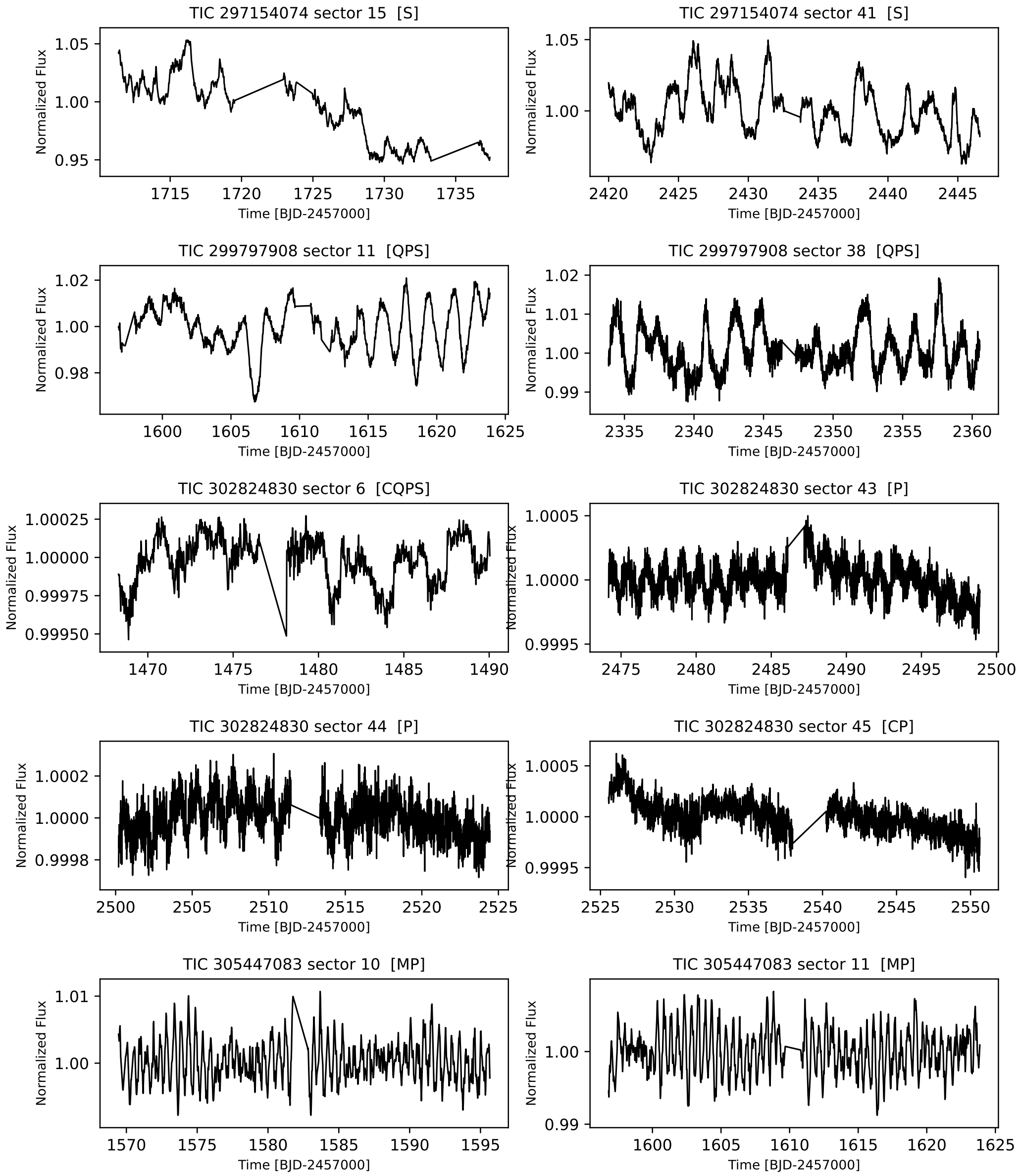

Figure 12. Cont.

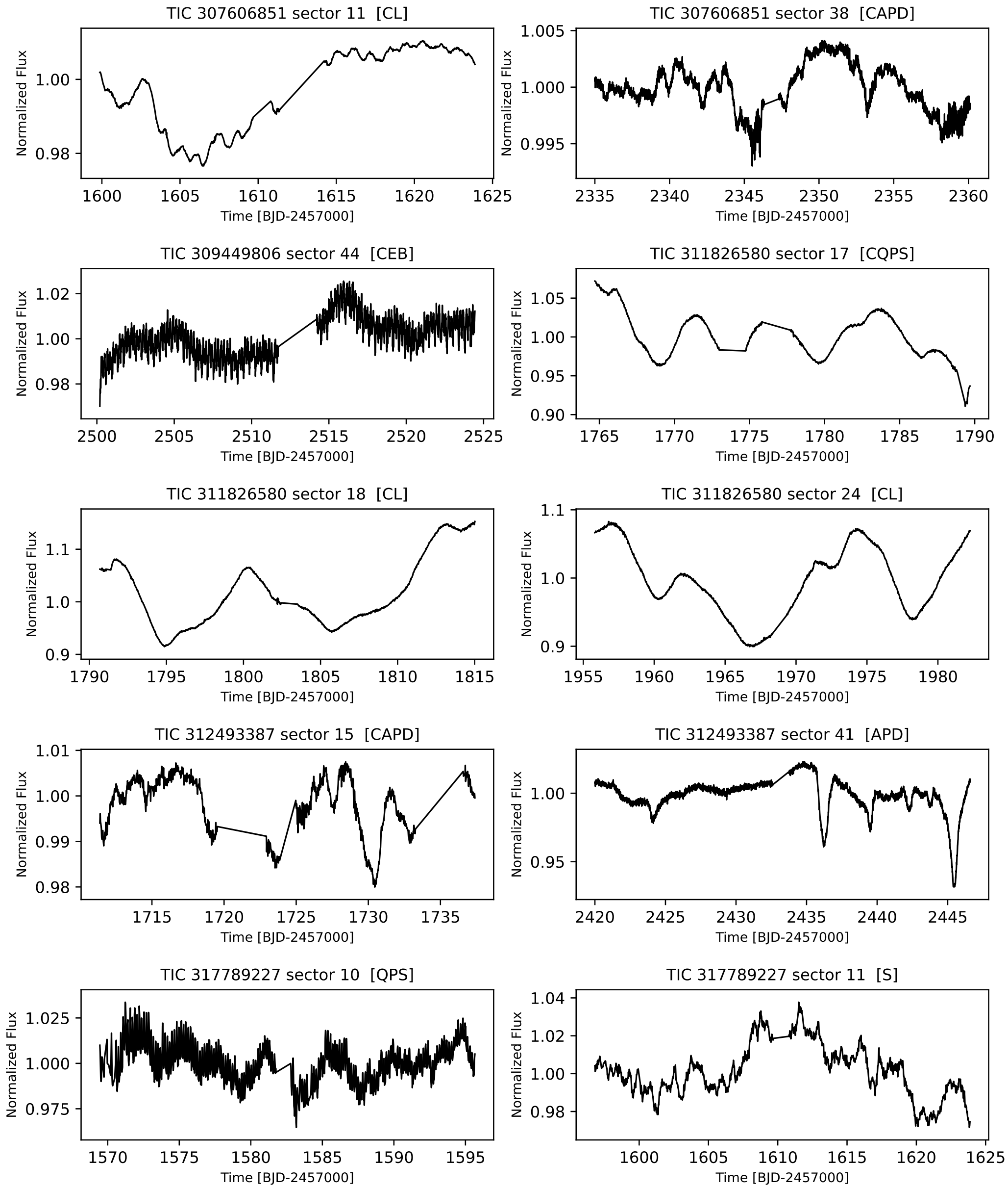

Figure 12. Cont.

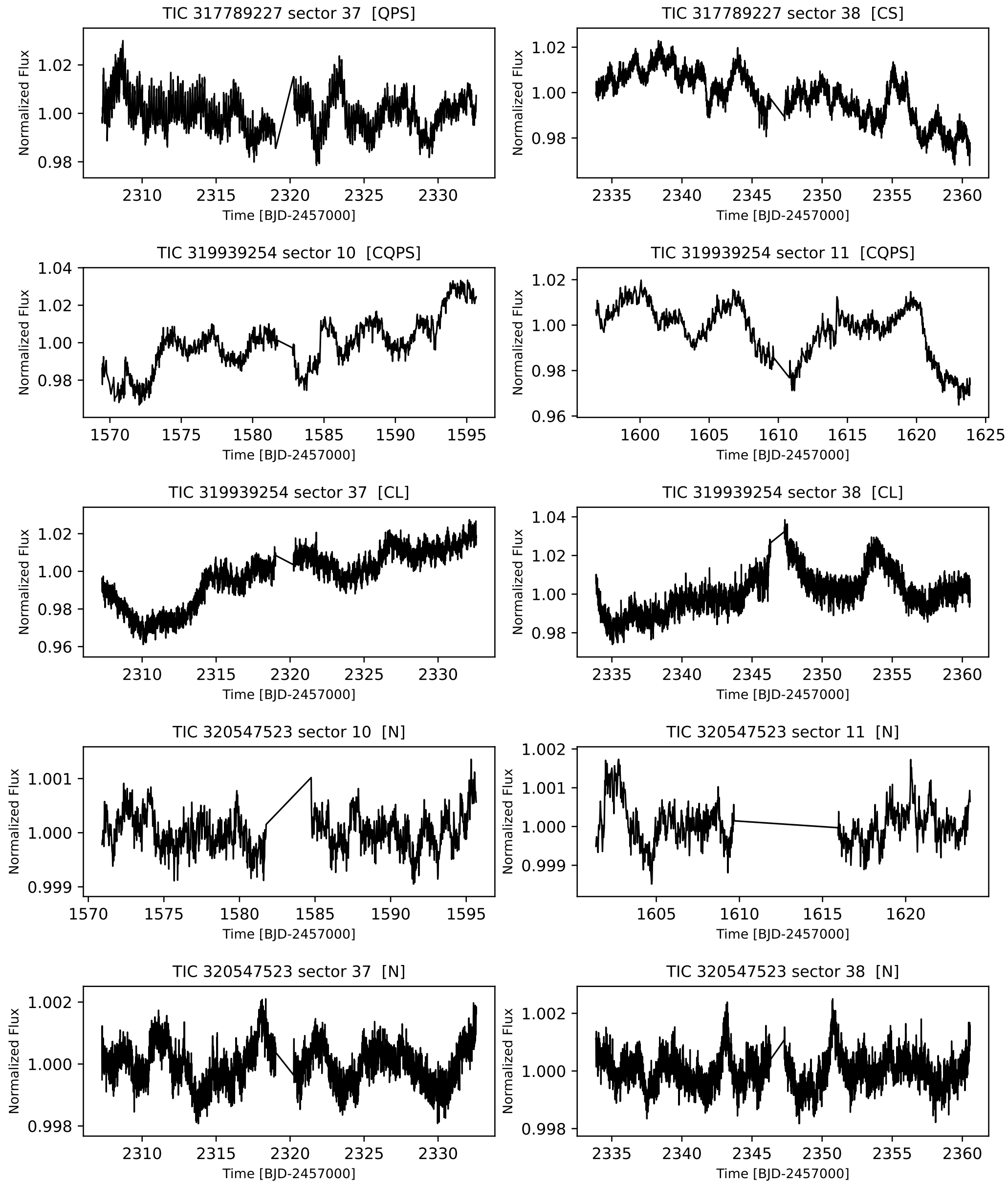

Figure 12. Cont.

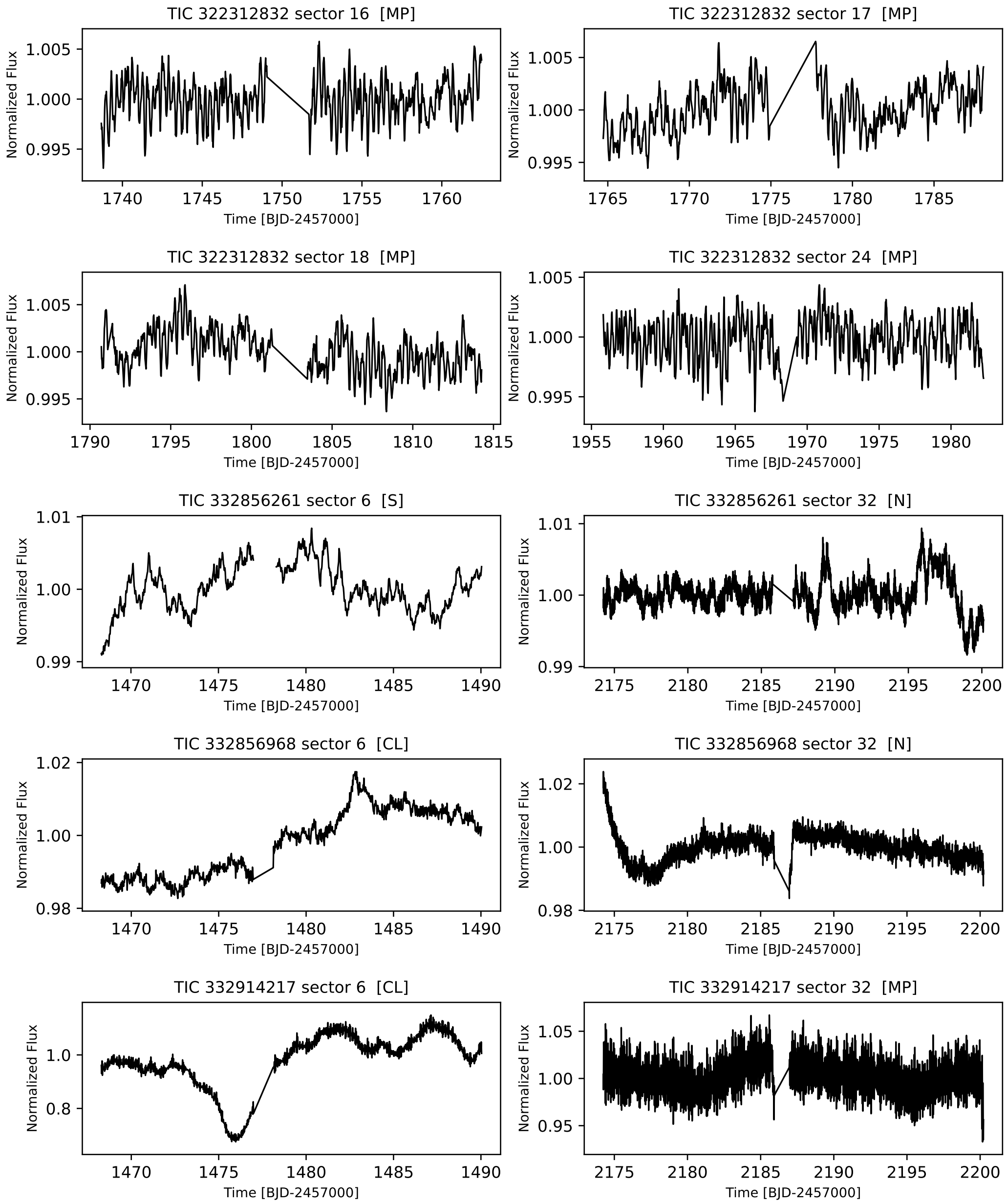

Figure 12. Cont.

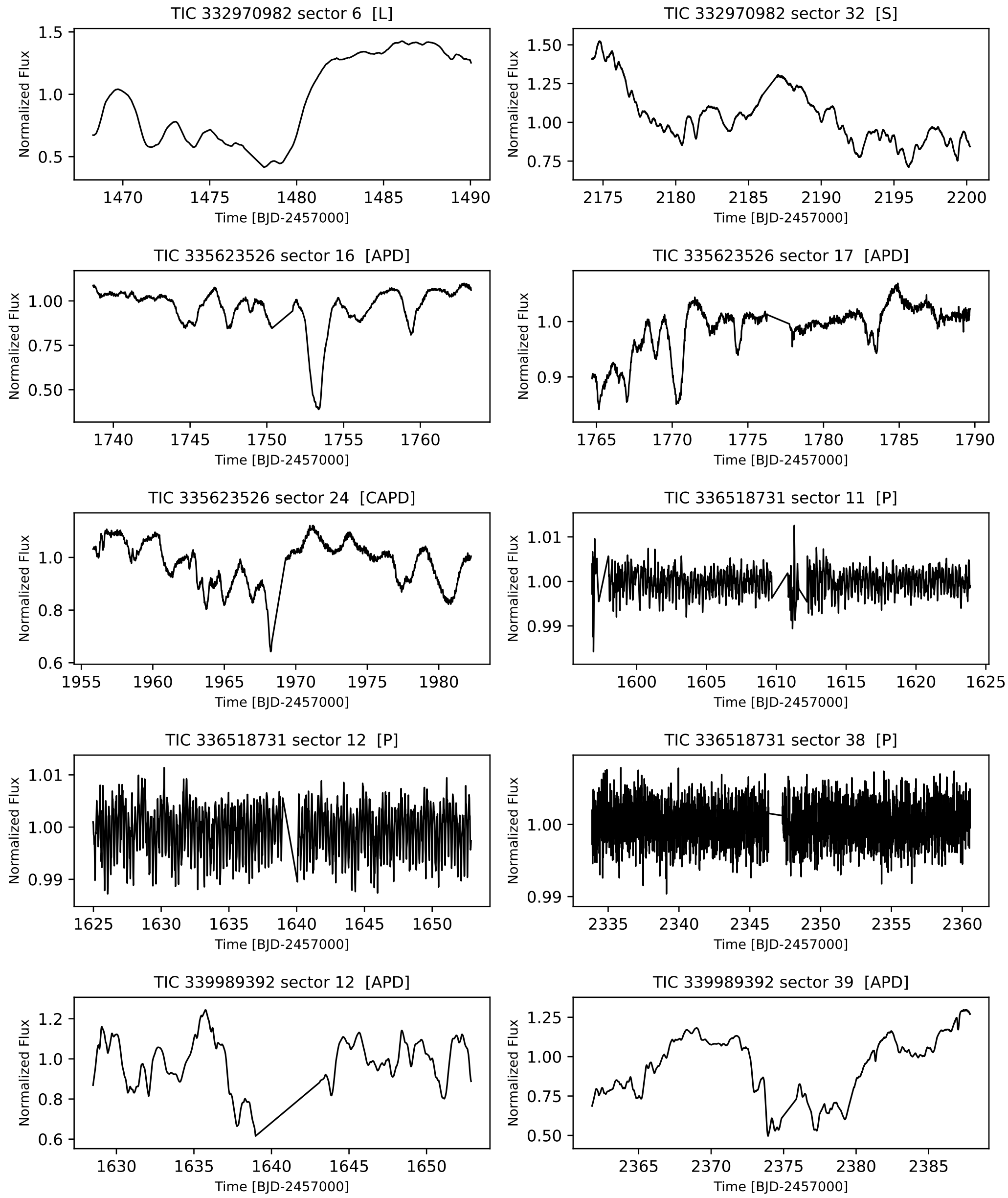

Figure 12. Cont.

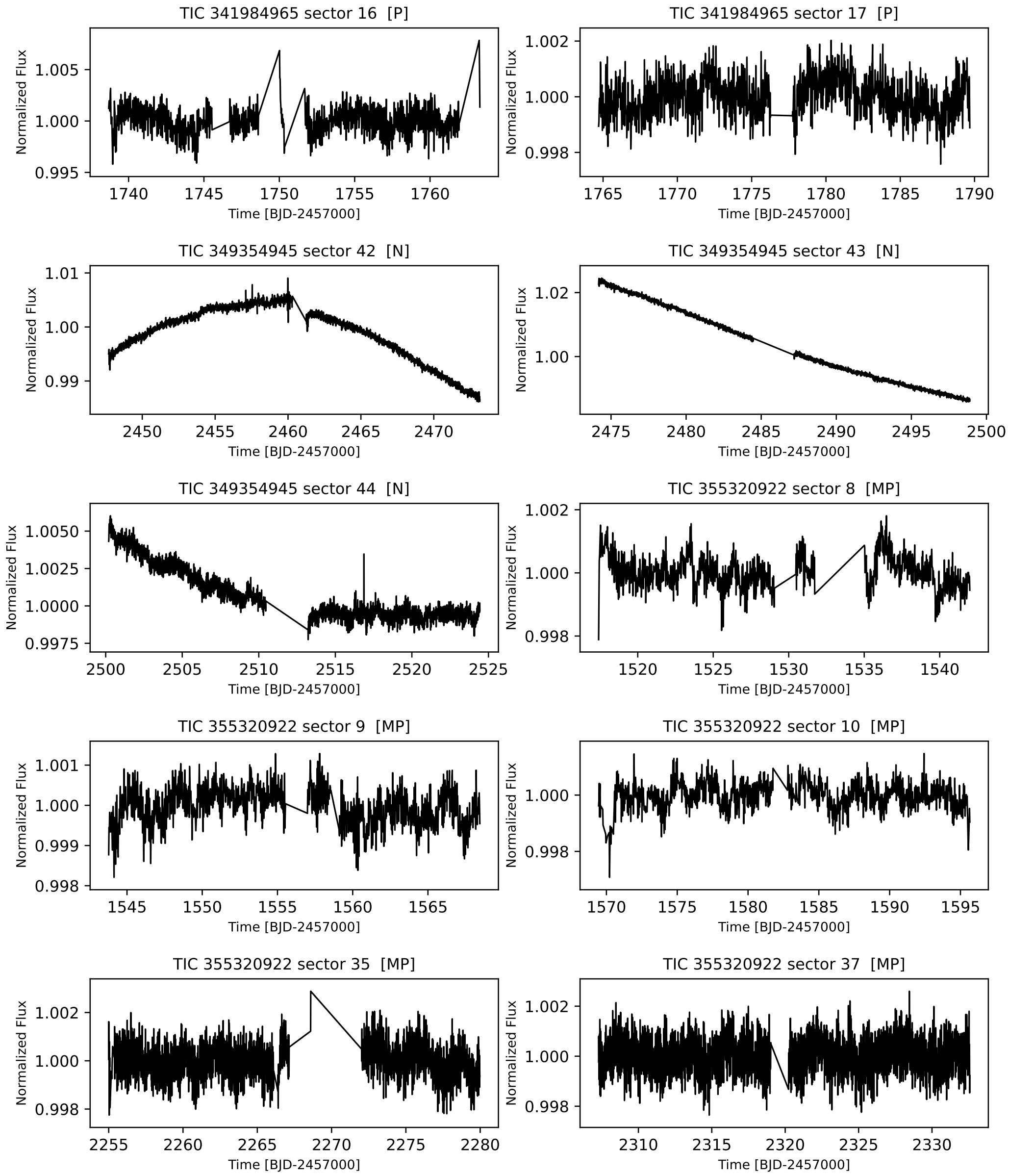

Figure 12. Cont.

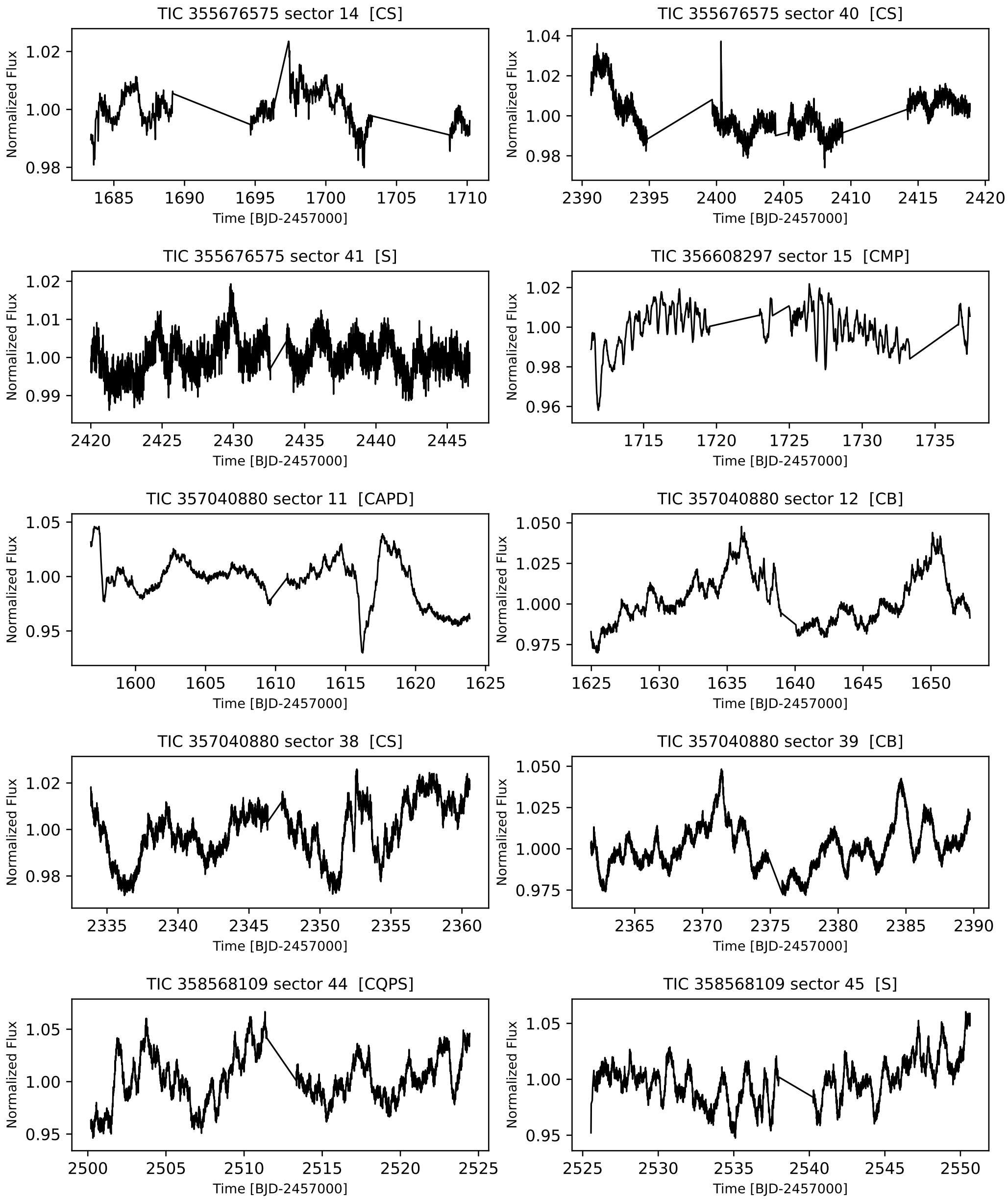

Figure 12. Cont.

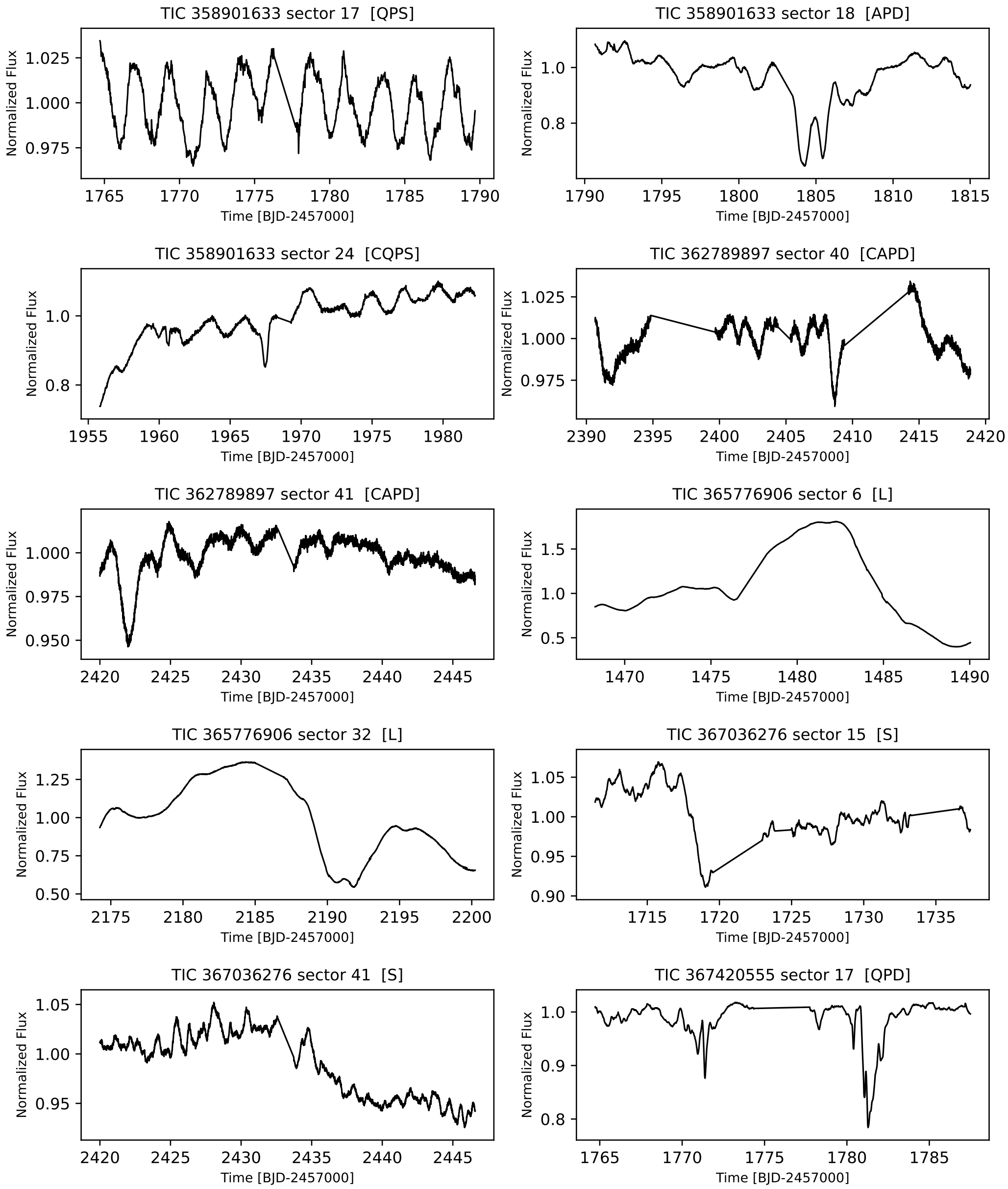

Figure 12. Cont.

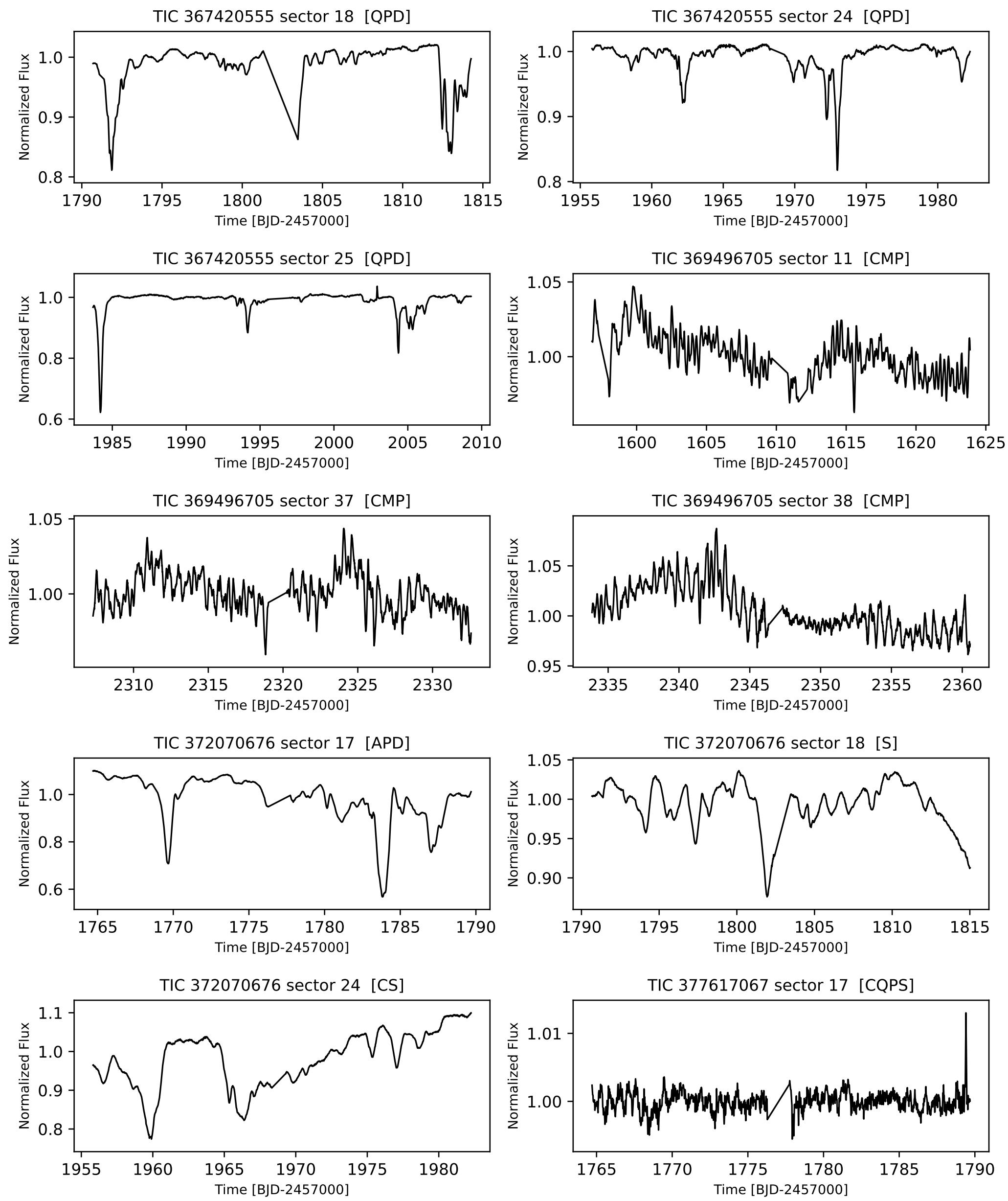

Figure 12. Cont.

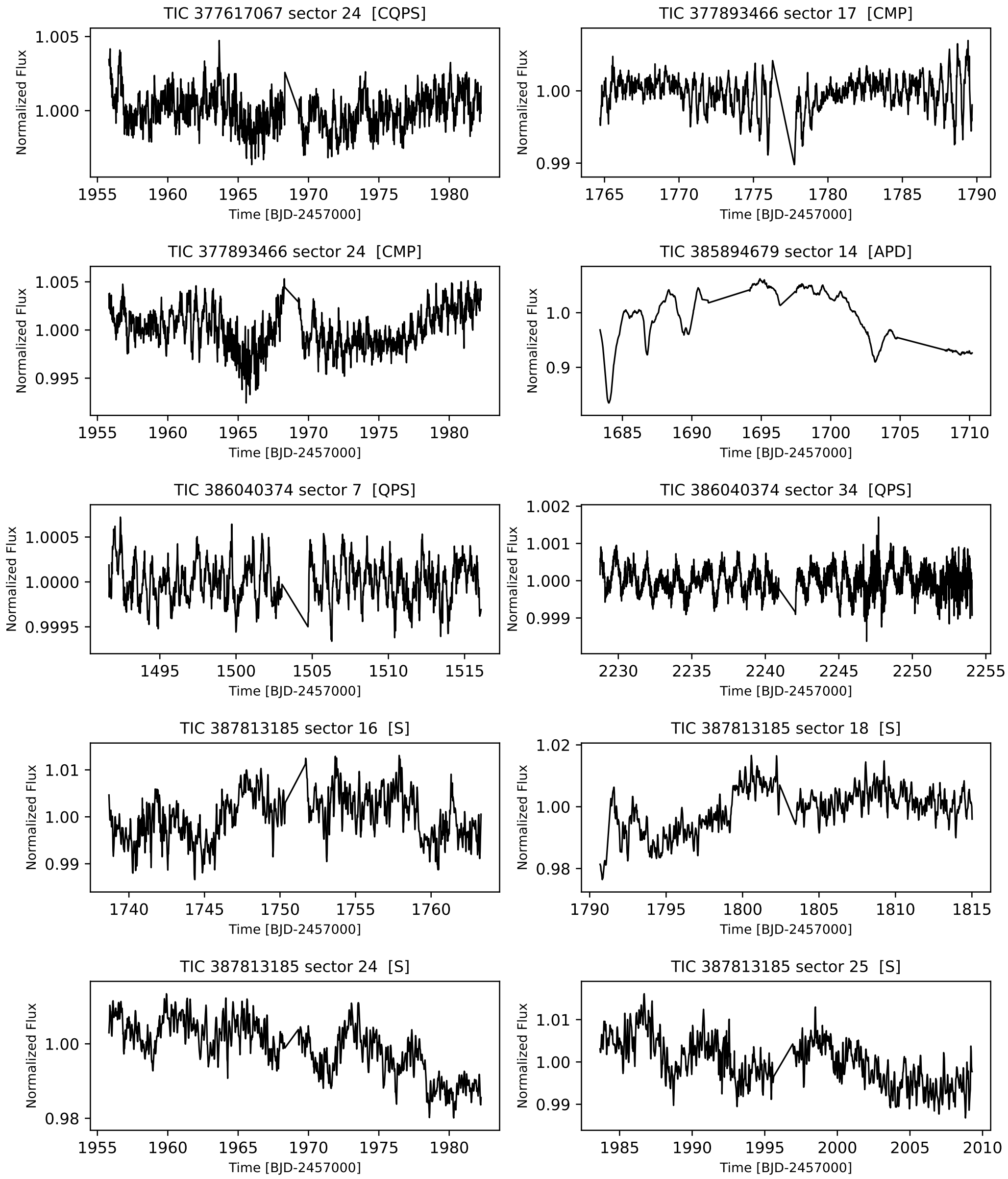

Figure 12. Cont.

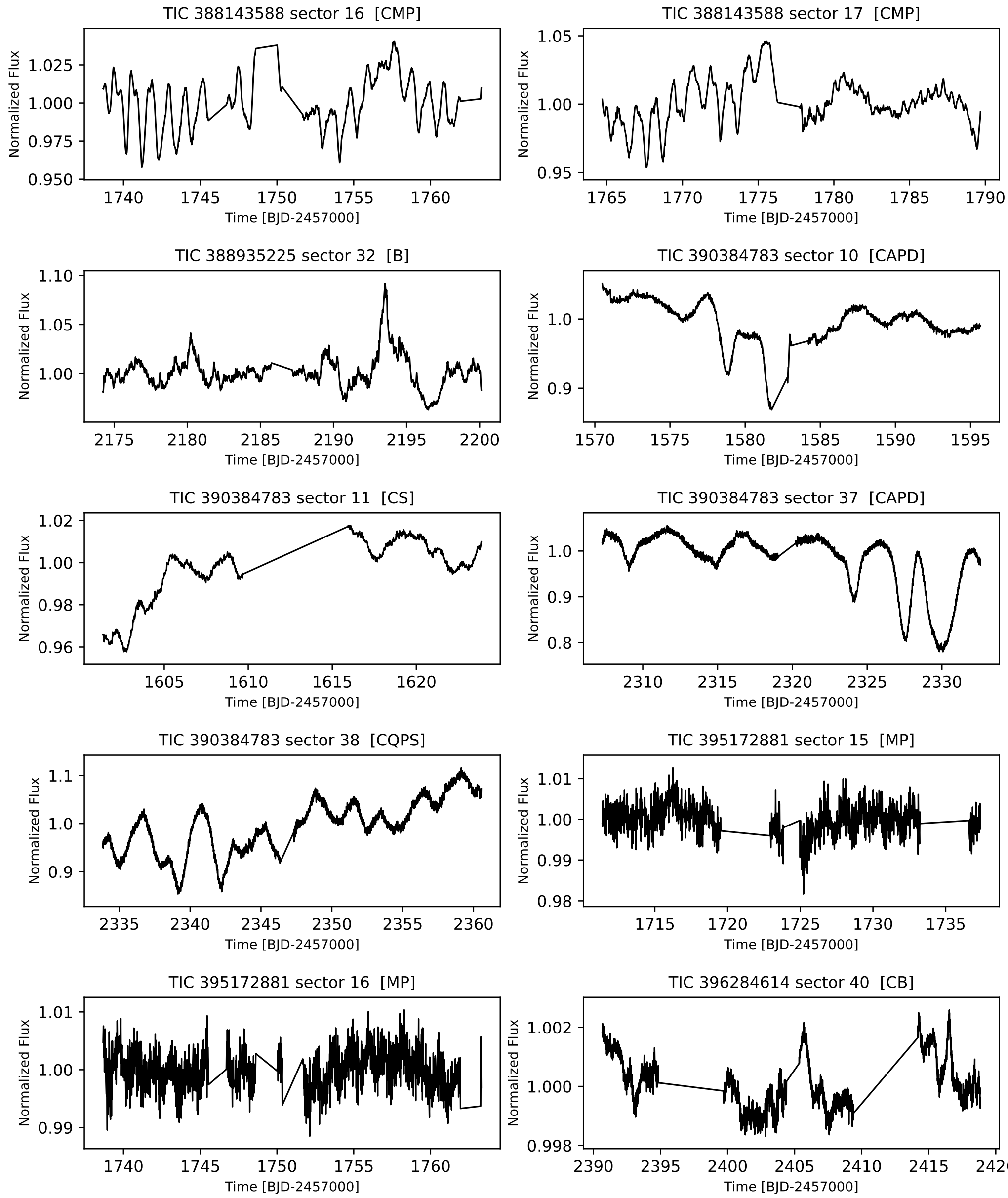

Figure 12. Cont.

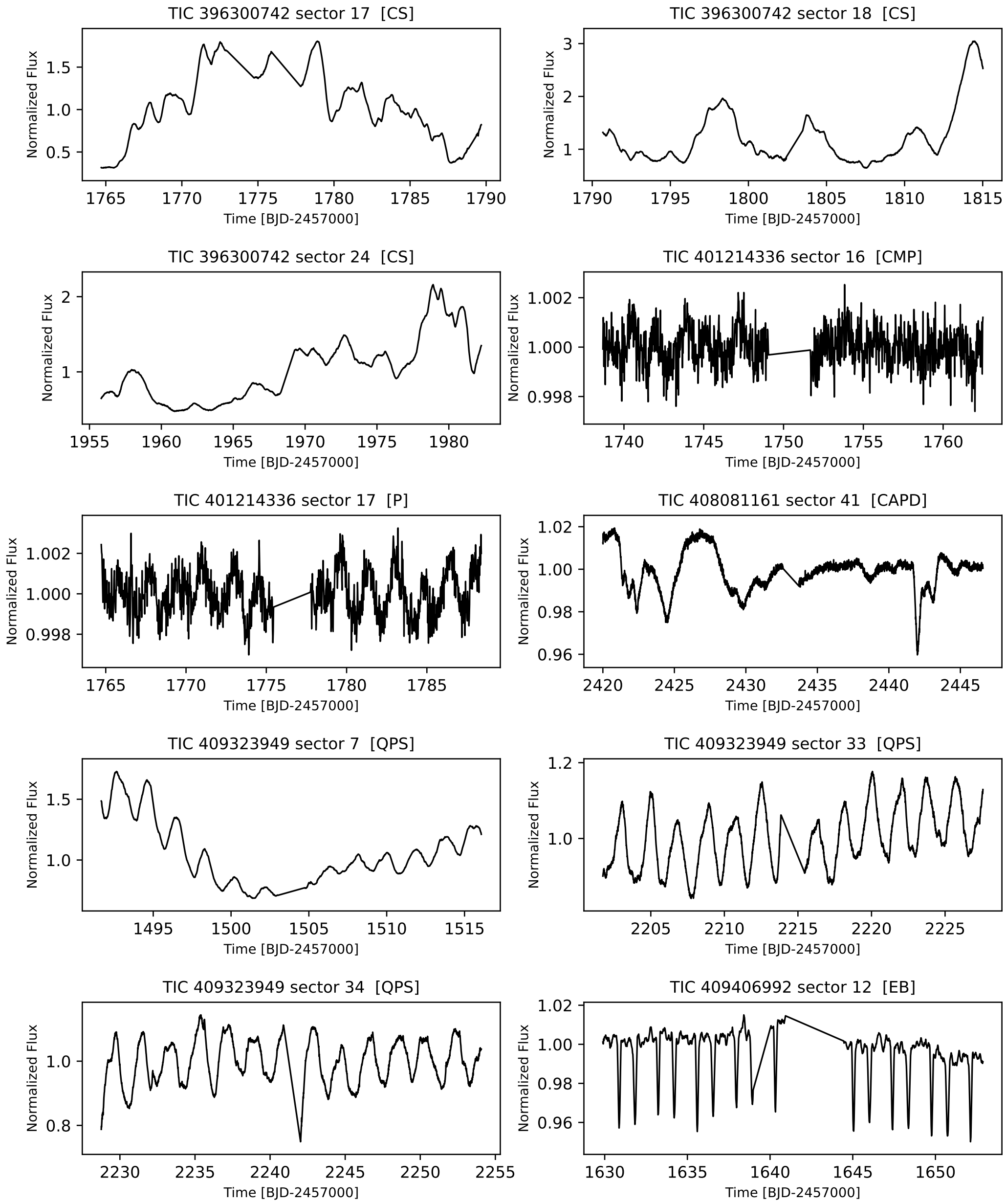

Figure 12. Cont.

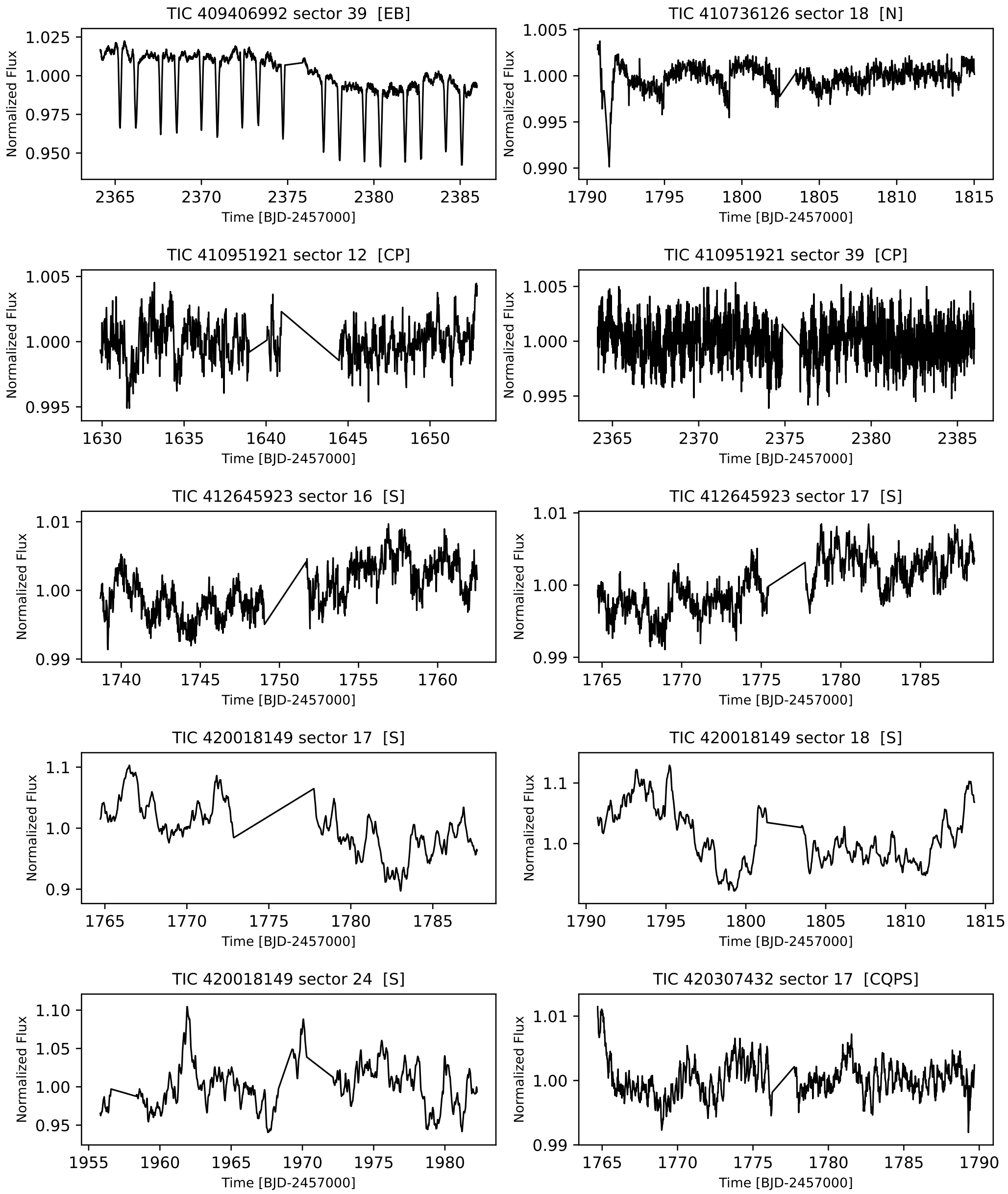

Figure 12. Cont.

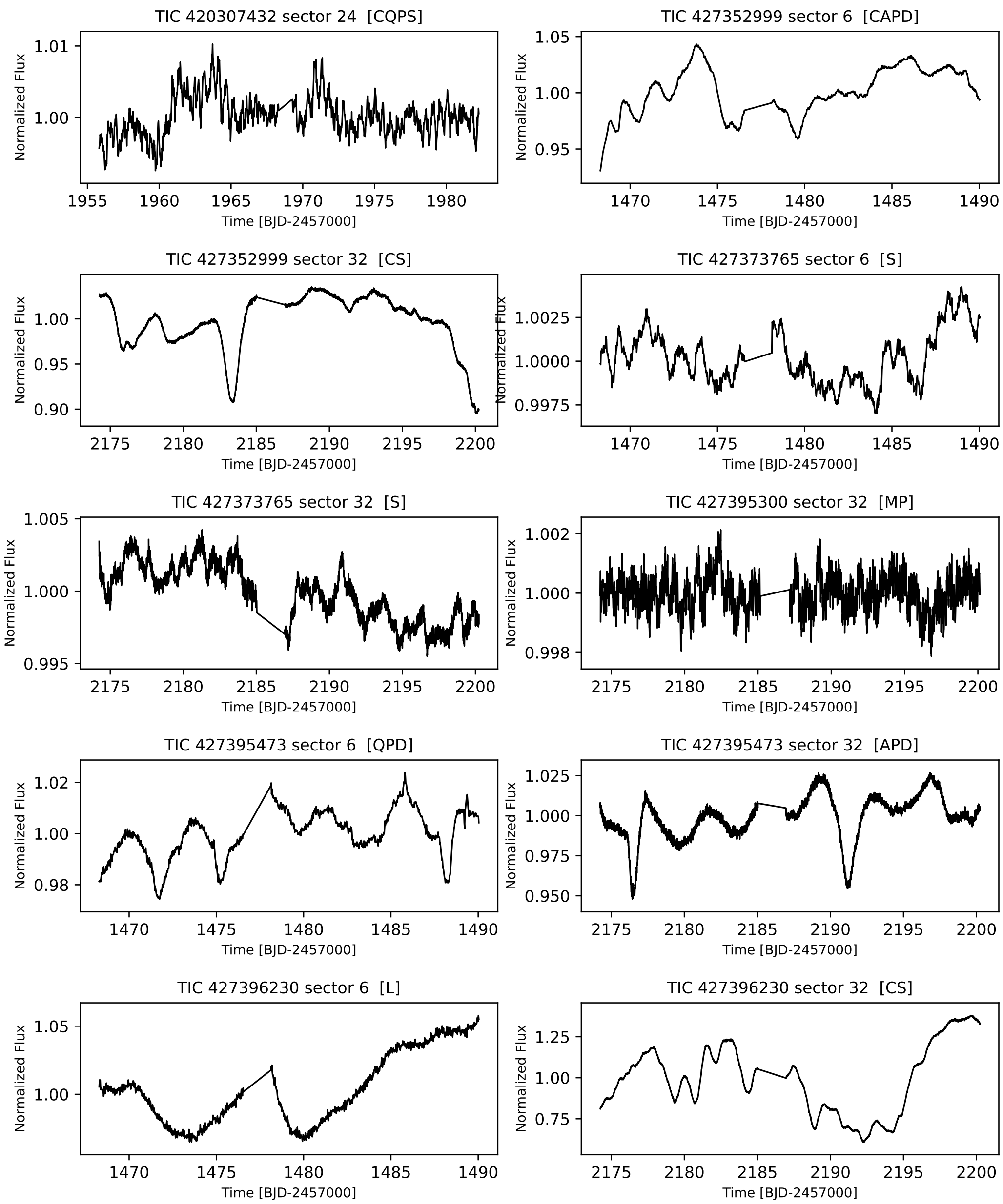

Figure 12. Cont.

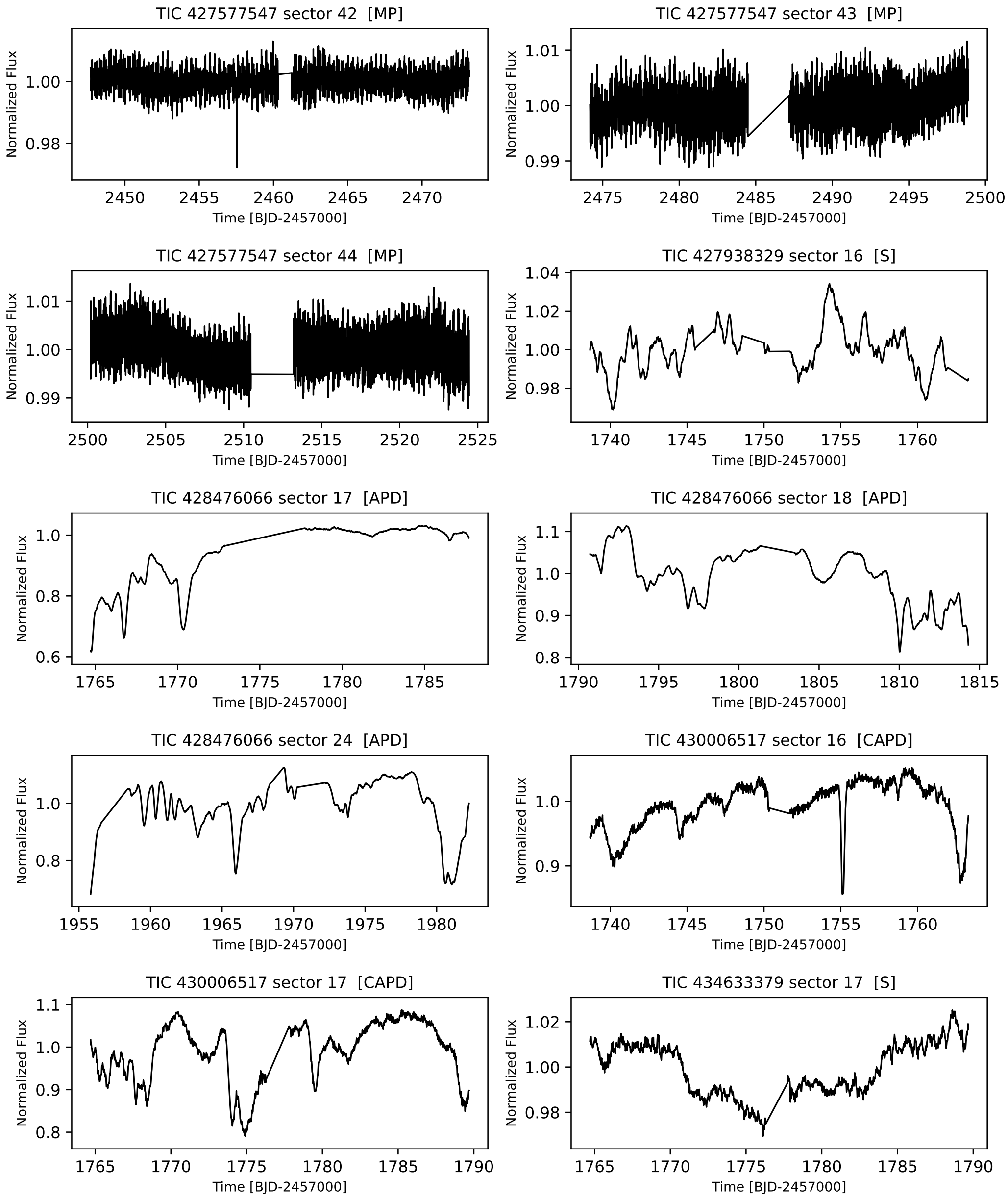

Figure 12. Cont.

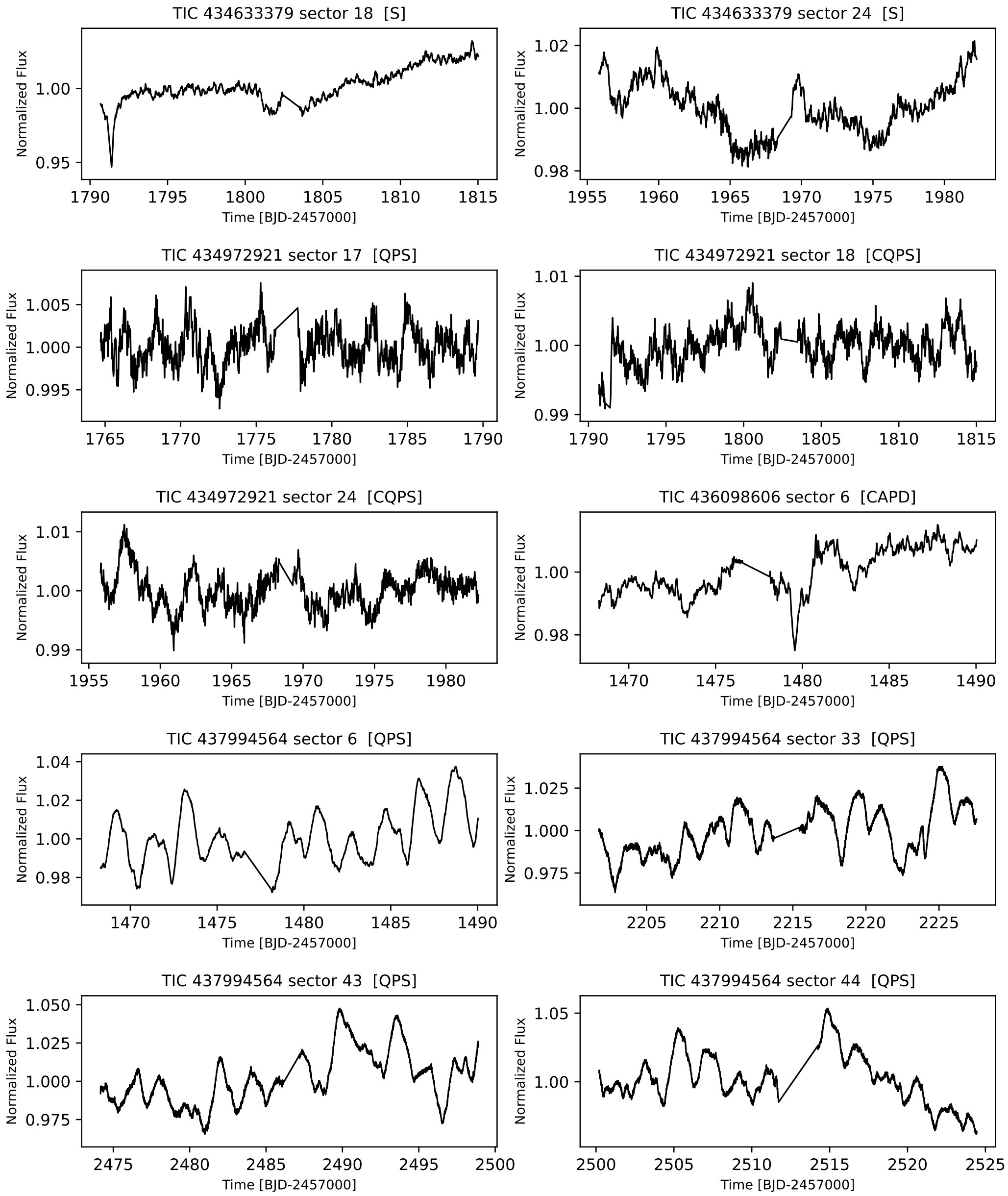

Figure 12. Cont.

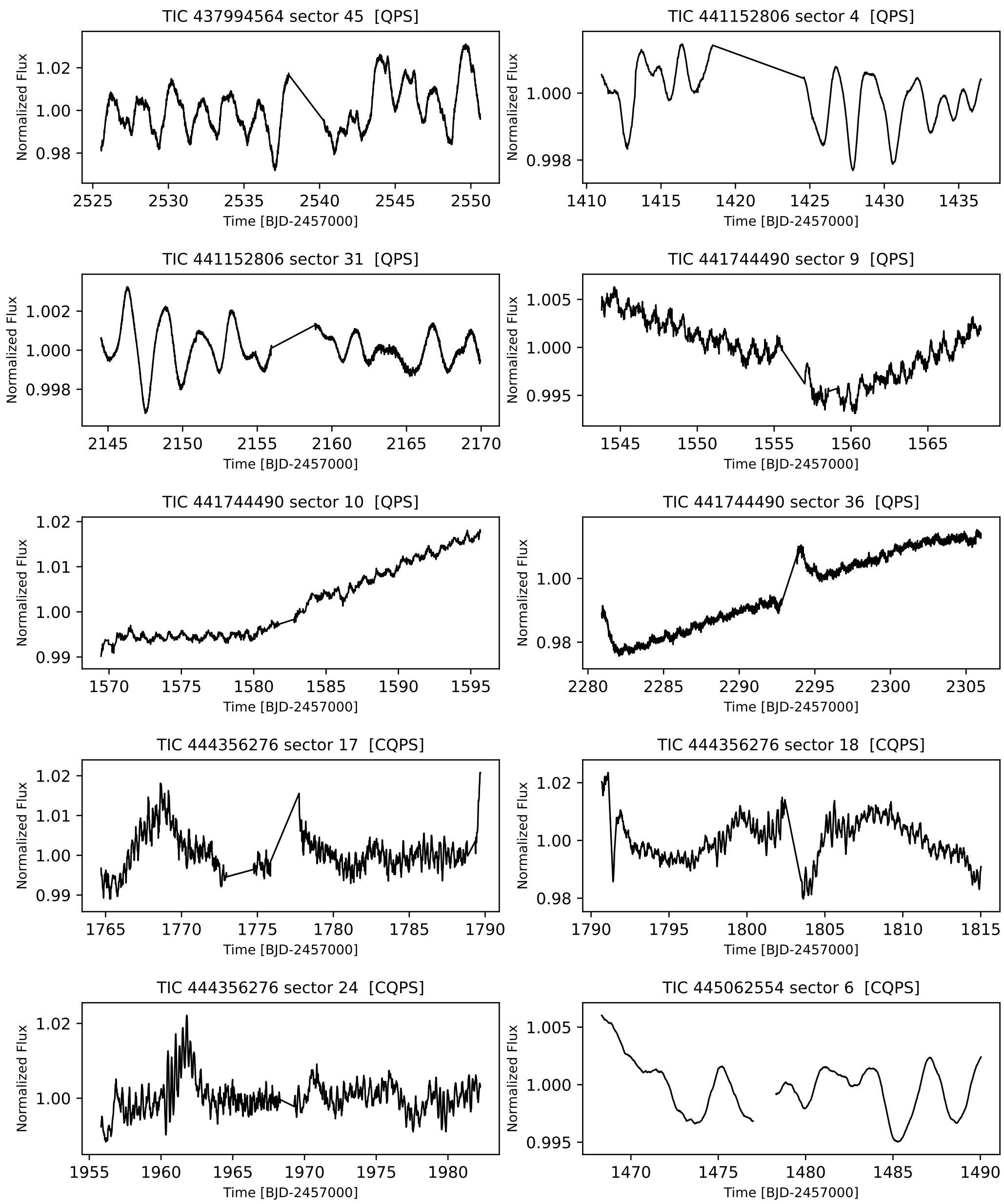

Figure 12. Cont.

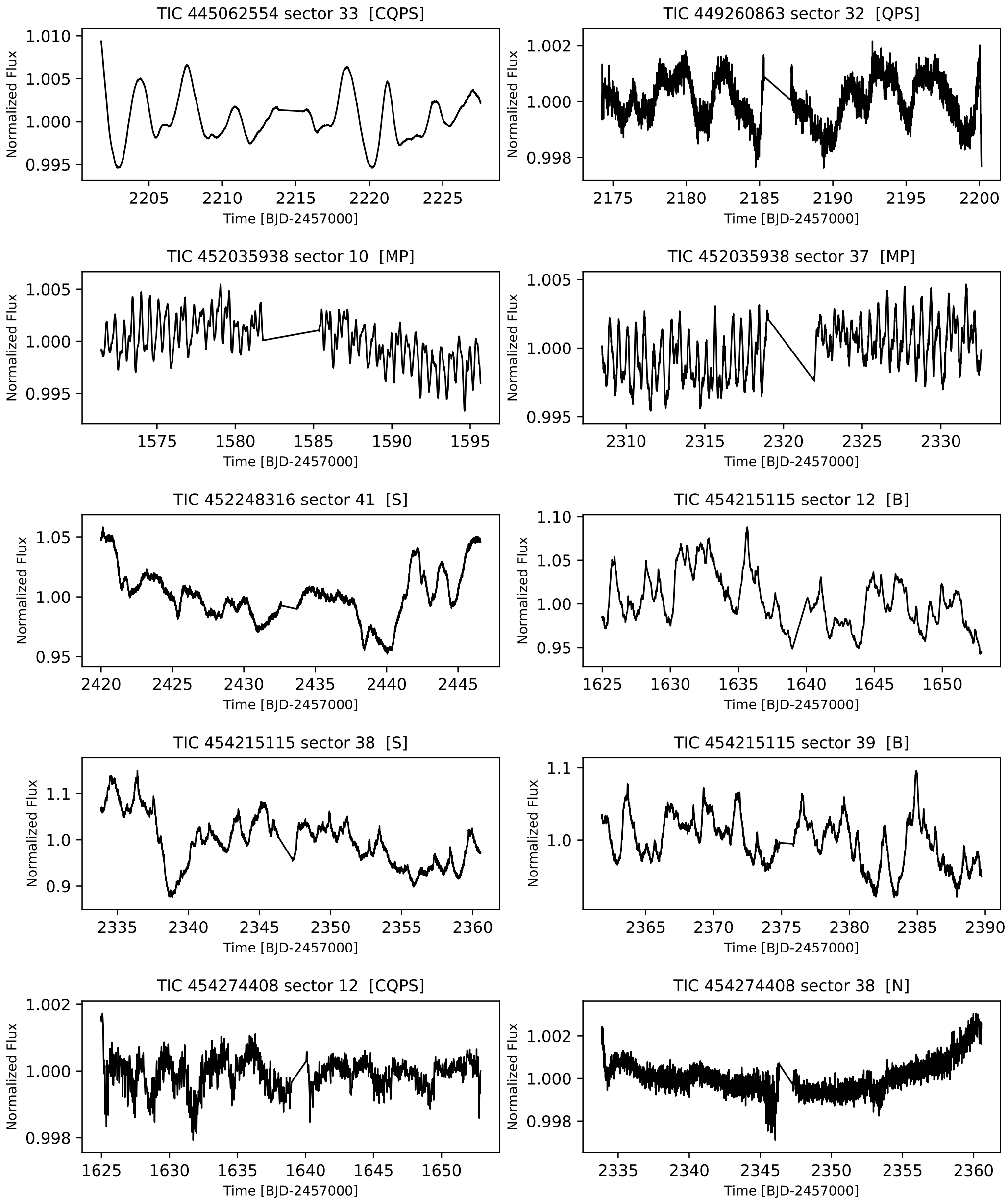

Figure 12. Cont.

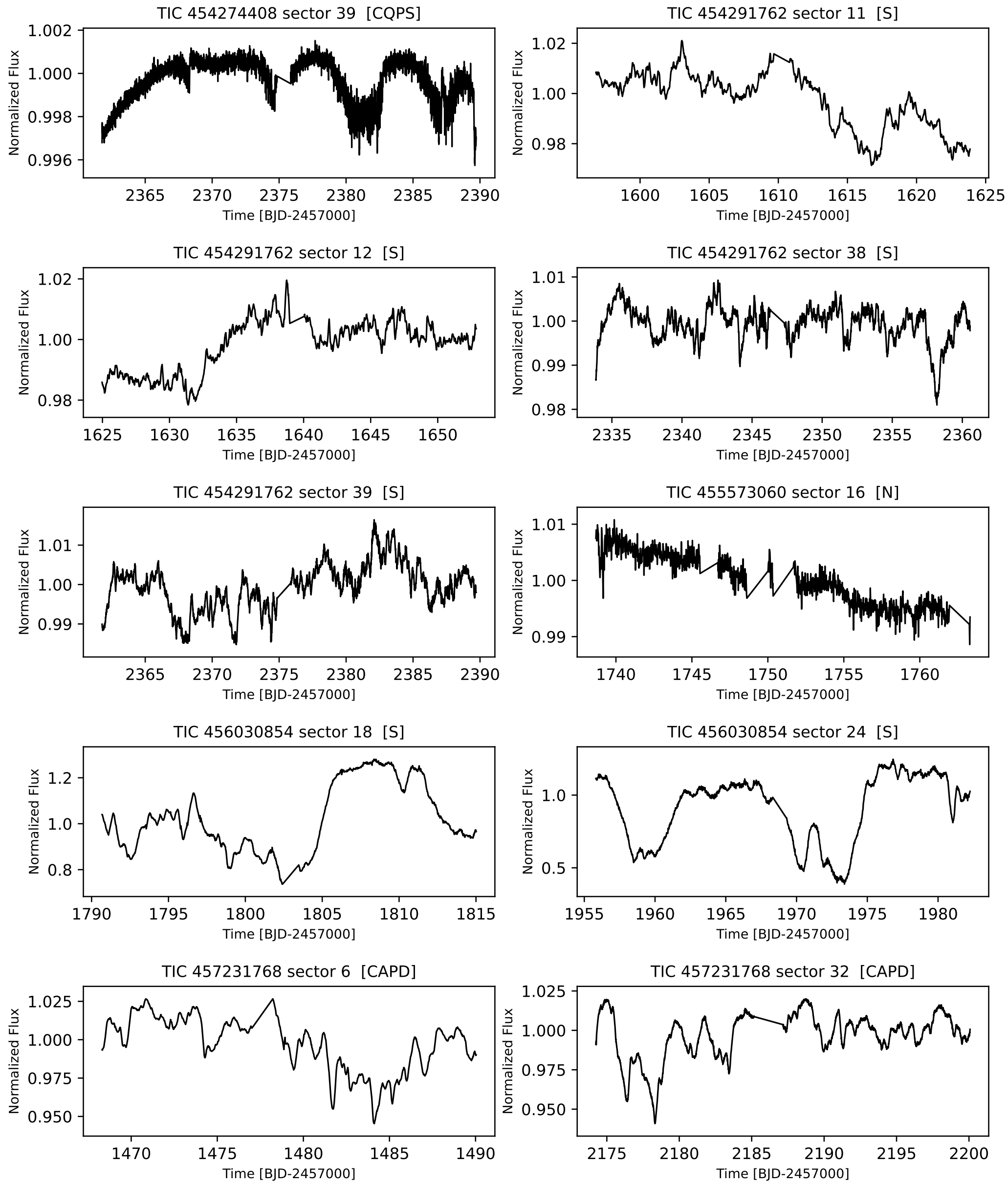

Figure 12. Cont.

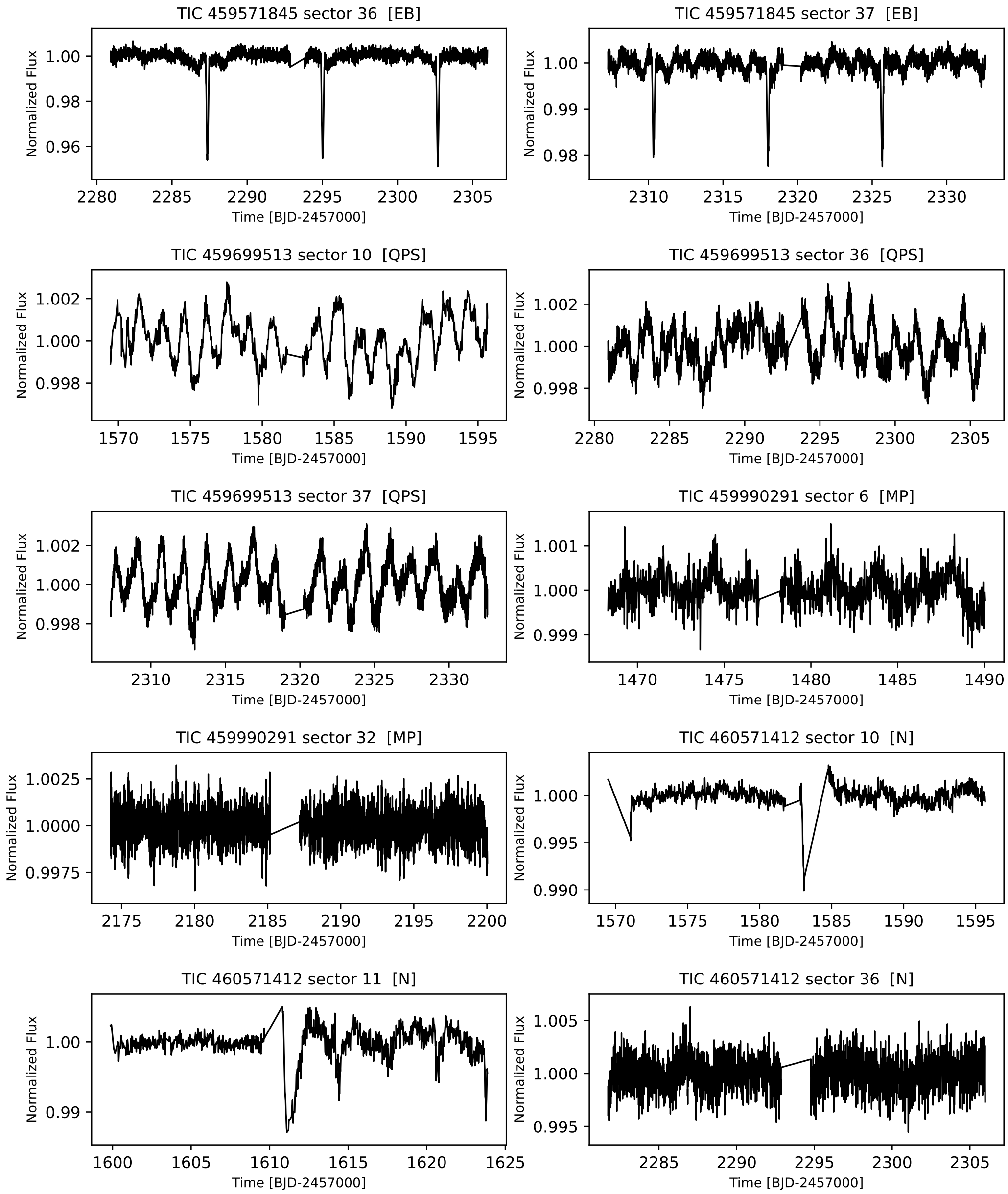

Figure 12. Cont.

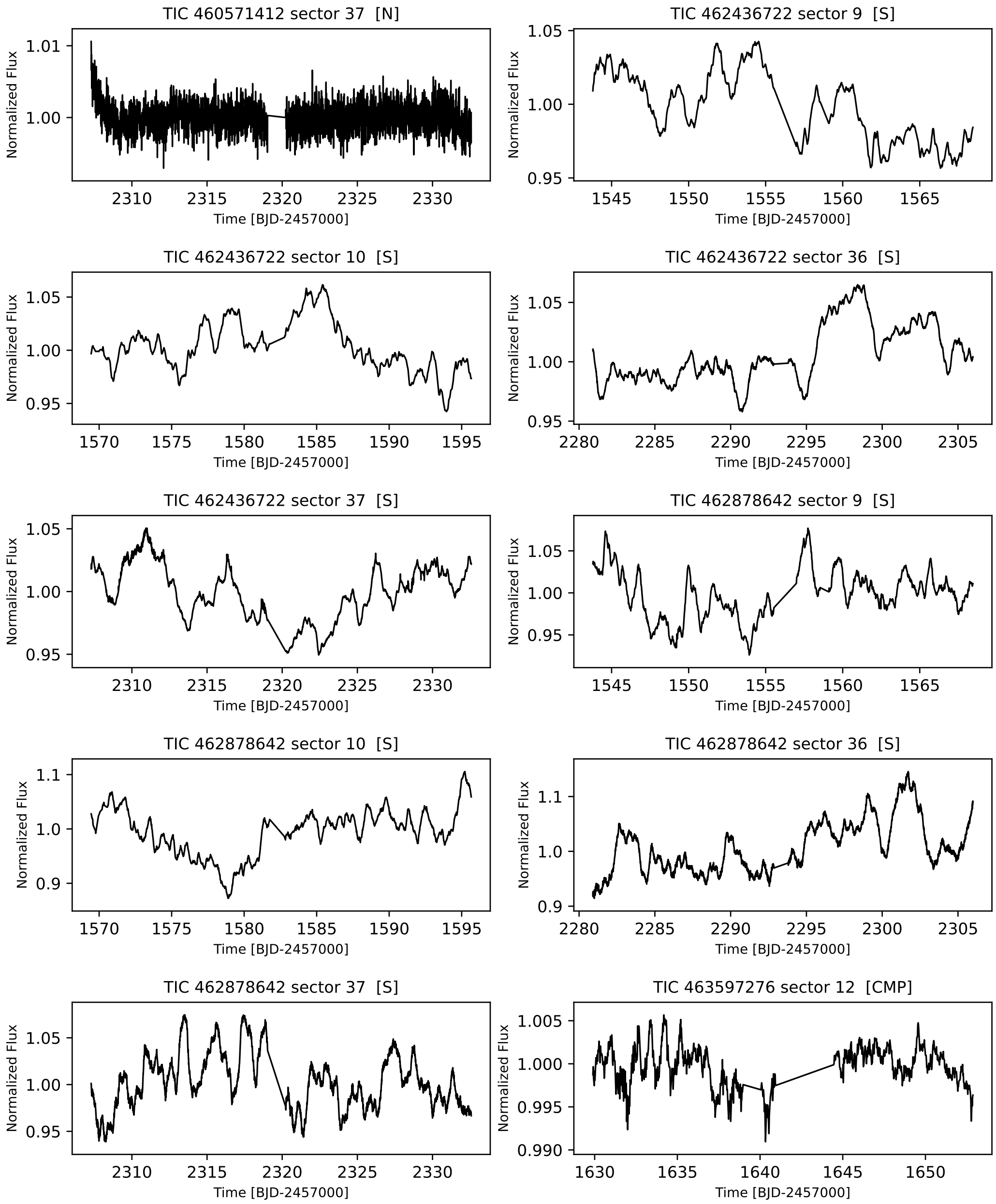

Figure 12. Cont.

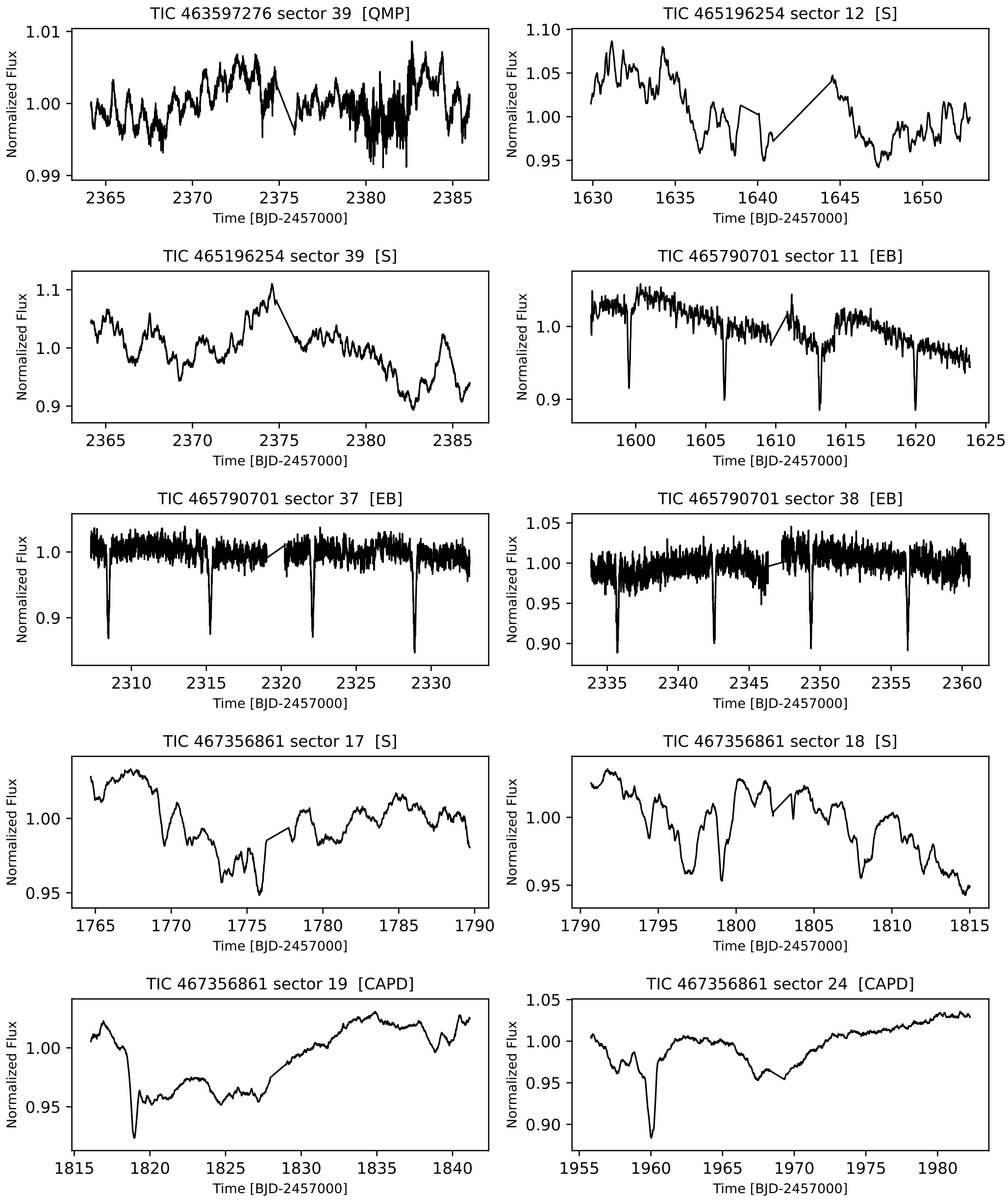

Figure 12. Cont.

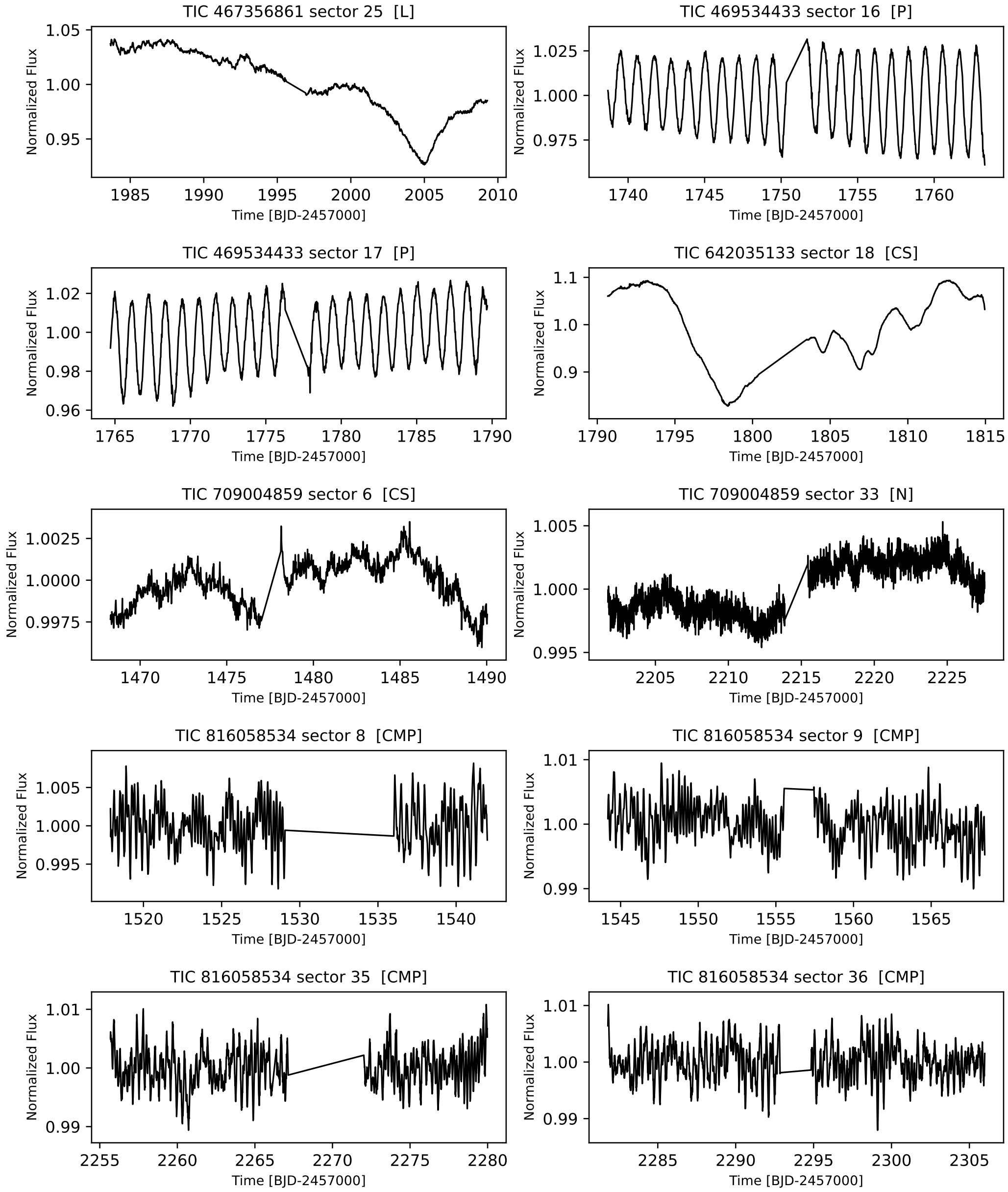

Figure 12. Cont.

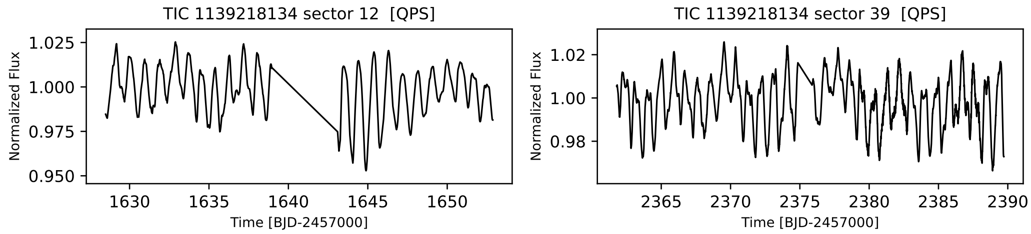

Figure 12. Cont.

REFERENCES

Alecian, E., Wade, G. A., Catala, C., et al. 2013, MNRAS, 429, 1027, doi: 10.1093/mnras/sts384

Arun, R., Mathew, B., Manoj, P., et al. 2019, AJ, 157, 159, doi: 10.3847/1538-3881/ab0ca1

Barsunova, O. Y., Mel'nikov, S. Y., Grinin, V. P., Katysheva, N. A., & Shugarov, S. Y. 2013, Astronomy Reports, 57, 89, doi: 10.1134/S1063772913020029

Benisty, M., Perraut, K., Mourard, D., et al. 2013, A&A, 555, A113, doi: 10.1051/0004-6361/201219893

Bibo, E. A., & The, P. S. 1991, A&AS, 89, 319

Bodman, E. H. L., Quillen, A. C., Ansdell, M., et al. 2017, MNRAS, 470, 202, doi: 10.1093/mnras/stx1034

Boehm, T., & Catala, C. 1995, A&A, 301, 155

Bouvier, J., Cabrit, S., Fernandez, M., Martin, E. L., & Matthews, J. M. 1993, A&A, 272, 176

Bouvier, J., Grankin, K. N., Alencar, S. H. P., et al. 2003, A&A, 409, 169, doi: 10.1051/0004-6361:20030938

Brasseur, C. E., Phillip, C., Hargis, J., et al. 2019, in Astronomical Society of the Pacific Conference Series, Vol. 523, Astronomical Data Analysis Software and Systems XXVII, ed. P. J. Teuben, M. W. Pound, B. A. Thomas, & E. M. Warner, 397

Brittain, S. D., Kamp, I., Meeus, G., Oudmaijer, R. D., & Waters, L. B. F. M. 2023, SSRv, 219, 7, doi: 10.1007/s11214-023-00949-z

Caldwell, D. A., Tenenbaum, P., Twicken, J. D., et al. 2020, Research Notes of the American Astronomical Society, 4, 201, doi: 10.3847/2515-5172/abc9b3

Calvet, N., & Hartmann, L. 1992, ApJ, 386, 239, doi: 10.1086/171010

Cardelli, J. A., Clayton, G. C., & Mathis, J. S. 1989, ApJ, 345, 245, doi: 10.1086/167900

Carmona, A., van den Ancker, M. E., Audard, M., et al. 2010, A&A, 517, A67, doi: 10.1051/0004-6361/200913800

Cauley, P. W., & Johns-Krull, C. M. 2015, ApJ, 810, 5, doi: 10.1088/0004-637X/810/1/5

Cody, A. M., & Hillenbrand, L. A. 2018, AJ, 156, 71, doi: 10.3847/1538-3881/aacead

Cody, A. M., Hillenbrand, L. A., & Rebull, L. M. 2022, AJ, 163, 212, doi: 10.3847/1538-3881/ac5b73

Cody, A. M., Stauffer, J., Baglin, A., et al. 2014, AJ, 147, 82, doi: 10.1088/0004-6256/147/4/82

Costa, G., Shepherd, K. G., Bressan, A., et al. 2025, A&A, 694, A193, doi: 10.1051/0004-6361/202452573

Donati, J. F., & Landstreet, J. D. 2009, ARA&A, 47, 333, doi: 10.1146/annurev-astro-082708-101833

Donehew, B., & Brittain, S. 2011, AJ, 141, 46, doi: 10.1088/0004-6256/141/2/46

Dullemond, C. P., van den Ancker, M. E., Acke, B., & van Boekel, R. 2003, ApJL, 594, L47, doi: 10.1086/378400

Efimova, N. V., Arkharov, A. A., Grinin, V. P., et al. 2022, Astronomy Reports, 66, 236, doi: 10.1134/S1063772922030027

Eiroa, C., Oudmaijer, R. D., Davies, J. K., et al. 2002, A&A, 384, 1038, doi: 10.1051/0004-6361:20020096

Fairlamb, J. R., Oudmaijer, R. D., Mendigutía, I., Ilee, J. D., & van den Ancker, M. E. 2015, MNRAS, 453, 976, doi: 10.1093/mnras/stv1576

Feinstein, A. D., Montet, B. T., Foreman-Mackey, D., et al. 2019, PASP, 131, 094502, doi: 10.1088/1538-3873/ab291c

Ferrario, L., Pringle, J. E., Tout, C. A., & Wickramasinghe, D. T. 2009, MNRAS, 400, L71, doi: 10.1111/j.1745-3933.2009.00765.x

Finkenzeller, U., & Mundt, R. 1984, A&AS, 55, 109

Folsom, C. P., Bagnulo, S., Wade, G. A., et al. 2012, MNRAS, 422, 2072, doi: 10.1111/j.1365-2966.2012.20718.x

Fossati, L., Zwintz, K., Castro, N., et al. 2014, A&A, 562, A143, doi: 10.1051/0004-6361/201323214

Gaia Collaboration, Prusti, T., de Bruijne, J. H. J., et al. 2016, A&A, 595, A1, doi: 10.1051/0004-6361/201629272

GRAVITY Collaboration, Perraut, K., Labadie, L., et al. 2019, A&A, 632, A53, doi: 10.1051/0004-6361/201936403

—. 2021, A&A, 655, A73, doi: 10.1051/0004-6361/202141624

Gürtler, J., Friedemann, C., Reimann, H. G., Splittgerber, E., & Rudolph, E. 1999, A&AS, 140, 293, doi: 10.1051/aas:1999423

Guzmán-Díaz, J., Mendigutía, I., Montesinos, B., et al. 2021, A&A, 650, A182, doi: 10.1051/0004-6361/202039519

Harris, C. R., Millman, K. J., van der Walt, S. J., et al. 2020, Nature, 585, 357, doi: 10.1038/s41586-020-2649-2

Hartmann, L., Herczeg, G., & Calvet, N. 2016, ARA&A, 54, 135, doi: 10.1146/annurev-astro-081915-023347

Hartmann, L., Hewett, R., & Calvet, N. 1994, ApJ, 426, 669, doi: 10.1086/174104

Herbig, G. H. 1960, ApJS, 4, 337, doi: 10.1086/190050

Herbst, W., Herbst, D. K., Grossman, E. J., & Weinstein, D. 1994, AJ, 108, 1906, doi: 10.1086/117204

Herbst, W., & Shevchenko, V. S. 1999, AJ, 118, 1043, doi: 10.1086/300966

Hernández, J., Calvet, N., Briceño, C., Hartmann, L., & Berlind, P. 2004, AJ, 127, 1682, doi: 10.1086/381908

Hernández, J., Calvet, N., Hartmann, L., et al. 2005, AJ, 129, 856, doi: 10.1086/426918

Hillenbrand, L. A., Kiker, T. J., Gee, M., et al. 2022, AJ, 163, 263, doi: 10.3847/1538-3881/ac62d8

Hillenbrand, L. A., Strom, S. E., Vrba, F. J., & Keene, J. 1992, ApJ, 397, 613, doi: 10.1086/171819

Hubrig, S., Järvinen, S. P., Schöller, M., et al. 2019, in Astronomical Society of the Pacific Conference Series, Vol. 518, Physics of Magnetic Stars, ed. D. O. Kudryavtsev, I. I. Romanyuk, & I. A. Yakunin, 18, doi: 10.48550/arXiv.1812.04482

Hubrig, S., & Schöller, M. 2021, Magnetic Fields in O, B, and A Stars, doi: 10.1088/2514-3433/abefcc

Hubrig, S., Schöller, M., Savanov, I., et al. 2010, Astronomische Nachrichten, 331, 361, doi: 10.1002/asna.201011346

Hubrig, S., Schöller, M., & Yudin, R. V. 2004, A&A, 428, L1, doi: 10.1051/0004-6361:200400091

Hunter, J. D. 2007, Computing in Science & Engineering, 9, 90, doi: 10.1109/MCSE.2007.55

Järvinen, S. P., Carroll, T. A., Hubrig, S., Ilyin, I., & Schöller, M. 2019, MNRAS, 489, 886, doi: 10.1093/mnras/stz2190

Lightkurve Collaboration, Cardoso, J. V. d. M., Hedges, C., et al. 2018, Lightkurve: Kepler and TESS time series analysis in Python, Astrophysics Source Code Library. http://ascl.net/1812.013

Luhman, K. L. 2022, AJ, 163, 25, doi: 10.3847/1538-3881/ac35e3

—. 2023, AJ, 165, 37, doi: 10.3847/1538-3881/ac9da3

Marconi, M., & Palla, F. 1998, ApJL, 507, L141, doi: 10.1086/311704

Marconi, M., Ripepi, V., Alcalá, J. M., et al. 2000, A&A, 355, L35, doi: 10.48550/arXiv.astro-ph/0002466

Meeus, G., Waters, L. B. F. M., Bouwman, J., et al. 2001, A&A, 365, 476, doi: 10.1051/0004-6361:20000144

Mendigutía, I., Eiroa, C., Montesinos, B., et al. 2011, A&A, 529, A34, doi: 10.1051/0004-6361/201015821

Meyer, M. R., Calvet, N., & Hillenbrand, L. A. 1997, AJ, 114, 288, doi: 10.1086/118474

Monnier, J. D., & Millan-Gabet, R. 2002, ApJ, 579, 694, doi: 10.1086/342917

Monnier, J. D., Millan-Gabet, R., Billmeier, R., et al. 2005, ApJ, 624, 832, doi: 10.1086/429266

Nguyen, C. T., Costa, G., Girardi, L., et al. 2022, A&A, 665, A126, doi: 10.1051/0004-6361/202244166

Paegert, M., Stassun, K. G., Collins, K. A., et al. 2021, arXiv e-prints, arXiv:2108.04778, doi: 10.48550/arXiv.2108.04778

Pecaut, M. J., & Mamajek, E. E. 2013, ApJS, 208, 9, doi: 10.1088/0067-0049/208/1/9

Poxon, M. 2015, JAAVSO, 43, 35

Ricker, G. 2019, in AAS/Division for Extreme Solar Systems Abstracts, Vol. 51, AAS/Division for Extreme Solar Systems Abstracts, 100.01

Ricker, G. R., Winn, J. N., Vanderspek, R., et al. 2015, Journal of Astronomical Telescopes, Instruments, and Systems, 1, 014003, doi: 10.1117/1.JATIS.1.1.014003

Rivinius, T., Carciofi, A. C., & Martayan, C. 2013, A&A Rv, 21, 69, doi: 10.1007/s00159-013-0069-0

Strom, S. E., Strom, K. M., Yost, J., Carrasco, L., & Grasdalen, G. 1972, ApJ, 173, 353, doi: 10.1086/151425

Suh, K.-W. 2016, Journal of Astronomy and Space Sciences, 33, 119, doi: 10.5140/JASS.2016.33.2.119

The, P. S. 1994, in Astronomical Society of the Pacific Conference Series, Vol. 62, The Nature and Evolutionary Status of Herbig Ae/Be Stars, ed. P. S. The, M. R. Perez, & E. P. J. van den Heuvel, 23

Thé, P. S., de Winter, D., & Perez, M. R. 1994, A&AS, 104, 315

Thomas, S. J., Rodgers, B., van der Bliek, N. S., et al. 2023, AJ, 165, 135, doi: 10.3847/1538-3881/aca803

Torres, C. A. O., Quast, G., de La Reza, R., Gregorio-Hetem, J., & Lepine, J. R. D. 1995, AJ, 109, 2146, doi: 10.1086/117440

Uemura, M., Kato, T., Ishioka, R., et al. 2004, PASJ, 56, S183, doi: 10.1093/pasj/56.sp1.S183

van den Ancker, M. E., de Winter, D., & Tjin A Djie, H. R. E. 1998, A&A, 330, 145

Venuti, L., Cody, A. M., Rebull, L. M., et al. 2021, AJ, 162, 101, doi: 10.3847/1538-3881/ac0536

Vieira, S. L. A., Corradi, W. J. B., Alencar, S. H. P., et al. 2003, AJ, 126, 2971, doi: 10.1086/379553

Vioque, M., Oudmaijer, R. D., Baines, D., Mendigutía, I., & Pérez-Martínez, R. 2018, A&A, 620, A128, doi: 10.1051/0004-6361/201832870

Vioque, M., Oudmaijer, R. D., Schreiner, M., et al. 2020, A&A, 638, A21, doi: 10.1051/0004-6361/202037731

Waters, L. B. F. M., & Waelkens, C. 1998, ARA&A, 36, 233, doi: 10.1146/annurev.astro.36.1.233

Wichittanakom, C., Oudmaijer, R. D., Fairlamb, J. R., et al. 2020, MNRAS, 493, 234, doi: 10.1093/mnras/staa169

Zhang, P., Yang, H. T., & Liu, J. 2006, Ap&SS, 305, 11, doi: 10.1007/s10509-005-9031-6

Zhang, Y.-J., Luo, A. L., Jiang, B., et al. 2022, ApJ, 936, 151, doi: 10.3847/1538-4357/ac84da